WIRELESS POWERED COMMUNICATION OVER INDUCTIVELY COUPLED CIRCUITS

by

Tomohiro Arakawa

A Dissertation

Submitted to the Faculty of Purdue University

In Partial Fulfillment of the Requirements for the degree of

Doctor of Philosophy

School of Electrical and Computer Engineering

West Lafayette, Indiana

May 2021

THE PURDUE UNIVERSITY GRADUATE SCHOOL
STATEMENT OF COMMITTEE APPROVAL

Dr. David J. Love, Co-Chair

School of Electrical and Computer Engineering

Dr. James V. Krogmeier, Co-Chair

School of Electrical and Computer Engineering

Dr. Borja M. Peleato-Iñarrea

School of Electrical and Computer Engineering

Dr. Raghuraman Mudumbai

Department of Electrical and Computer Engineering

University of Iowa

Approved by:

Dr. Dimitrios Peroulis

ACKNOWLEDGMENTS

The time that I have spent pursuing the degree of Ph.D. at Purdue has been one of the most fulfilling moments of my life. I have been incredibly fortunate that I have met and worked with so many wonderful people through various opportunities, including the DARPA Spectrum Collaboration Challenge (SC2), the Open Ag Technology and Systems Center (OATS), and the research on inductive wireless powered communication.

First, I would like to extend my deepest gratitude and appreciation to my advisors Professor David J. Love and Professor James V. Krogmeier, for their continued guidance and encouragement in my journey to the degree of Ph.D. They have always given me fresh insights into every research project that I have worked on and exposed me to diverse academic and industrial experiences.

I would like to thank Professor Raghu Mudumbai for allowing me to collaborate on the research project on the wireless power transfer problem and Professor Borja Peleato, who brought us technical insights when we were working for DARPA SC2.

A huge thanks to all of the past and present fellow graduate students who supported me academically and socially. Special thanks to Aaron Neustedter, Alex Layton, Andrew Balmos, Andrew Marcum, Dennis Ogbe, Eric Ruzomberka, Fabio Castiblanco, Jing Guo, Junghoon Kim, Kyle Willstatter, Mai Zhang, Peng Cheng, Rodrigo Castellanos, Sam Noel, Servio Palacios, Sneha Jha, Stephen Larew, Tzu-Hsuan "Henry" Chou, Vinayak Suresh, Yaguang Zhang, and Yang Wang.

I thank my parents, grandparents, cousins, aunts, and uncles for all the support that I have received and for allowing me to spend an extended period of time abroad. A special thank you to my mother and father for their unconditional love and support throughout my life.

Lastly, I acknowledge the National Science Foundation (NSF), the Defense Advanced Research Projects Agency (DARPA), the Foundation for Food and Agricultural Research (FFAR), and Funai Foundation for Information Technology (FFIT) for their financial support during this research[1].

[1]↑The work in this dissertation was supported in part by the National Science Foundation under Grant EEC-1941529 and the Foundation for Food and Agriculture Research under Grant 534662.

TABLE OF CONTENTS

LIST OF TABLES

LIST OF FIGURES

ABBREVIATIONS

AP	access point
BPSK	binary phase shift keying
CSI	channel state information
CW	continuous wave
DFT	discrete Fourier transform
EH	energy harvesting
FEM	finite element method
GLS	generalized least squares
IC-SWIPT	inductively-coupled simultaneous wireless information and power transfer
ID	information decoding
IoT	Internet of Things
KKT	Karush-Kuhn-Tucker
LM	load modulation
MIMO	multiple-input multiple-output
MISO	multiple-input single-output
ML	maximum likelihood
MRC	maximum ratio combining
NFC	near-field communication
PTE	power transfer efficiency
QAM	quadrature amplitude modulation
QPSK	quadrature phase shift keying
R-E	rate-energy
RF	radio frequency
RFID	radio-frequency identification
RMS	root mean square
SER	symbol error rate
SISO	single-input single-output
SNR	signal-to-noise ratio

SVD	singular value decomposition
SWIPT	simultaneous wireless information and power transfer
WPC	wireless powered communication
WPCN	wireless powered communication network
WPT	wireless power transfer

ABSTRACT

Wireless powered communication (WPC) is an emerging paradigm where wireless devices are powered over the air while exchanging information with them. This technology is attractive for various wireless applications, including classical radio-frequency identification (RFID) systems, implantable sensors, environmental sensing as found in agriculture and forestry, and simultaneous charging and telemetry communications for electric vehicles. While recent studies have shown that inductive coupling provides a more energy-efficient and robust channel for short and middle-range wireless transmission, most of the previous analyses on WPC have been limited to far-field transmission models. To this end, this work provides a comprehensive framework to design and analyze WPC over inductively coupled circuits. We consider three problems, namely, wireless power transfer (WPT), simultaneous wireless information and power transfer (SWIPT), and wireless powered communication network (WPCN) using multiple coupled coils. Each configuration is modeled by an abstract circuit model in which various effects, including mutual coupling and parasitic elements, are captured by a small number of measurable parameters. This technique allows us to not only eliminate the need for solving the circuit but also apply well-known signal processing techniques such as beamforming and channel estimation to inductively coupled models. For each of the three models, we derive the properties of the optimal source signal. In addition, we propose methods to design the load impedance of WPCN by taking into account the nonlinear effects due to impedance mismatches in the circuits.

1. INTRODUCTION

1.1 Overview

As the number of Internet of Things (IoT) devices increases rapidly, there is an urgent need for new technology to prolong the lifetime of wireless communication devices by eliminating the manual replacement of batteries. Replacement or wired-charging of the batteries of IoT devices, including underground sensors, wireless structural sensors, and medical implants, is often very challenging. The conventional approach to supporting these devices was implementing distinct wireless power transfer (WPT) and wireless communication protocols, which require two wireless channels and the corresponding pairs of transmitter and receiver circuits. Therefore, new technologies such as wireless powered communication (WPC) are desired to jointly design and optimize WPT and wireless communications for IoT devices.

Historically, WPT and wireless communication have evolved as two distinct research areas. In wireless communications, various intelligent data transmission techniques have been developed based on signal processing and information theory to implement reliable, fast, and low-latency wireless communication channels. For WPT systems, on the other hand, the main focus has been to create an energy-efficient wireless charging system that transfers large energy with minimal loss. While wireless power transfer and communication are fundamentally the same physical phenomena, the two research areas had rarely been jointly studied until recently because of their vastly different objectives.

WPC is an emerging paradigm in which WPT and wireless communication systems are jointly designed and analyzed [1]. In general, a WPC system consists of one or more access points (APs) that supply energy to remote wireless devices over the air. The APs and wireless devices also exchange information using uplink, downlink, or both channels. This technique has been extensively studied recently in the signal processing community based on microwave transmission models. The concept of WPC captures various wireless information and power transfer configurations, from the traditional WPT to the emerging simultaneous wireless information and power transfer (SWIPT) and wireless powered communication network (WPCN) models.

While most of the previous work on WPC has been limited to far-field microwave transmission models, near-field inductive coupling is a promising technique to establish an energy-efficient wireless channel for short and middle-range wireless signal transmission [2]. In contrast to far-field transmission models based on the propagating electromagnetic field, an inductively coupled system primarily uses a near-field magnetic field. Since the invention of inductive wireless transfer by Tesla [3], the near-field inductive coupling technique has been used for various wireless charging applications, including wireless chargers for cell phones, smartwatches, electric vehicles (EVs), medical implants, and underground and underwater wireless charging systems in which far-field microwave signals suffer from a significant attenuation. Furthermore, a recent breakthrough on inductive WPT, referred to as magnetic resonant coupling, has shown to significantly increase the range of power transmission while maintaining a high power transfer efficiency (PTE) by utilizing additional resonant coils [4].

One of the difficulties of using a wireless channel over inductively coupled circuits is that the channel is sensitive to the misalignment of coils. One approach to compensate for the performance degradation is to physically adjust the position of the coils using magnets or other mechanical techniques so that the best wireless channel is obtained [5]. However, this technique often requires a complex mechanical system to control the position as well as the orientation of coils. Therefore, this dissertation considers applying multi-antenna technology, a widely used technique in the signal processing community, to an inductively coupled system. Specifically, we employ multiple transmit coils to transmit signals, which are optimized based on the information about the inductive wireless channel.

This dissertation investigates three types of inductive WPC configurations. First, we consider WPT from a transmitter with multiple transmit coils to a receiver with a single coil as illustrated in Fig. 1.1a. In contrast to the traditional approach in which a circuit system is directly solved, the proposed model uses a "black-box" approach in which unknown channel parameters are estimated in real-time. Secondly, we consider a multiple-input multiple-output (MIMO) SWIPT in which both information and power are simultaneously transferred from a multi-coil transmitter to a multi-coil receiver, as illustrated in Fig. 1.1b. The optimal transmit covariances for three objectives, namely, the maximum data rate, maximum harvested power, and maximum data rate subject to the minimum harvested power constraint,

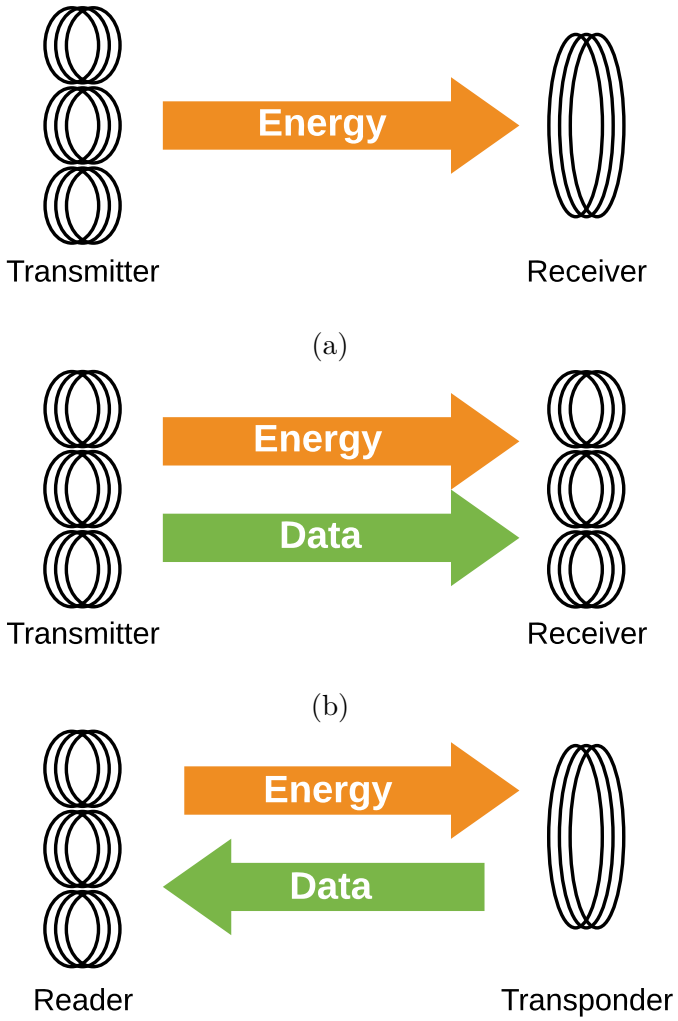

Figure 1.1. Three inductive WPC operating modes considered in this dissertation. (a) MISO WPT. (b) MIMO SWIPT. (c) MISO WPCN.

are derived. Lastly, we propose an inductive multiple-input single-output (MISO) WPCN in which energy is transferred from a reader to a passive transponder while information is transferred to the other direction, as illustrated in Fig. 1.1c. We present methods to design reflection coefficients and estimate the unknown channel (scattering parameters) based on a combination of active channel sounding and passive load modulation techniques.

1.2 Optimizing Wireless Power Transfer from Multiple Transmit Coils

Inductive WPT allows remote devices to receive energy at high power transfer efficiency using magnetically coupled transmit and receive coils. Traditionally, inductive WPT systems have been designed and analyzed using the circuit analysis technique, which considers individual circuit parameters such as self and mutual inductances as well as parasitic components in the circuits. While this approach works well if the exact properties and orientations of the transmit and receive coils are known and fixed, the power transfer efficiency quickly drops when the coil geometry is altered. Furthermore, it is challenging to correctly model all of the individual parasitic components that exist in a WPT system. Therefore, this dissertation introduces a black-box approach in which the linear circuit interconnections between the transmitter and receiver are represented by a small number of measurable parameters. The optimal source currents that maximize the power transfer efficiency are derived using the proposed black-box model. The experimental results confirmed the improvement in PTE compared to the conventional beamforming solutions. A short discussion on a method to estimate the unknown black-box parameters is also provided.

This is joint work with David J. Love, James V. Krogmeier, Matthew A. Swabey at Purdue University, Sairam Goguri at Qualcomm Inc., Raghuraman Mudumbai, and Anton Kruger at the University of Iowa.

1.3 MIMO Simultaneous Wireless Information and Power Transfer over Inductively Coupled Circuits

SWIPT is an emerging research topic in the signal processing community to study joint optimization of power transfer and wireless communication using a common transmit signal. In particular, MIMO SWIPT has shown to be a promising technique to implement a robust and efficient SWIPT system using multi-antenna technology [6]. This dissertation extends MIMO SWIPT to a generic black-box circuit model, which takes into account impedance mismatches and various parasitic losses. The optimal transmit covariance matrices for three optimization objectives, namely, maximum delivered power, maximum data rate, and maximum data rate under the minimum delivered power constraint, are derived. The tradeoffs

between the data rate and harvested power are computed for direct-fed and indirect-fed inductive SWIPT models using finite element method (FEM) analysis.

This is joint work with David J. Love and James V. Krogmeier at Purdue University. This work was presented in part at the 2019 Asilomar Conference on Signals, Systems, and Computers [7].

1.4 Near-Field Wireless Powered Communication Network Using a Coil Array

Many IoT devices such as underground sensors and implantable medical sensors transfer the collected data over an uplink wireless communication channel. This dissertation studies a simultaneous downlink power transfer and uplink communication system, which is often referred to as WPCN in the signal processing community [8]. In particular, we consider data transfer from an inductively coupled single-coil transponder to a multi-coil reader based on passive load modulation, a widely-used radio-frequency identification (RFID) technique that does not require any active signal transmission or modulation at the transponder. The inductive WPCN is modeled using the black-box model, and the optimal source gains and the receive combiner are derived to maximize the harvested power and receive signal-to-noise ratio (SNR). In addition, a novel scattering parameter estimation method, which determines the unknown channel using a combination of active and passive pilot sequences, was proposed. The numerical analysis confirmed that the proposed multi-coil reader model yields higher delivered power and receive SNR than the traditional single-coil reader model in coil misalignment scenarios.

This is joint work with David J. Love and James V. Krogmeier at Purdue University. This work was originally presented in part at the 2020 Asilomar Conference on Signals, Systems, and Computers [9].

1.5 Organization of Dissertation

The rest of the dissertation is organized as follows. Chapter 2 discusses optimizations of WPT from a transmitter with multiple coils to a receiver with a single coil. In Chapter 3, point-to-point MIMO SWIPT over an inductively coupled circuits is studied. Chapter 4

analyzes WPCN with simultaneous downlink WPT and uplink wireless communication over inductively coupled MISO channel. Chapter 5 summarizes the dissertation.

2. OPTIMIZING WIRELESS POWER TRANSFER FROM MULTIPLE TRANSMIT COILS

 T. Arakawa, S. Goguri, J. V. Krogmeier, *et al.*, "Optimizing wireless power transfer from multiple transmit coils," *IEEE Access*, vol. 6, pp. 23 828–23 838, 2018. DOI: 10.1109/ACCESS.2018.2825290.

2.1 Introduction

2.1.1 Overview of Inductive WPT

Inductive coupling has long been recognized as an effective method to transfer power to remote devices without wires. Unlike radiative far-field power transmission, which uses propagating electromagnetic waves, near-field inductive coupling techniques utilize the magnetic fields generated by one or more coils [11]. The fundamental idea of WPT using inductive coupling involves applying an AC voltage to drive current in a transmitter coil that induces a current in a receiver coil to supply power to a resistive load. This technique dates back to the 19th century, and there is a long history of attempts to build practical devices for wireless power transfer based on this principle [2], [12].

The explosion of mobile devices has invigorated industrial work on WPT, driven by the possibility of eliminating the last remaining wire for mobile computing devices such as smartphones and watches [13], [14]. Recent applications include mobile device charging [15], passive RFID tags [16], medical implants [17], [18], and electric vehicles [19]. There are already several international standards, including the Wireless Power Consortium Qi standard [20] and the Alliance for Wireless Power Rezence standard [21], and there are a variety of commercial products developed from these standards. Despite this significant amount of work, most present-day WPT devices are still limited by short ranges (e.g., a few millimeters to centimeters) and/or low efficiencies [22], [23].

2.1.2 The Key Challenge

A common challenge in most of the previous work on WPT systems is the difficulty of building accurate models that can predict the power transfer efficiency well enough to tune

and optimize the system. The common approach in previous work is to model a WPT system as a lumped RLC circuit that is then analyzed using standard circuit-solving techniques. Some previous work has also used models for WPT systems based on coupled-mode theory [4], which has been shown to be equivalent to the RLC circuit modeling [24], [25].

There are two major limitations to using standard circuit solving techniques. First, the self inductance (L) and mutual inductance (M) circuit elements require complex numerical calculations, and the mutual inductance values are very sensitive to small changes in the geometry of the system. Second, and more crucially, a realistic circuit model requires a complex circuit with a large number of lumped circuit elements.

This latter difficulty appears to be fundamental and arises from the fact that there are at least two dominant loss mechanisms in WPT systems: Ohmic losses in parasitic resistances and radiation losses, which are often modeled by multiple lumped circuit elements [26], [27]. Furthermore, an accurate analysis requires consideration of small losses, e.g., Eddy currents in conducting surfaces near the transmitter coils. These losses are physically dispersed and cannot be modeled with a small number of lumped circuit elements.

The above reasoning leads directly to the fundamental question that motivates this work. *Can we devise an alternative to the lumped element circuit model that captures the cumulative effect of the various loss mechanisms in a WPT system without explicitly modeling every loss source individually?*

2.1.3 Approach

The approach followed here is most easily explained using an analogy with channel modeling for wireless communication systems. Wireless communication engineers have long faced the problem of accurately calculating the frequency response of the propagation channel. A physics-based approach is to apply Maxwell's equations to intricate models of the propagation environment. While this can be useful in a carefully controlled setting, practical wireless communication devices must be deployed in innumerable scenarios and perform real-time channel adaptation. To solve this problem, researchers have long resorted to signal processing inspired techniques. The channel is viewed as a black box, and the system

response is typically estimated in real-time at the receiver using a known training sequence. This omits the need for careful, and usually inaccurate, electromagnetic (EM) modeling, succinctly captures the mathematical properties of the channel needed for optimization, and allows for real-time adaptation.

This is exactly what we propose to do for multiple coil WPT systems. Specifically, we assume that the WPT system is represented by an unknown multi-terminal linear circuit. We consider the transmitter terminals as the inputs, receiver terminal as the output, and express the input-output relationship between the terminal voltages and currents using a minimal number of unknown transimpedance and gain parameters. We propose to directly estimate these parameters using a series of simple measurements based on a predetermined sequence of input currents. We refer to this technique as *circuit sounding*. Calculating the input excitations to this multiple coil system that yield the maximum power transfer efficiency is then a simple optimization.

Note that this approach is different from impedance matching, which intends to maximize power transfer by determining optimal circuit parameters which minimize the wave reflection ratio [28]–[30]. Instead, we aim to find optimal coil excitation currents which deliver maximum power to a receiver for a given WPT system with fixed circuit parameters.

The specific contributions of this chapter are as follows:

1. We describe an abstract circuit model that captures the coupling between the transmitters and the receiver as well as losses using a minimal number of unknown parameters. A simple procedure to estimate the unknown model parameters is also described.

2. We present a simple derivation of the input excitations that maximize the power transfer in terms of the parameters of the abstract model. We demonstrate that it yields solutions that differ from standard assumptions commonly found in the existing literature.

3. We describe an extensive set of experiments that we designed to test and validate the abstract model.

2.1.4 Survey of Recent Work

Resonant coupling is one recently-developed technique for improving the efficiency and range of multi-coil WPT systems. A typical configuration used with this method involves a four-coil system where the transmitter and receiver are designed to resonate with a high Q factor at precisely the same frequency [4]. Since the performance of resonant coupled systems is sensitive to coil geometry and the presence of other conducting objects near the coils [31], [32], maintaining resonance is extremely challenging in practice [31], [33], [34].

A recently proposed technique is to use multiple transmit coils [35]–[37] to focus the energy of the magnetic field towards the receiver. This idea is superficially similar to beamforming from phased array antennas [38]. However, it is important to keep in mind that the physics of radiative electromagnetic fields from antennas is very different from that of magnetic near-fields. Indeed, the experimental results in this paper illustrate that phase coherence at the receiver is not necessarily optimal for WPT systems.

Convex optimization methods have been used to find the optimal reactances and current excitations that maximize the power transfer efficiency of resonant multiple-input single-output (MISO) WPT systems [39]. While the optimization problem presented in this paper is closely related to the one in [39], we do not consider optimizing the impedances, and our formulation can be applied to non-resonant WPT systems. Recently, [40] presented an optimization problem for maximizing the efficiency of multiple-input multiple-output (MIMO) WPT systems. However, this approach relies on a specific lumped RLC circuit model, which requires prior knowledge of the circuit parameters such as parasitic resistances. Both [39] and [40] use numerical simulations, instead of experimental validation, to verify the correctness. In contrast, we present experimental evidence based on direct real-time measurements to verify the validity of the model and analysis.

The rest of the paper is organized as follows. Section 2.2 presents the abstract model for MISO WPT systems. The efficiency-maximizing excitation for the transmitters is derived in Section 2.3. A series of experiments designed to illustrate and verify the model is described in Section 2.4 and an analysis of the experimental results is presented in Section 2.5. Section 2.6 concludes.

In this paper, we use the following notation: for a matrix or vector $\mathbf{A}$, $\mathbf{A}^H$ stands for its Hermitian transpose, $\mathbf{A}^T$ means transpose, $\mathbf{A}^{-1}$ indicates its matrix inverse, and $\mathbf{A}^*$ stands for the conjugate of $\mathbf{A}$. For a complex number c, the complex conjugate is written as c^*, and the real part of c is denoted by $\mathrm{Re}(c)$.

2.2 Model Description

2.2.1 Abstract Circuit Model

Consider an arbitrary MISO WPT system (e.g., WPT model with lumped circuit elements shown in Fig. 2.1(a)) which can be translated into an abstract circuit model illustrated in Fig. 2.1(b). In these models, N current sources connected to N input terminals with currents $i_1, i_2, ..., i_N$ represent the transmitters. These transmitters aim to deliver maximum power to a receiver which is modeled as a load as shown. The voltage across source k, for $k = 1, \ldots, N$, is denoted by v_k, and the load voltage and current are denoted by v_0 and i_0, respectively.

It is assumed that all the elements in the circuit are linear and the N sources are the only active elements. Beyond that, we make no assumptions about the interconnections between the different terminals, the geometry of the coils, and the complexity of the circuit. Specifically, the model allows i) arbitrarily weak or strong coupling for the transmitter coils with each other and with the receiver and ii) applies to both resonant or non-resonant systems. Since Maxwell's equations are linear, this model also automatically accounts for all parasitic resistances and reactances including radiation and skin effects and the presence of shielding materials.

For simplicity, we limit consideration to a time-invariant single-frequency AC circuit system, where phasor voltages and currents are represented by complex numbers and the linear load by a complex impedance Z_0. The generalization of the circuit model to arbitrary time-varying non-sinusoidal voltages and currents is straightforward. However, the general non-sinusoidal case presents a far richer design space and a variety of interesting optimization problems. We defer detailed consideration of these to future work.

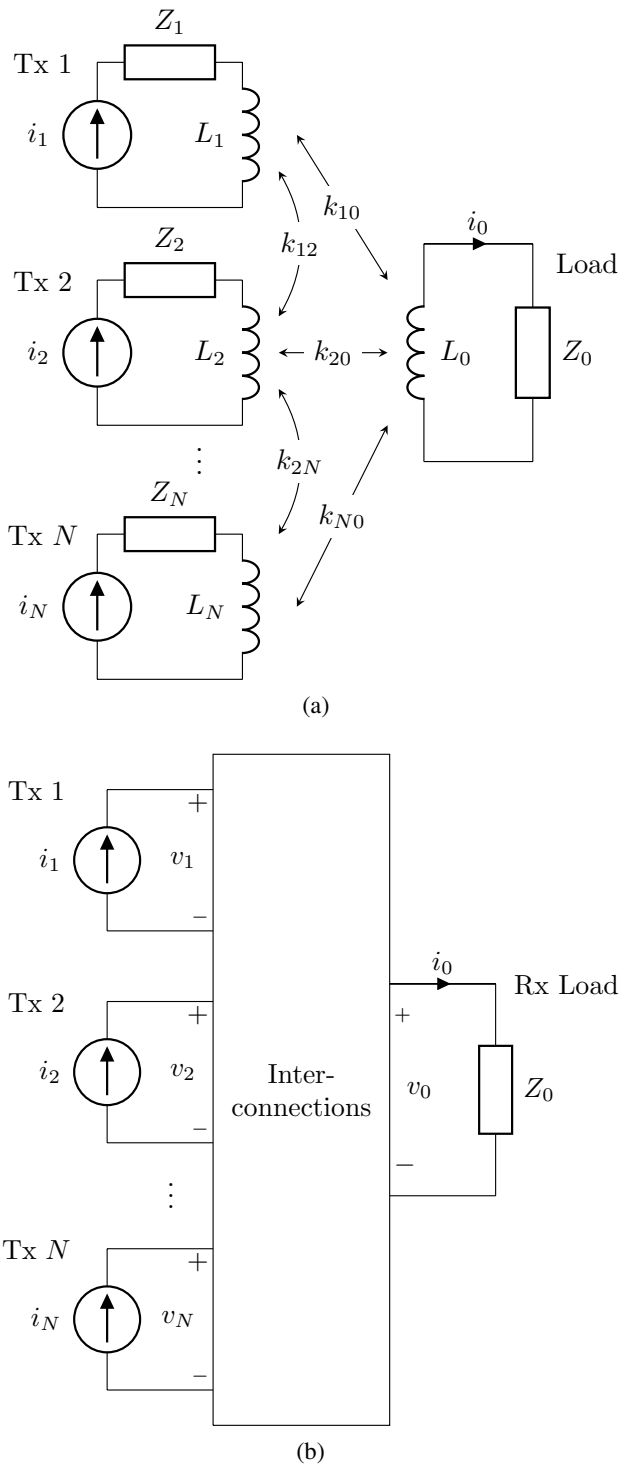

Figure 2.1. (a) Lumped circuit model and (b) abstract circuit model for inductive WPT systems.

Under the assumptions of linearity and time invariance, the voltage v_0 and current i_0 across the receiver load can be computed using the superposition principle as the sum of contributions proportional to each of the phasor currents i_k's:

$$v_0 = a_{0,1}^* i_1 + a_{0,2}^* i_2 + \ldots + a_{0,N}^* i_N \equiv \mathbf{a}_0^H \mathbf{i}, \tag{2.1}$$

$$\text{and} \quad i_0 = b_{0,1}^* i_1 + b_{0,2}^* i_2 + \ldots + b_{0,N}^* i_N \equiv \mathbf{b}_0^H \mathbf{i}, \tag{2.2}$$

where $\mathbf{i} = [i_1, i_2, ..., i_N]^T$ is an input current vector, $\mathbf{a}_0 = [a_{0,1}, a_{0,2}, ..., a_{0,N}]^T$ is a transimpedance vector, and $\mathbf{b}_0 = [b_1, b_2, ..., b_N]^T$ is a dimensionless current gain vector. Using (2.1) and (2.2), the power consumed by the receiver load is given by

$$\begin{aligned} P_L(\mathbf{i}) &= \mathrm{Re}(v_0^* i_0) \\ &= \frac{1}{2}\left(v_0^* i_0 + i_0^* v_0\right) \\ &= \frac{1}{2}\mathbf{i}^H \left(\mathbf{a}_0 \mathbf{b}_0^H + \mathbf{b}_0 \mathbf{a}_0^H\right) \mathbf{i}. \end{aligned} \tag{2.3}$$

Using Ohm's law, we can write the current i_0 and voltage v_0 of the load Z_0 as

$$i_0 = \frac{v_0}{Z_0} = \mathbf{b}_0^H \mathbf{i} \quad \text{and} \quad v_0 = \mathbf{a}_0^H \mathbf{i}.$$

This gives $\mathbf{a}_0^H = Z_0 \mathbf{b}_0^H$ which gives for the load power,

$$P_L(\mathbf{i}) = \mathrm{Re}\left(Z_0\right) \mathbf{i}^H \left(\mathbf{b}_0 \mathbf{b}_0^H\right) \mathbf{i} = \mathbf{i}^H \left(\mathbf{c}\mathbf{c}^H\right) \mathbf{i}, \tag{2.4}$$

where the vector $\mathbf{c} \triangleq \sqrt{\mathrm{Re}\left(Z_0\right)} \mathbf{b}_0$.

Similarly for the k-th source terminal, the voltage across transmit coil k can be written as

$$v_k = a_{k,1}^* i_1 + a_{k,2}^* i_2 + \ldots + a_{k,N}^* i_N \equiv \mathbf{a}_k^H \mathbf{i}, \tag{2.5}$$

where $\mathbf{a}_k$ is a transimpedance vector $\mathbf{a}_k = [a_{k,1}, a_{k,2}, ..., a_{k,N}]^T$. The current i_k is trivially written as $i_k = \boldsymbol{\delta}_k^H \mathbf{i}$ where $\boldsymbol{\delta}_k$ is the k-th column of the $N \times N$ identity matrix. The power P_k generated by the transmitter k can then be written as

$$P_k(\mathbf{i}) = \frac{1}{2}\mathbf{i}^H \left(\mathbf{a}_k \boldsymbol{\delta}_k^H + \boldsymbol{\delta}_k \mathbf{a}_k^H\right) \mathbf{i} \equiv \mathbf{i}^H \mathbf{A}_k \mathbf{i}, \tag{2.6}$$

where $\mathbf{A}_k = \frac{1}{2}\left(\mathbf{a}_k \boldsymbol{\delta}_k^H + \boldsymbol{\delta}_k \mathbf{a}_k^H\right)$ is a positive semidefinite Hermitian matrix. This allows us to write for the total power transmitted by all the sources as

$$P_T(\mathbf{i}) = \mathbf{i}^H \left(\sum_{k=1}^{N} \mathbf{A}_k\right) \mathbf{i} \equiv \mathbf{i}^H \overline{\mathbf{A}} \mathbf{i}, \tag{2.7}$$

where $\overline{\mathbf{A}}$ is the transmitted power matrix and $P_T(\mathbf{i}) \leq P_T$ for total available transmit power P_T.

The power loss in the WPT system is defined as

$$P_{loss}(\mathbf{i}) = \mathbf{i}^H \mathbf{B} \mathbf{i}, \tag{2.8}$$

using a positive semi-definite Hermitian "loss matrix" $\mathbf{B} = \mathbf{B}^H \equiv \overline{\mathbf{A}} - \mathbf{c}\mathbf{c}^H$. Therefore, using (2.7) and (2.8), we can rewrite the total power delivered to the load as

$$P_L(\mathbf{i}) = P_T(\mathbf{i}) - P_{loss}(\mathbf{i}) = \mathbf{i}^H \left(\overline{\mathbf{A}} - \mathbf{B}\right) \mathbf{i}. \tag{2.9}$$

2.2.2 Real-time Measurement Procedure

We describe a simple method to estimate the unknown "channel" parameters $\mathbf{B}$ and $\mathbf{c}$ using least-squares. We define a full-rank matrix $\mathbf{Q} \in \mathbb{C}^{N \times K}$ to represent pilot sequences, which is given by

$$\mathbf{Q} = \begin{bmatrix} q_{11} & q_{12} & \cdots & q_{1K} \\ q_{21} & q_{22} & \cdots & q_{2K} \\ \vdots & \vdots & \ddots & \vdots \\ q_{N1} & q_{N2} & \cdots & q_{NK} \end{bmatrix} \text{ (A)}, \tag{2.10}$$

where q_{ij} is a pilot symbol transmitted from coil i at time instant j. When the pilot symbols are transmitted, the voltage across the i-th transmit coil can be represented by

$$\mathbf{x}_i = \mathbf{a}_i^H \mathbf{Q} + \mathbf{w}_i \ \ (\text{V}), \tag{2.11}$$

where $\mathbf{a}_i$ are transimpedance vectors and $\mathbf{w}_i \in \mathbb{C}^{1\times K}$ are noise. Similarly, the current of the receiver load is represented by

$$\mathbf{y} = \mathbf{b}_0^H \mathbf{Q} + \mathbf{w}_0 \ \ (\text{A}), \tag{2.12}$$

where $\mathbf{w}_0 \in \mathbb{C}^{1\times K}$ is the noise. Using the measured transmitter voltages $\mathbf{x}_i$ and load current $\mathbf{y}$, we can estimate the parameters $\mathbf{a}_i$ and $\mathbf{b}_0$ by

$$\hat{\mathbf{a}}_i = (\mathbf{x}_i \mathbf{Q}^\dagger)^H, \quad \text{and} \quad \hat{\mathbf{b}}_0 = (\mathbf{y}\,\mathbf{Q}^\dagger)^H, \tag{2.13}$$

where $\mathbf{Q}^\dagger$ is a pseudo-inverse of $\mathbf{Q}$, which is given by $\mathbf{Q}^\dagger = \mathbf{Q}^H(\mathbf{Q}\mathbf{Q}^H)^{-1}$. The estimate of the matrix $\mathbf{B}$ can then be calculated as $\hat{\mathbf{B}} = \frac{1}{2}\sum_{i=1}^{N}\left(\hat{\mathbf{a}}_i\boldsymbol{\delta}_i^H + \boldsymbol{\delta}_i\hat{\mathbf{a}}_i^H\right) - \hat{\mathbf{c}}\hat{\mathbf{c}}^H$, where $\hat{\mathbf{c}} = \sqrt{\text{Re}\,(Z_0)}\hat{\mathbf{b}}_0$.

If $\mathbf{w}_0$ and $\mathbf{w}_i$ are zero-mean white noise vectors, then the estimation error $\mathbb{E}\left[\|\mathbf{a}_i - \hat{\mathbf{a}}_i\|^2\right]$ and $\mathbb{E}\left[\|\mathbf{b}_0 - \hat{\mathbf{b}}_0\|^2\right]$ are minimized when $\mathbf{Q}$ is constructed by orthogonal rows with the same norm [41]. Some examples that satisfy this condition include the identity matrix and DFT matrix.

Note: The above estimation procedure involves measurements only at the input terminals and the load and does not involve any measurements anywhere else in the circuit.

2.3 Problem Formulation and Optimal Solution

2.3.1 Maximizing Delivered Power

To maximize power transfer, we want to find the excitation current vector $\mathbf{i}$ that maximizes the total power delivered to the load given a maximum total transmit power P_T. As described in Section 2.2.2, $\mathbf{B}$ and $\mathbf{c}$ are treated as unknown channel parameters and estimated

directly using real-time measurements. For this section, we assume that these parameters are known and formulate a general optimization problem for the WPT system.

Formally, we state the WPT optimization problem as

$$\begin{aligned} \mathbf{i}_{opt} &= \arg\max_{\mathbf{i}} \ \mathbf{i}^H \mathbf{c}\mathbf{c}^H \mathbf{i}, \\ \text{subject to } & \ \mathbf{i}^H \left(\mathbf{c}\mathbf{c}^H + \mathbf{B}\right) \mathbf{i} \leq P_T. \end{aligned} \tag{2.14}$$

For convenience, we define the efficiency of the WPT system for a given excitation current vector $\mathbf{i}$ as

$$\eta(\mathbf{i}) \triangleq \frac{P_L(\mathbf{i})}{P_T(\mathbf{i})} \equiv \frac{\mathbf{i}^H \mathbf{c}\mathbf{c}^H \mathbf{i}}{\mathbf{i}^H \left(\mathbf{c}\mathbf{c}^H + \mathbf{B}\right) \mathbf{i}}. \tag{2.15}$$

The optimal solution to (2.14) is stated in the following theorem.

Theorem 2.3.1. *Assuming that* $\mathbf{B}$ *is non-singular, the optimal solution to the problem (2.14) is given by*

$$\mathbf{i}_{opt} = \ell \, \mathbf{B}^{-1} \mathbf{c}, \tag{2.16}$$

where ℓ *is a constant determined by the transmit power constraint. In addition, the maximum achievable transfer efficiency* $\eta(\mathbf{i}_{opt})$ *is always strictly less than 100%.*

Proof. The loss matrix $\mathbf{B}$ is assumed to be non-singular. If $\mathbf{B}$ is singular, it is possible to choose nonzero $\mathbf{i}$ that satisfies $\mathbf{B}\mathbf{i} = \mathbf{0}$. According to (2.8), such an excitation $\mathbf{i}$ produces zero losses and the resulting power transfer efficiency is unity. This means that it is possible to excite this system to achieve perfectly lossless power transfer which is physically unrealistic.

We now derive the optimal current excitation vector that maximizes the delivered power for given total available power P_T. Consider the Lagrangian of (2.14) with Lagrange multiplier $\lambda \in \mathbb{R}$,

$$\begin{aligned} J(\mathbf{i}, \lambda) &= \mathbf{i}^H \mathbf{c}\mathbf{c}^H \mathbf{i} - \lambda(\mathbf{i}^H \left(\mathbf{c}\mathbf{c}^H + \mathbf{B}\right) \mathbf{i} - P_T) \\ &= \mathbf{i}^H \left((1-\lambda)\mathbf{c}\mathbf{c}^H - \lambda \mathbf{B}\right) \mathbf{i} + \lambda P_T. \end{aligned}$$

Setting the partial derivatives of the Lagrangian to zero, we get the optimal solution:

$$\frac{\partial J}{\partial \mathbf{i}} = \mathbf{i}^H \left((1-\lambda)\mathbf{c}\mathbf{c}^H - \lambda \mathbf{B}\right) = 0, \tag{2.17}$$

$$\frac{\partial J}{\partial \lambda} = \mathbf{i}^H \left(\mathbf{c}\mathbf{c}^H + \mathbf{B}\right)\mathbf{i} - P_T = 0. \tag{2.18}$$

Simplifying (2.17), we get

$$\begin{aligned} & \mathbf{i}^H \left((1-\lambda)\mathbf{c}\mathbf{c}^H - \lambda \mathbf{B}\right) = 0. \\ \Rightarrow \quad & (1-\lambda)\mathbf{c}\mathbf{c}^H \mathbf{i} = \lambda \mathbf{B}\mathbf{i}. \end{aligned} \tag{2.19}$$

Equation (2.19) represents a generalized eigenvalue problem.

Under the assumption that $\mathbf{B}$ is non-singular, we can rewrite (2.19) as

$$\mathbf{B}^{-1}\mathbf{c} = \left(\frac{\lambda}{1-\lambda}\right)\left(\frac{1}{\mathbf{c}^H\mathbf{i}}\right)\mathbf{i}, \tag{2.20}$$

and hence, the optimizing vector $\mathbf{i}_{opt}$ is a scalar multiple of $\mathbf{B}^{-1}\mathbf{c}$,

$$\mathbf{i}_{opt} = \ell\, \mathbf{B}^{-1}\mathbf{c}, \tag{2.21}$$

where ℓ is a constant and can be computed using (2.18) as

$$\begin{aligned} \ell^2 \mathbf{c}^H \mathbf{B}^{-1}\left(\mathbf{c}\mathbf{c}^H + \mathbf{B}\right)\mathbf{B}^{-1}\mathbf{c} &\equiv \ell^2\left(\alpha^2 + \alpha\right) = P_T. \\ \Rightarrow \ell &= \sqrt{\frac{P_T}{\alpha(\alpha+1)}}. \end{aligned}$$

where $\alpha = \mathbf{c}^H\mathbf{B}^{-1}\mathbf{c} > 0$. Now, using (2.4) and (2.18), we get

$$\mathbf{i}^H \left(\mathbf{c}\mathbf{c}^H + \mathbf{B}\right)\mathbf{i} \equiv P_L(\mathbf{i}) + \mathbf{i}^H\mathbf{B}\mathbf{i} = P_T.$$

With $\mathbf{i} = \mathbf{i}_{opt}$,

$$\begin{aligned} P_T &= \bar{P}_L + P_T \frac{\mathbf{c}^H \mathbf{B}^{-1} \mathbf{B} \mathbf{B}^{-1} \mathbf{c}}{\alpha(\alpha+1)} \\ &= \bar{P}_L + P_T \frac{\alpha}{\alpha(\alpha+1)}. \\ \Rightarrow \ \frac{\bar{P}_L}{P_T} &= \frac{\alpha}{1+\alpha} \ < 1, \end{aligned}$$

where $\bar{P}_L$ denotes the maximum delivered load power (i.e., $\bar{P}_L = P_L(\mathbf{i}_{opt})$). □

2.3.2 Suboptimal Power Transfer based on Conjugate Beamforming

A suboptimal method is proposed to find an excitation current vector. When a large number of transmit coils are employed, calculation of optimal excitation vector, which involves both $\mathbf{B}$ and $\mathbf{c}$, becomes computationally intensive. This method reduces the complexity by computing the excitation current vector without knowledge of loss matrix $\mathbf{B}$. This scheme is inspired by the conjugate beamforming, a common precoding technique in multi-antenna wireless communication systems.

The optimization problem can be written as

$$\begin{aligned} \tilde{\mathbf{i}} &= \arg\max_{\mathbf{i}} \ \mathbf{i}^H \mathbf{c}\mathbf{c}^H \mathbf{i}, \\ &\text{subject to} \ \ \mathbf{i}^H \mathbf{i} \leq w. \end{aligned} \tag{2.22}$$

where $w > 0$. Note that the units of w are A^2 but not W.

The problem (2.22) is a well-known optimization problem on maximizing a quadratic form. The solution is given by

$$\tilde{\mathbf{i}} = \sqrt{\frac{w}{\mathbf{c}^H \mathbf{c}}}\, \mathbf{c}^*.$$

Therefore, the excitation current is chosen to be the complex conjugate of the current gain at each node. Since the total power consumption for an excitation current vector $\mathbf{i}$ is given by $\mathbf{i}^H \left(\mathbf{c}\mathbf{c}^H + \mathbf{B}\right) \mathbf{i}$, the current vector can be written as

$$\mathbf{i}_{conj} = \beta \, \tilde{\mathbf{i}}, \tag{2.23}$$

where β is an excitation gain given by

$$\beta = \sqrt{\frac{P_T}{\tilde{\mathbf{i}}^H \left(\mathbf{c}\mathbf{c}^H + \mathbf{B}\right) \tilde{\mathbf{i}}}}. \tag{2.24}$$

Note that the gain β is introduced to simply satisfy the maximum power constraint and it does not affect the overall power transfer efficiency for $\beta > 0$. Therefore, in practice, the gain can be determined empirically by real time measurement of transmit power $P_T(\mathbf{i})$ without computing (2.24).

2.4 Experimental Design

A series of experiments was designed and performed to (a) verify the model for real-world inductive systems, (b) show that the optimal solution can achieve significantly better performance than previously known methods, and (c) demonstrate the method's feasibility for estimating the model parameters from real-time measurements.

It is important to emphasize that the purpose of this experimental study is to test and validate the correctness of the abstract model, but not to demonstrate a practical charging application. This guided design choices some of which may otherwise seem counter-intuitive. For instance, we used a non-resonant power transfer system, which does not include a capacitor or additional resonant coils. A resonant WPT system would have allowed increased power levels delivered to the receiver as well as higher efficiency, but it would have resulted in a more complex system and less reliable measurements. Also, while this paper is focused on a MISO WPT system with a single receiver, the experimental setup includes two receivers to allow us to study the effect of parasitic inductances on the WPT system. Thus, we can treat one of the receivers as the intended charging device and the other receiver as

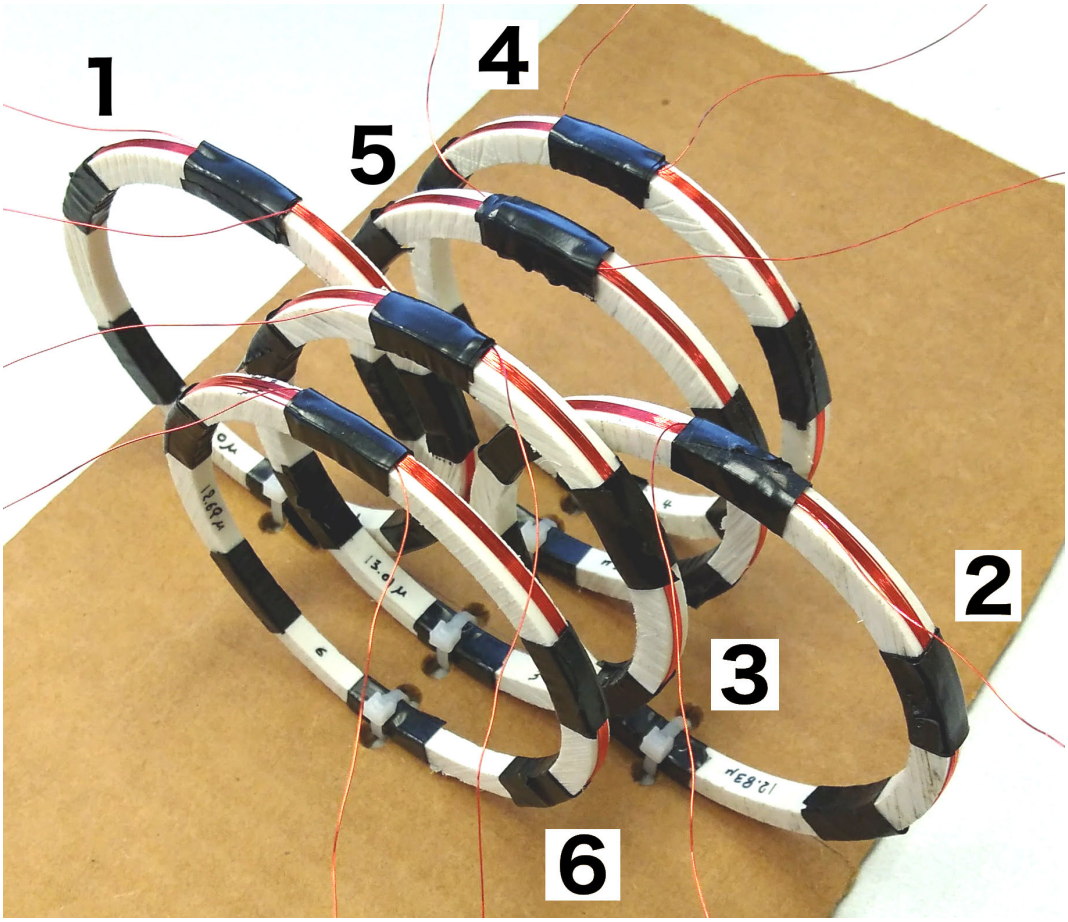

Figure 2.2. Experimental setup.

an undesired loss element. The results confirm the intuitive expectation that optimizing the power transfer to the desired receiver has the effect of reducing the power transferred to the undesired receiver.

Specific details are as follows. The setup consists of four transmitter coils, which can transfer power to any one of two receiver coils. All the coils are fixed to a cardboard base as shown in Fig. 2.2. Four coils including two transmitter coils and two receiver coils are located coaxially while the other two transmitter coils are on the same plane (co-planar coils).

The circuit schematics of the experimental setup and locations of the coils are shown in Fig. 2.3. The receiver coils are connected with loads $Z_L = 100\ \Omega$ at all times, and the transmitter coils are connected to a power source only when the coils are used for transmission. Otherwise, the transmitter coils are open. Note that no converter is used in

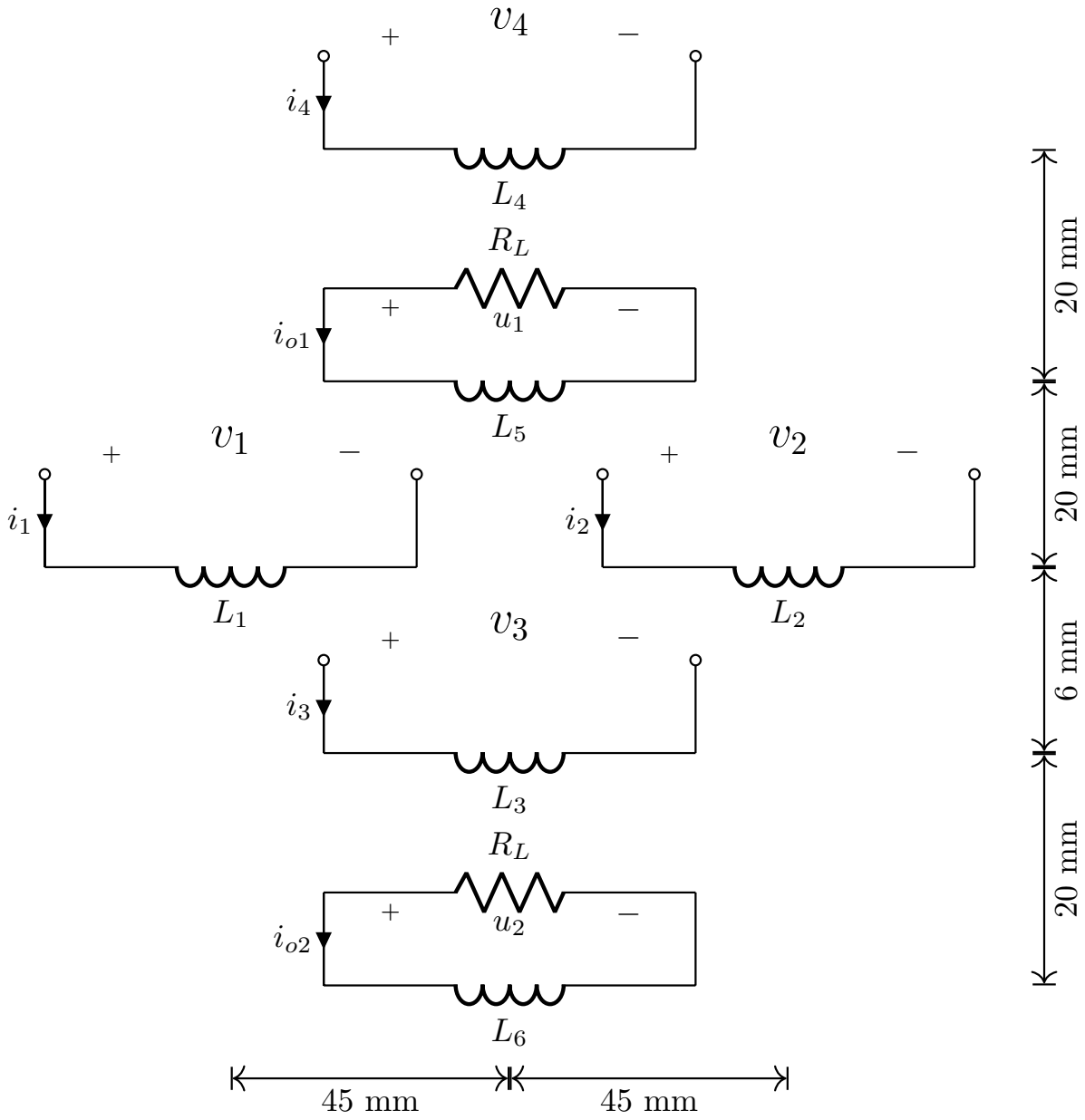

Figure 2.3. Circuit configuration of experimental setup. Dimensions indicate center-to-center distances of the coils.

this configuration. The coils have a 90 mm diameter, 2 mm coil length, and 7 turns. The inductance and resistance of the coils are listed in Table 2.1.

The interaction between two coils is represented by a coupling coefficient defined as

$$k_{ij} \triangleq \frac{M_{ij}}{\sqrt{L_i L_j}}, \tag{2.25}$$

Table 2.1. Inductance and resistance of coils.

i	L_i (μH)	R_i (Ω)	i	L_i (μH)	R_i (Ω)
1	13.2	0.892	4	12.8	0.938
2	12.8	0.888	5	12.9	0.885
3	13.0	0.940	6	12.7	0.897

Table 2.2. Coupling coefficient between coil i and j.

i	j	k_{ij}	i	j	k_{ij}	i	j	k_{ij}
1	2	0.06	2	3	0.11	3	5	0.19
1	3	0.10	2	4	0.04	3	6	0.12
1	4	0.05	2	5	0.08	4	5	0.22
1	5	0.08	2	6	0.07	4	6	0.05
1	6	0.07	3	4	0.09	5	6	0.09

where L_i and L_j are self inductances as shown in Fig. 2.3, and M_{ij} is the mutual inductance of the two coils [42]. The measured coupling coefficients are listed in Table 2.2.

The measurements are performed as follows. First, 200 kHz AC voltages (whose amplitude and phase can be arbitrarily controlled) are applied to one or more transmitter coils. The operating frequency is chosen to comply with Qi and PMA standards [20], [21]. The resulting voltages and currents on the transmit and receiver coils are measured. The voltages are directly measured using an oscilloscope, and the currents are measured by inserting current sensing resistors in series to the coils and measuring the resulting voltage drops. Note that the current flowing through a non-excited transmitter coil is zero since the circuit is open.

One transmitter coil's current is used as a common phase reference, and the remaining phasor voltages and currents are measured with respect to the phase reference. Similarly, the voltages and currents of all of the receiver coils are measured. Since the loads connected to the receiver coils are purely resistive and resistances are known, the current can be calculated from the voltage measurement and vice versa.

Table 2.3. Single coil excitation measurements.

Index	i_1 (mA)	i_2 (mA)	i_3 (mA)	i_4 (mA)	v_1 (mV)	v_2 (mV)	v_3 (mV)	v_4 (mV)	u_1 (mV)	u_2 (mV)
1	$33.2\angle 0°$	0	0	0	$550.2\angle -86.8°$	$32.9\angle 89.0°$	$51.9\angle -85.8°$	$24.9\angle -84.2°$	$39.2\angle -78.2°$	$36.2\angle -77.4°$
2	0	$33.1\angle 0°$	0	0	$33.2\angle 89.2°$	$543.4\angle -85.4°$	$60.1\angle -86.2°$	$23.4\angle -84.1°$	$40.0\angle -78.4°$	$37.6\angle -78.3°$
3	0	0	$32.9\angle 0°$	0	$55.6\angle -86.4°$	$60.0\angle -86.1°$	$551.4\angle -86.3°$	$45.5\angle -83.4°$	$92.0\angle -78.4°$	$118.3\angle -78.0°$
4	0	0	0	$33.2\angle 0°$	$28.3\angle -85.3°$	$27.4\angle -84.7°$	$45.7\angle -83.6°$	$549.5\angle -86.8°$	$118.74\angle -79.2°$	$26.5\angle -75.7°$

2.5 Results and Analysis

2.5.1 Overview of Experiment

We performed two sets of experiments. In the first set of experiments, each of the four transmitter coils is excited one at a time and the resulting voltages and currents of transmitter coils and receiver load are measured. In the second set of experiments, the transmitter coils are excited *two* at a time resulting in $\binom{4}{2} = 6$ sets of voltage and current measurements.

The single coil excitation measurements are used to measure the model parameters and analyze the efficiency of the WPT system, and the two coil excitation measurements are conducted for verification. The proposed solutions were compared with the equal power beamforming, which is the most widely used method in the literature on WPT systems with multiple transmitters in which the phase of the excitation current is chosen to be the negative of the phase of the current gain at each transmitter [43]. This ensures that the contributions from each transmitter to the total load current are aligned in phase and thus add up coherently at the receiver load.

2.5.2 Computation of Excitation Vectors

The measurement results when a single transmitter coil is excited are shown in Table 2.3. The pilot symbol q_{ij} in (2.10) corresponds to the current i_i of measurement index j. Since there are two receiver coils, we use $\mathbf{b}_0^{(1)}$ and $\mathbf{b}_0^{(2)}$ to denote the current gain vectors between the transmitter coil array and receiver coil 1 and 2, respectively, i.e.,

$$i_0^{(1)} = \mathbf{b}_0^{(1)H}\mathbf{i} \quad \text{and} \quad i_0^{(2)} = \mathbf{b}_0^{(2)H}\mathbf{i}, \tag{2.26}$$

Table 2.4. Two coil excitation measurements.

Index	i_1 (mA)	i_2 (mA)	i_3 (mA)	i_4 (mA)	v_1 (mV)	v_2 (mV)	v_3 (mV)	v_4 (mV)	u_1 (mV)	u_2 (mV)
5	32.9∠0°	33.2∠2.5°	0	0	525.6∠−85.1°	537.2∠−85.6°	119.4∠−85.0°	59.1∠−83.9°	88.4∠−77.5°	79.0∠−77.0°
6	32.5∠0°	0	32.6∠1.7°	0	601.5∠−85.0°	45.2∠−82.7°	604.0∠−85.6°	71.7∠−83.0°	134.9∠−77.3°	155.7∠−78.0°
7	32.7∠0°	0	0	32.8∠2.6°	577.9∠−85.6°	3.5∠−4.9°	99.6∠−83.8°	593.3∠−85.6°	160.9∠−78.3°	60.9∠−76.3°
8	0	31.4∠0°	32.6∠2.0°	0	28.2∠−81.0°	597.2∠−85.5°	616.5∠−85.5°	82.4∠−86.4°	138.8∠−77.4°	153.3∠−78.0°
9	0	32.5∠0°	0	32.8∠2.2°	4.0∠42.5°	594.6∠−85.4°	114.9∠−84.2°	600.9∠−86.0°	166.5∠−78.1°	68.9∠−76.3°
10	0	0	32.3∠0°	32.6∠1.0°	82.4∠−85.2°	86.2∠−85.5°	614.5∠−85.3°	599.1∠−86.5°	206.0∠−78.8°	156.3∠−77.9°

and calculate the transimpedance gain as

$$\mathbf{c}^{(1)} = \sqrt{\mathrm{Re}\left(Z_0^{(1)}\right)}\,\mathbf{b}_0^{(1)} \quad \text{and} \quad \mathbf{c}^{(2)} = \sqrt{\mathrm{Re}\left(Z_0^{(2)}\right)}\,\mathbf{b}_0^{(2)}, \tag{2.27}$$

where $Z_0^{(1)}$ and $Z_0^{(2)}$ are the load resistances in receiver coil 1 and 2, respectively.

The estimation procedure described in Section 2.2.2 with four measurements is used to measure the model parameters. The estimated transmitted power matrix is

$$\overline{\mathbf{A}} = \begin{bmatrix} 0.93\angle 0° & 0.02\angle 21.1° & 0.13\angle -30.4° & 0.10\angle -35.6° \\ 0.02\angle -21.1° & 1.31\angle 0° & 0.12\angle -1.8° & 0.10\angle -38.8° \\ 0.13\angle 30.4° & 0.12\angle 1.8° & 1.08\angle 0° & 0.16\angle 1.0° \\ 0.10\angle 35.6° & 0.10\angle 38.8° & 0.16\angle -1.0° & 0.92\angle 0° \end{bmatrix}$$

and the transimpedance vectors are

$$\mathbf{c}^{(1)} = \begin{bmatrix} 0.12\angle 78.2° \\ 0.12\angle 78.2° \\ 0.28\angle 78.4° \\ 0.36\angle 79.2° \end{bmatrix}, \quad \text{and} \quad \mathbf{c}^{(2)} = \begin{bmatrix} 0.11\angle 77.4° \\ 0.11\angle 78.4° \\ 0.36\angle 78.0° \\ 0.08\angle 75.7° \end{bmatrix}.$$

The optimal excitation vector for transferring power to coil 5 (receiver coil 1) in Fig. 2.3 is computed as

$$\mathbf{i}_{opt}^{(1)} = k_1 \Big[1\angle 0°; 0.6\angle -3.2°; 2.2\angle -26.3°; 4.0\angle -23.8°\Big]^T \text{(A)}.$$

The corresponding equal power and conjugate beamforming excitation vector are

$$\mathbf{i}_{eq}^{(1)} = k_2 \Big[1\angle 0°; 1\angle 0°; 1\angle 0.2°; 1\angle 1.0°\Big]^T \text{(A)},$$

and

$$\mathbf{i}_{conj}^{(1)} = k_3 \left[1.0\angle 0°; 1.0\angle 0°; 2.3\angle 0.2°; 3.0\angle 1.0°\right]^T \text{(A)},$$

respectively, where $k_1, k_2, k_3 > 0$ are determined based on the maximum available transmit power P_T.

Similarly, if we aim to deliver power to coil 6 (receiver coil 2), the optimal solution is given by

$$\mathbf{i}_{opt}^{(2)} = k_4 \left[1\angle 0°; 0.6\angle -10.4°; 3.4\angle -15.9°; 0.4\angle -35.9°\right]^T \text{(A)},$$

and the equal power ($\mathbf{i}_{eq}^{(2)}$) and conjugate beamforming ($\mathbf{i}_{conj}^{(2)}$) solution for receiver coil 2 are

$$\mathbf{i}_{eq}^{(2)} = k_5 \left[1\angle 0°; 1\angle 1.0°; 1\angle 0.6°; 1\angle -1.7°\right]^T \text{(A)},$$

and

$$\mathbf{i}_{conj}^{(2)} = k_6 \left[1.0\angle 0°; 1.0\angle 1.0°; 3.3\angle 0.6°; 0.7\angle -1.7°\right]^T \text{(A)},$$

where $k_4, k_5, k_6 > 0$ are determined based on P_T.

2.5.3 Comparison of Power Transfer Efficiencies

We first look at maximizing the power delivered to coil 5 (receiver coil 1). As a result of strong coupling between transmitter coils 3 and 4 to the receiver coil 1, the optimal solution $\mathbf{i}_{opt}^{(1)}$ is heavily weighted to these two coils. The maximum achievable efficiency is 19.1% which is significantly better than 14.1% efficiency obtained by using the well-known method of equal power beamforming and marginally better than 18.3% efficiency achieved by conjugate beamforming. The phase of the received voltage due to transmitter coils 1, 2, 3 and 4 are 22.5°, 18.2°, −3.2°, and −1.5°, respectively and it can be observed that this is different from the beamforming excitation. Note that the efficiency degradation due to the non-optimal phase excitation of the conjugate beamforming solution is small. Most of the efficiency improvement of the optimal solution as compared to equal power beamforming is due to the amplitude mismatch, i.e., the power transmitted by coils that are very weakly coupled to the receiver.

This observation highlights an important oversight in previous work. The beamforming solution seems intuitively reasonable following an analogy with beamforming used in multiple-antenna communications: coherent beamforming allows the individual induced currents from each transmitter to combine constructively at the intended receiver and therefore achieves the largest possible signal levels at the receiver *for a given set of signal levels at each transmitter*. Thus, beamforming is optimal in a certain sense. The flaw in this reasoning is that it neglects the effect of coherent excitation on power losses. While the received signal is enhanced by coherent beamforming, the overall power transfer efficiency may not increase proportionally depending on what it does to the power losses.

The above intuitive interpretation is supported by the experimental results. When we attempt to transmit power to receiver 1, receiver 2 acts as a parasitic loss element. The beamforming solutions are independent of the channels from the transmitters to receiver 2, and depend only on the channels to receiver 1. In contrast, the optimal solution fully incorporates all the relevant channel information. When we observe the amount of power transferred to the undesired receiver 2, we find that the optimal solution $\mathbf{i}_{opt}^{(1)}$ results in a power loss of 6.9% for receiver coil 2, which is smaller than the 8.9% power loss obtained by using equal power and conjugate beamforming. In other words, the optimal solution not only maximizes the power at receiver coil 1 but also minimizes the power delivered to parasitic receiver coil 2.

Now, we examine the case where the aim is maximizing power delivered to coil 6 (receiver coil 2). As a result of this strong coupling between transmitter coil 3 and receiver coil 2, the optimal solution is heavily weighted to transmitter coil 3. The maximum achievable efficiency is 13.4% which is significantly better than the 8.2% efficiency obtained by using the equal power beamforming and marginally better than the 12.6% efficiency achieved by conjugate beamforming. The phase of the received voltage due to transmitter coils 1, 2, 3 and 4 are 15.3°, 4.0°, −1.2°, −18.9°, respectively and is different from the beamforming excitation. Similar to the case of maximizing efficiency to receiver coil 1, the effect of amplitude mismatch between optimal and equal power beamforming excitation has a more pronounced effect on efficiency as compared to phase mismatch between optimal excitation and beamforming. Since most of the received power is due to coil 3, the conjugate beamforming solution, by

virtue of having roughly the same magnitude on transmitter coil 3 as that of the optimal excitation, suffers only a small efficiency degradation as compared to the optimal solution.

The optimal solution, $\mathbf{i}_{opt}^{(2)}$ results in loss of 9.9% to the undesired receiver coil 1 which is again the smallest as compared to the 14.1% loss obtained by using equal power and the 11.7% loss obtained by conjugate beamforming. Note that equal power beamforming solution, $\mathbf{i}_{eq}^{(2)}$ delivers more power to the parasitic receiver coil 1 instead of the desired receiver coil 2, which confirms the intuitive explanation of the sub-optimality of beamforming.

2.5.4 Verification of Results

Additional measurements were made in order to check the reliability of the estimated model parameters and efficiency calculations. Table 2.4 shows the phasor measurements which were obtained by simultaneously exciting two of the four transmitter coils. The measured efficiency is computed as the ratio of measured load power and measured input power. Using the measurements, the total input power (P_T) and the load power (P_L) can be calculated as

$$P_T = \sum_k \mathrm{Re}(v_k i_k^*) \quad \text{and} \quad P_L = \mathrm{Re}(v_0 i_0^*). \tag{2.28}$$

The measured efficiency is compared against the predicted efficiency, where the latter is computed by using the estimated model parameters to estimate the load and total input power for the given excitation current vectors using (2.4) and (2.7), respectively.

Figure 2.5 shows the measured and predicted efficiencies in receiver coil 2 for the measurements shown in Table 2.4. It can be observed that the predicted efficiency closely matches with the measured efficiency (the difference being less than 2%). Similarly, for receiver coil 1 with the measurements in Table 2.4, the predicted and measured efficiencies are shown in Fig. 2.4 and in this case too, the predicted efficiency matches the measured efficiency for most of the measurements (to within an error of 2%) expect one measurement (index 9), where the error is slightly higher at 4%. Hence, we conclude that the measurements are quite stable. We also observed that the measurements are highly repeatable.

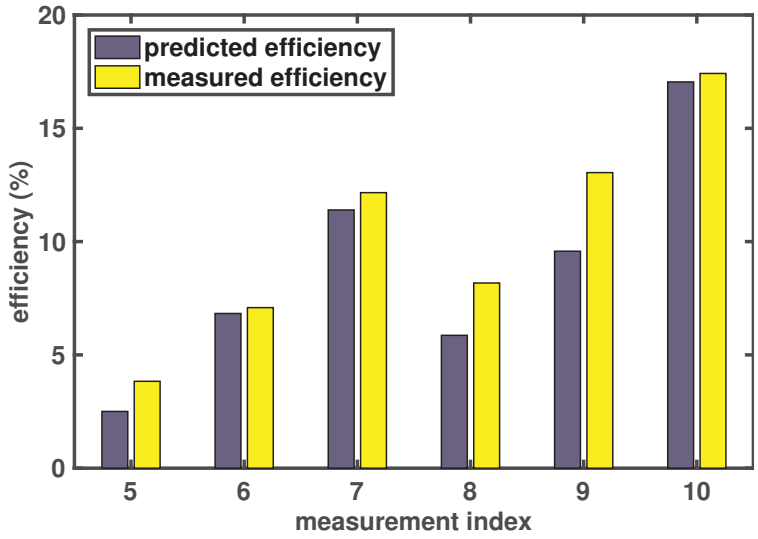

Figure 2.4. Predicted and measured efficiency for receiver coil 1 when two transmitter coils are simultaneously excited.

2.6 Conclusion

We presented a simple abstract approach to model a WPT system with multiple transmitter coils that seek to transfer power to a single receiver coil. We derived an expression for the optimal excitation current vector that maximizes the efficiency of power transfer, which is a function of the abstract model parameters. We presented a simple procedure to estimate these model parameters. We also presented experimental results with four transmitter coils and two receiver coils and showed that the optimal excitation vector has significant gains as compared to sub-optimal alternatives like equal power beamforming.

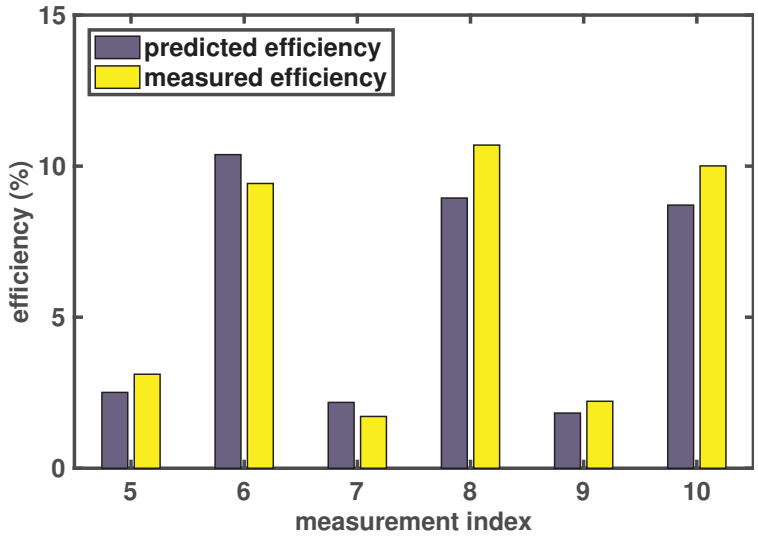

Figure 2.5. Predicted and measured efficiency for receiver coil 2 when two transmitter coils are simultaneously excited.

3. MIMO SIMULTANEOUS WIRELESS INFORMATION AND POWER TRANSFER OVER INDUCTIVELY COUPLED CIRCUITS

Reprinted from: T. Arakawa, J. V. Krogmeier, and D. J. Love, "MIMO simultaneous wireless information and power transfer over inductively coupled circuits," submitted for publication.

3.1 Introduction

There is an urgent need to develop new ways to power the increasing number of mobile devices. Ideally, any power transfer signal can also be used for data transfer, which is commonly referred to as SWIPT [1], [45]–[47]. Intuitively, since power transfer and data transfer are fundamentally the same phenomena, in the sense that they both involve transfer of energy from one device to the other, the data and power transfer should be jointly optimized. This technique is particularly attractive for applications such as RFID tags and IoT devices, which require both energy to drive circuits and a communication channel to transfer data [48].

In most deployment scenarios, SWIPT will suffer from low data rate and low energy transfer efficiency due to various losses and channel impairments [49]. One approach to overcoming these challenges is the use of multiple transmit and/or multiple receive elements coupled with MIMO system design. MIMO SWIPT has been extensively studied for radio frequency (RF)[1] scenarios as a natural extension of MIMO wireless communication systems. In [6], SWIPT for a RF MIMO model was investigated and the optimal transmit waveforms were derived. The wideband SWIPT over frequency selective RF channel was considered in [50]. A multiuser MISO beamforming for SWIPT model was discussed in [51].

Among numerous wireless transmission approaches, inductive WPT is an efficient short and medium distance wireless energy transmission technique [2], [52]–[54]. In contrast to wireless transmission over an RF channel, inductive WPT primarily uses a non-propagating magnetic field generated, which results in a significantly higher power transfer efficiency

[1]↑We use the term *RF* to describe a wireless transmission method in which a radiative electromagnetic wave is primarily used.

in short and middle distance scenarios [2]. In 2007, it was demonstrated that 60 W of power can be transferred over a distance of two meters with approximately 40 % power efficiency [4]. The properties of inductive WPT, including the efficiency, antenna design, and configurations, have been actively studied recently [39], [55]–[58]. Additionally, it has been shown that the power transfer efficiency can be increased by using multiple transmit coils [32]. Recently, a channel-estimation based optimization technique for a MISO inductive WPT system was proposed [10].

In this paper, a single-user MIMO SWIPT model using inductive coupling is considered. We refer to this model as MIMO inductively-coupled simultaneous wireless information and power transfer (IC-SWIPT). Inductive communication allows us to exploit the unique properties of near-field coupling, including negligible multipath effects and low absorption energy loss from water [59]–[62]. Because of these properties, inductive communication has been studied for RF challenging scenarios including underground and underwater communications [63], [64]. In this paper, however, we consider *both* communication and charging where inductively coupled coils offer robust communication channels and high power transfer efficiency. The rate-energy tradeoff over a frequency-selective inductively coupled channel was initially studied in [65]. In [66], MIMO SWIPT with a single information receiver and multiple power receivers was considered.

While inductive coupling suffers from somewhat different impairments than RF channels, an adaptation of the transmit waveform is an effective way to maintain the performance of IC-SWIPT. Since RF channels use radiative electromagnetic waves, the signal is largely affected by fading effects including signal reflection, refraction, multipath, and propagation delays. In contrast, the inductive channel is generated primarily from near-field coupling, which will be affected only minimally by the standard causes of wireless channel small-scale fading. Instead, the main impairment of the channel is primarily due to coil geometry (i.e., relative location and orientation of mutually coupled coils). To illustrate the effect of transmitter-receiver geometry on the channel, the gain of 2×1 inductive MIMO model for different receiver angle θ is shown in Fig. 3.1. By choosing the optimal amplitude and phase of the transmit signals, the power transfer efficiency can be improved and maintained even when the geometry changes.

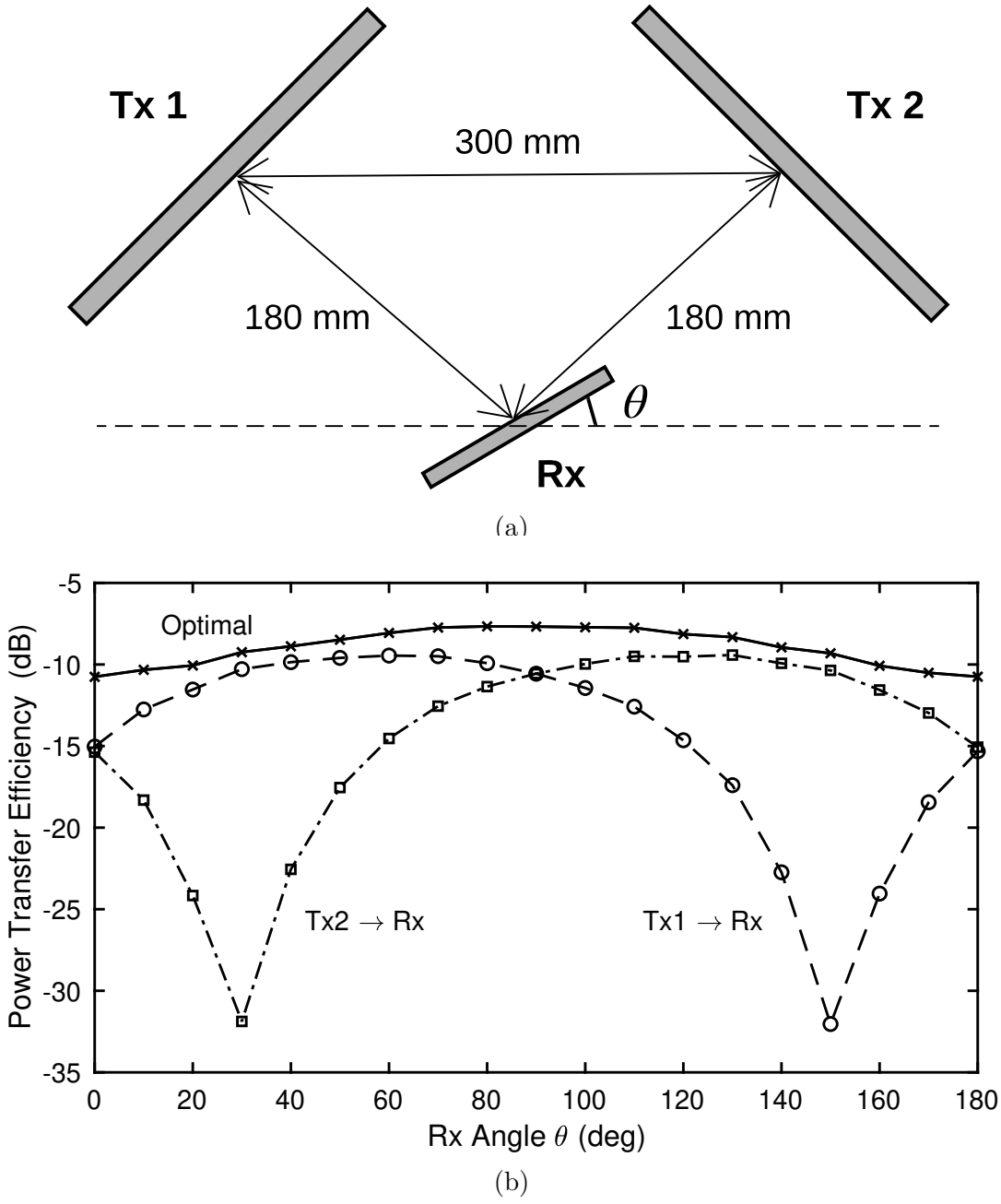

Figure 3.1. The 2×1 MISO system illustrated in (a) results in the efficiencies shown in (b) when the receiver is rotated from $\theta = 0°$ to 180°. The solid line in (b) represents the efficiency of the optimal waveform.

The main difficulty of analyzing IC-SWIPT is that WPT and wireless communication are usually analyzed by two distinct approaches. Traditionally, an inductive WPT system is studied using tools from circuit theory in which signals are represented by voltages and

currents, and the system is modeled with lumped circuit elements (e.g., [10], [40]). However, this approach quickly becomes intractable when a multi-coil system is considered. RF wireless communication, on the other hand, is represented by a linear communication model in which the system is given as the canonical multiplicative gain and additive noise model [67]. The wireless channel is treated as a "black box" and estimated by transmitting pilot symbols instead of directly solving a physical propagation model [41]. While this approach greatly reduces the complexity of the model and provides an intuitive representation of wireless communication system, it often fails to capture some important physical phenomena such as impedance mismatch and signal reflections, which need to be considered when analyzing inductively coupled circuits. Furthermore, most of the previous studies on inductive wireless communication have derived the characteristics of wireless channel (e.g., bit error rate and information capacity) *solely* based on the transmit and receive power [63], [64], [68]. While these works present the theoretical communication performance for a given system, they do not provide the input-output signal relationships, which makes it difficult to analyze and develop MIMO signal processing techniques such as beamforming[2].

To study IC-SWIPT, this paper proposes a new analysis framework by employing tools from microwave network theory. The properties of coupled circuits are represented by scattering parameters, which allow us to analyze inductively coupled circuits in the same manner as far-field transmission models. The circuit representation based on scattering parameters captures effects such as impedance mismatches, which have been overlooked in most signal processing-oriented work on SWIPT. We then show how the performance of IC-SWIPT is affected by different configurations of coupled coils using numerical analysis. The framework and results presented in this paper are readily applicable to various types of SWIPT models including far-field (microwave) SWIPT with standard RF antennas. The preliminary results of this method were presented in [7].

Specifically, the contributions of this paper are as follows:

1. To propose a framework to analyze an IC-SWIPT system using traveling waves and scattering parameters [69]. This notation allows us to describe the characteristics of

[2]↑When we use the term *beamforming*, we are referring to a rank-one transmit signal that is constructed by sending a common signal on each antenna/coil that is gain and/or phase shifted.

channels and the flow of signals while utilizing well-developed standard communication representations.

2. To provide analytical solutions for the optimal transmit covariance matrices for i) maximum information capacity, ii) maximum harvested power, and iii) maximum information capacity subject to a minimum harvested power.

3. To provide a simple, real-time estimation procedure to determine unknown scattering parameters and a noise covariance based on a *circuit sounding* technique. Unlike typical wireless communication channel estimation, we have to explicitly impose the constraint from the law of conservation of energy.

4. To show the average magnetic fields of two simple MIMO IC-SWIPT model for information transfer and power transfer cases based on FEM computations[70]. The corresponding rate-energy region is also provided using the results of FEM computations.

The following notations are used in this paper: for a matrix $\mathbf{A}$, $\mathrm{tr}(\mathbf{A})$, $\mathbf{A}^T$, $\mathbf{A}^H$, and $\det(\mathbf{A})$ indicate the trace, transpose, Hermitian conjugate, and determinant of the matrix $\mathbf{A}$, respectively. The conjugate of a complex number c is denoted by c^*.

The rest of the paper is organized as follows. Section 3.2 describes the proposed IC-SWIPT system model based on traveling waves and scattering parameters. Section 3.3 presents the optimization problems and their solutions for information transfer, power transfer, and SWIPT systems. A real-time estimation method to determine the scattering parameters is given in Section 3.4. In Section 3.5, the scattering parameters for two IC-SWIPT models are obtained by simulation, and the performances of the information transfer, power transfer, and SWIPT are analyzed by numerical analysis.

3.2 System Model

3.2.1 Abstract MIMO IC-SWIPT Model

Consider a single-user downlink MIMO IC-SWIPT system in which the transmitter and receiver are equipped with N_t and N_r coils, respectively, as shown in Fig. 3.2. In this paper,

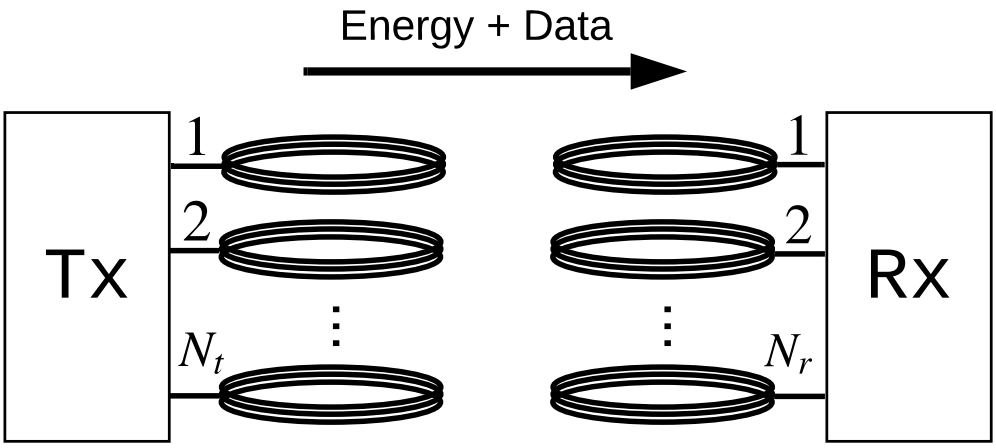

Figure 3.2. An illustration of a downlink MIMO IC-SWIPT system with N_t transmit coils and N_r receive coils.

we consider a co-located receiver model in which both of the information and energy are received by common coils.

Instead of directly solving the circuit system, we translate the model to an *abstract circuit model* in which the interconnections are treated as a "black box" as shown in Fig. 3.3. The interconnection captures the circuit elements and effects between the transmitter and receiver, including impedance matching circuits, coil shapes, mutual inductance, and parasitic losses of the coils. We only assume that the interconnection is linear[3] and make no further assumptions. The transmitter is modeled with N_t voltage sources, each with source impedance $R_s > 0$. The receiver is connected to the information decoding (ID) and energy harvesting (EH) receivers (denoted by R_{ID} and R_{EH}, respectively) via power dividers. This receiver structure is referred to as *power splitting*. To illustrate the flow of the signals, an equivalent block diagram is shown in Fig. 3.4.

Each signal is represented by a *traveling wave*, which is defined as a function of voltage, current, and a reference impedance [69]. The traveling waves $a_{T,i}$ and $b_{T,i}$, where $i = 1, \ldots, N_t$, are defined as a linear transformation of voltage and current expressed as

$$\begin{bmatrix} a_{T,i} \\ b_{T,i} \end{bmatrix} = \frac{1}{\sqrt{R_{\text{ref}}}} \begin{bmatrix} 1 & R_{\text{ref}} \\ 1 & -R_{\text{ref}} \end{bmatrix} \begin{bmatrix} V_{T,i} \\ I_{T,i} \end{bmatrix} \tag{3.1}$$

[3]↑The linearity assumption of inductively coupled coils has been experimentally verified in [10].

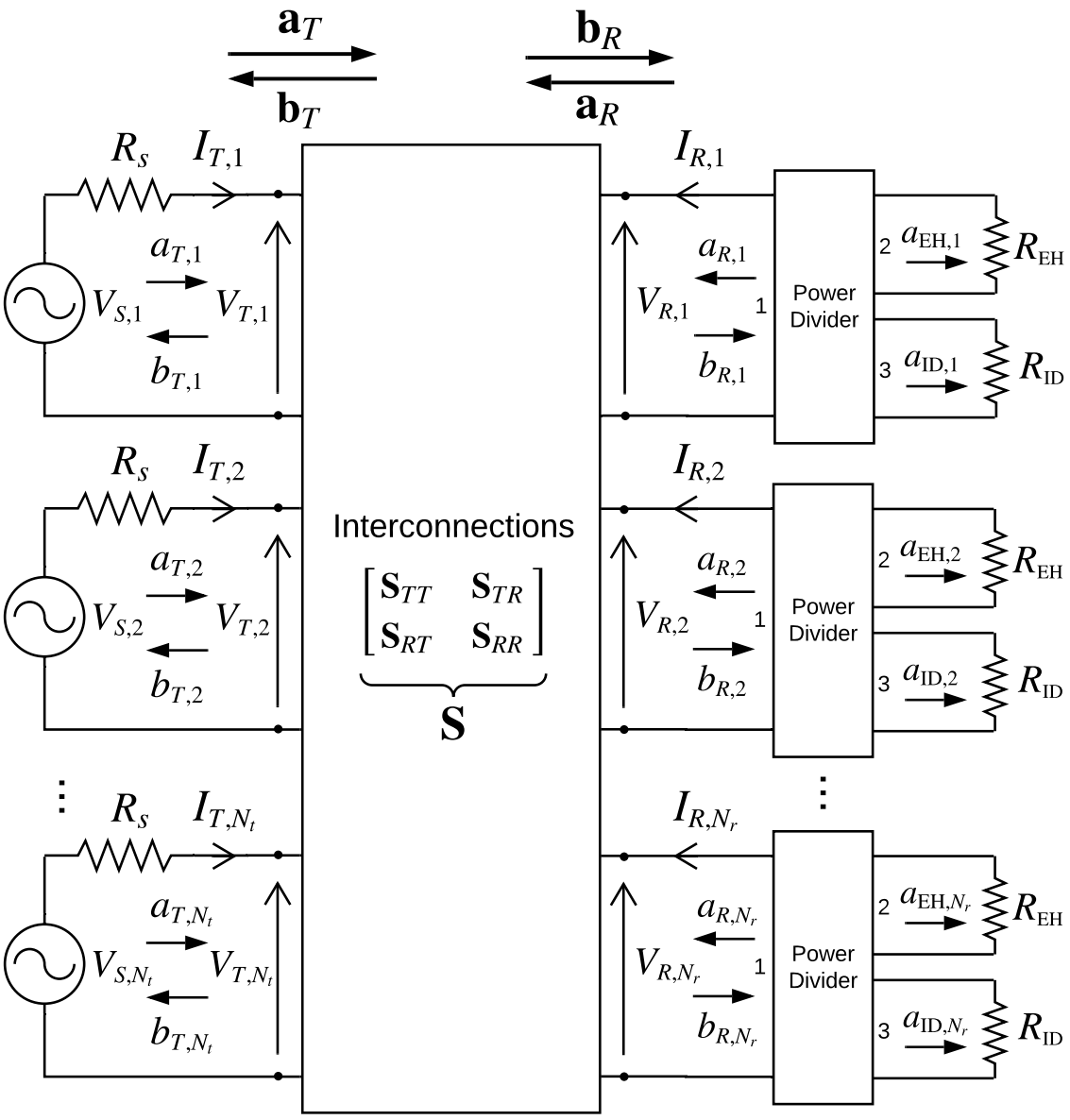

Figure 3.3. An abstract circuit model of IC-SWIPT system with a power-splitting receiver. The interconnections is represented by the scattering matrix $\mathbf{S}$.

where $V_{T,i}$ and $I_{T,i}$ are root mean square (RMS) values of the voltages and currents, and R_{ref} is a reference impedance. For simplicity, we assume $R_{\text{ref}} = R_s$ in this paper. The traveling waves $a_{R,i}$ and $b_{R,i}$, where $i = 1, \ldots, N_r$, are defined using $V_{R,i}$ and $I_{R,i}$ in the same manner. The representation based on traveling waves allows us to directly relate them to the "signals" commonly used in linear communication models [71]. The power of a_i and b_i

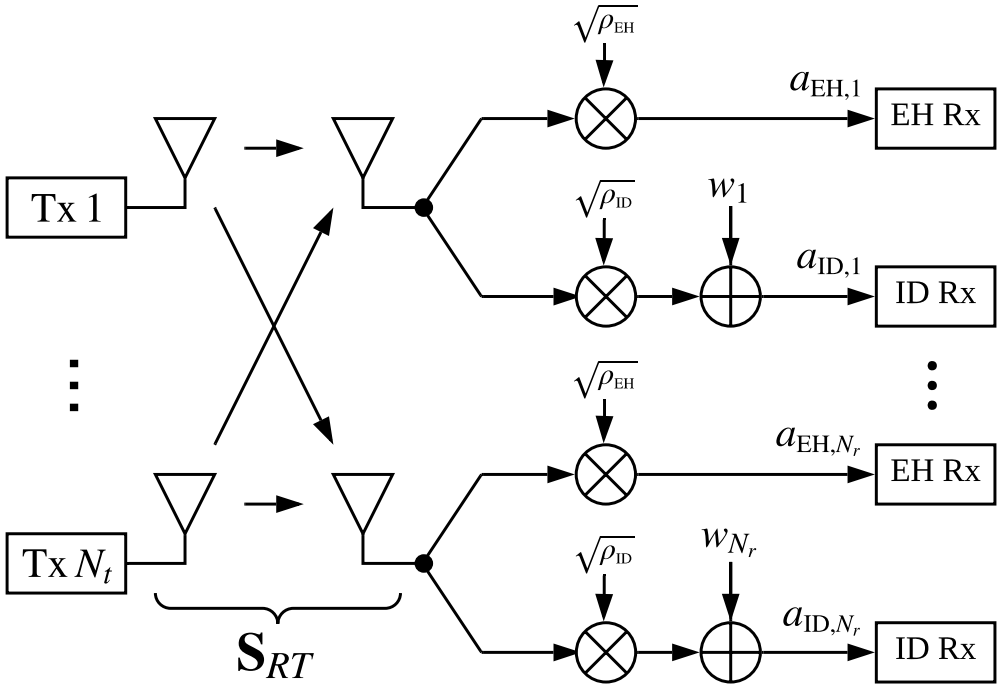

Figure 3.4. Block diagram of IC-SWIPT.

are given by $|a_i|^2$ and $|b_i|^2$, respectively [69]. The network's response to an external incident wave is described by a *scattering parameter*, defined as a ratio of incoming waves to the outgoing waves.

We describe a MIMO system as a vector-input vector-output two-port network. A similar formulation was used in [72] to analyze an RF coupled antenna array, which we extend to an inductively coupled circuit. The traveling waves $\mathbf{a}_T \in \mathbb{C}^{N_t \times 1}$, $\mathbf{b}_T \in \mathbb{C}^{N_t \times 1}$, $\mathbf{a}_R \in \mathbb{C}^{N_r \times 1}$, and $\mathbf{b}_R \in \mathbb{C}^{N_r \times 1}$ are defined in a vector form as

$$\begin{aligned} \mathbf{a}_T &= [a_{T,1} \cdots a_{T,N_t}]^T, \quad \mathbf{b}_T = [b_{T,1} \cdots b_{T,N_r}]^T, \\ \mathbf{a}_R &= [a_{R,1} \cdots a_{R,N_t}]^T, \quad \mathbf{b}_R = [b_{R,1} \cdots b_{R,N_r}]^T, \end{aligned} \tag{3.2}$$

respectively. The responses to the incident waves are described by the scattering matrices $\mathbf{S}_{TT} \in \mathbb{C}^{N_t \times N_t}$, $\mathbf{S}_{TR} \in \mathbb{C}^{N_t \times N_r}$, $\mathbf{S}_{RT} \in \mathbb{C}^{N_r \times N_t}$, and $\mathbf{S}_{RR} \in \mathbb{C}^{N_r \times N_r}$. Using the power waves defined in (3.2), the full network's input-output model is

$$\begin{bmatrix} \mathbf{b}_T \\ \mathbf{b}_R \end{bmatrix} = \underbrace{\begin{bmatrix} \mathbf{S}_{TT} & \mathbf{S}_{TR} \\ \mathbf{S}_{RT} & \mathbf{S}_{RR} \end{bmatrix}}_{\mathbf{S}} \begin{bmatrix} \mathbf{a}_T \\ \mathbf{a}_R \end{bmatrix}. \tag{3.3}$$

For ease of notation, we define $\mathbf{S}$ as shown in (3.3).

The power dividers shown in Fig. 3.3 are three-port passive networks which divide the received signal into two signal streams. We assume that the all ports of the divider are matched and the loads R_{EH} and R_{ID} are also matched to the output of the ports ($R_{\text{ref}} = Z_L$). This assumption allows us to eliminate the signal reflections at the divider and loads to zero. The power splitting ratios are denoted by $\rho_{\text{EH}} = P_{\text{EH}}/P_r > 0$ and $\rho_{\text{ID}} = P_{\text{ID}}/P_r > 0$, where P_r, P_{EH}, and P_{ID} are the total power admitted to the divider, the power harvested by EH receiver, and the power received by ID receiver, respectively.

3.2.2 Information Transfer Model

The data symbols transmitted from the N_t transmit coils are received by the ID receiver via N_r receive coils. The received signal at the ID receiver $\mathbf{y}_R \in \mathbb{C}^{N_r \times 1}$ is

$$\mathbf{y}_R = \sqrt{\rho_{\text{ID}}}\mathbf{S}_{RT}\mathbf{a}_T + \mathbf{w}_R, \tag{3.4}$$

where $\mathbf{w}_R = [w_1, \ldots, w_{N_r}]^T \sim \mathcal{CN}(\mathbf{0}, \mathbf{K}_w)$ is zero-mean complex Gaussian noise with covariance matrix $\mathbf{K}_w$. Note that mutual coupling between antennas (coils) results in correlated noise at the receiver in general [73], [74]. While most of the previous studies on inductive WPT have ignored the effects of noise, an additive noise term is explicitly given in (3.4) since the analysis of information transfer requires the noise model. A detailed analysis of correlated noise resulting from a passive network is given in [75].

By rewriting $\mathbf{H} \triangleq \sqrt{\rho_{\text{ID}}}\mathbf{S}_{RT}$ and $\mathbf{x} \triangleq \mathbf{a}_T$, we can represent the transmission from the transmit coils to the ID receivers as

$$\mathbf{y}_R = \mathbf{H}\mathbf{x} + \mathbf{w}_R, \tag{3.5}$$

where $\mathbf{x} \in \mathbb{C}^{N_t \times 1}$ is the transmit signal and $\mathbf{H} \in \mathbb{C}^{N_r \times N_t}$ is the effective communication channel. The transmit signal $\mathbf{x}$ is zero-mean complex Gaussian with covariance matrix $\mathbf{Q}_x = \mathbb{E}[\mathbf{x}\mathbf{x}^H]$ with $\mathbb{E}[\cdot]$ denoting the expected value. The maximum achievable rate given an input covariance $\mathbf{Q}_x$ (i.e., which some might call the capacity for a fixed input covariance) is [67]

$$C = \log_2 \det\left(\mathbf{I} + \mathbf{K}_w^{-1}\mathbf{H}\mathbf{Q}_x\mathbf{H}^H\right). \tag{3.6}$$

The capacity expression in (3.6) is highly dependent on the channel matrix $\mathbf{H}$. The structure of $\mathbf{H}$ can be extremely complicated, especially when combined with an optimization over $\mathbf{Q}_x$.

3.2.3 Power Transfer Model

The transmit power and the harvested power are represented as functions of the scattering parameters and the transmit covariance matrix. Using (3.3), the reflected signal to the transmitter is represented by

$$\mathbf{b}_T = \mathbf{S}_{TT}\mathbf{a}_T + \mathbf{w}_T. \tag{3.7}$$

where $\mathbf{w}_T \sim \mathcal{CN}(\mathbf{0}, \mathbf{K}_t)$. For the calculation of power transfer, the magnitude of the additive noise is assumed to be negligible. The total instantaneous generated power is

$$\begin{aligned} P_G &= \|\mathbf{a}_T\|^2 - \|\mathbf{b}_T\|^2 \\ &= \|\mathbf{a}_T\|^2 - \|\mathbf{S}_{TT}\mathbf{a}_T\|^2 \\ &= \mathbf{a}_T^H\left(\mathbf{I} - \mathbf{S}_{TT}^H\mathbf{S}_{TT}\right)\mathbf{a}_T \\ &= \mathbf{a}_T^H\mathbf{A}\mathbf{a}_T, \end{aligned} \tag{3.8}$$

where $\mathbf{A} \triangleq \mathbf{I} - \mathbf{S}_{TT}^H \mathbf{S}_{TT}$ and $\|\cdot\|$ indicates the two-norm. Note that $\mathbf{A}$ is positive-definite since the law of conservation of energy and non-zero coupling coefficients require $\|\mathbf{a}_T\|^2 > \|\mathbf{S}_{TT}\mathbf{a}_T\|^2$ for any $\mathbf{a}_T$. The average generated power is

$$\bar{P}_G = \mathbb{E}[\mathbf{a}_T^H \mathbf{A} \mathbf{a}_T] = \mathrm{tr}(\mathbf{Q}_x \mathbf{A}). \tag{3.9}$$

It is worth noting that if the network $\mathbf{S}$ is matched to the sources (i.e., all entries of $\mathbf{S}_{TT}$ are zero), we get $\mathbf{A} = \mathbf{I}$. The average generated power (3.9) simplifies to $\bar{P}_G = \mathrm{tr}(\mathbf{Q})$, which aligns with the standard definition of transmit power of RF communication models.

The total instantaneous harvested power is given by

$$\begin{aligned} P_{\text{EH}} &= \rho_{\text{EH}} \|\mathbf{b}_R\|^2 \\ &= \rho_{\text{EH}} \|\mathbf{S}_{RT}\mathbf{a}_T\|^2 \\ &= \rho_{\text{EH}}\, \mathbf{a}_T^H \mathbf{S}_{RT}^H \mathbf{S}_{RT} \mathbf{a}_T \\ &= \mathbf{a}_T^H \mathbf{G}^H \mathbf{G} \mathbf{a}_T, \end{aligned} \tag{3.10}$$

where $\mathbf{G} \triangleq \sqrt{\rho_{\text{EH}}}\mathbf{S}_{RT}$. The average harvested power is

$$\bar{P}_{\text{EH}} = \mathbb{E}\left[\|\mathbf{G}\mathbf{x}\|^2\right] = \mathrm{tr}(\mathbf{G}\mathbf{Q}_x\mathbf{G}^H). \tag{3.11}$$

Therefore, the harvested power is fully characterized by the channel $\mathbf{G}$ and the transmit covariance matrix $\mathbf{Q}_x$. Note that the result (3.11) is equally valid for non-Gaussian transmit signals (e.g., a single frequency sinusoidal signal).

3.3 Simultaneous Wireless Information and Power Transfer

In this section, we consider optimizing the transmit covariance matrix $\mathbf{Q}_x$ for each of three objectives, namely, i) maximizing the information capacity, ii) maximizing the harvested power, and iii) maximizing the capacity subject to a minimum harvested power constraint. For all the optimization problems, we assume a total average transmit power of P_T (W).

First, we find the transmit covariance matrix $\mathbf{Q}_{x,opt}^{(\mathrm{WIT})}$ that maximizes the information capacity of the MIMO IC-SWIPT link. The optimization problem is

Max Capacity Waveform

$$\begin{aligned} \arg\max_{\mathbf{Q}_x} \quad & \log_2 \det\left(\mathbf{I} + \mathbf{K}_w^{-1}\mathbf{H}\mathbf{Q}_x\mathbf{H}^H\right), && \text{(P1-1)} \\ \text{subject to} \quad & \mathrm{tr}(\mathbf{Q}_x\mathbf{A}) \leq P_T, && (3.12) \\ & \mathbf{Q}_x \succeq 0, && (3.13) \end{aligned}$$

where (3.12) represents the total average generated power constraint and (3.13) indicates that $\mathbf{Q}_x$ is positive semidefinite.

The problem (P1-1) can be equivalently written as

$$\begin{aligned} \arg\max_{\tilde{\mathbf{Q}}_x} \quad & \log_2 \det\left(\mathbf{I} + \tilde{\mathbf{H}}\tilde{\mathbf{Q}}_x\tilde{\mathbf{H}}^H\right), && \text{(P1-2)} \\ \text{subject to} \quad & \mathrm{tr}(\tilde{\mathbf{Q}}_x) \leq P_T, && (3.14) \\ & \tilde{\mathbf{Q}}_x \succeq 0, && (3.15) \end{aligned}$$

where $\tilde{\mathbf{H}} \triangleq \mathbf{K}_w^{-1/2}\mathbf{H}\mathbf{U}_A\mathbf{D}_A^{-1/2}$, $\tilde{\mathbf{Q}}_x \triangleq \mathbf{D}_A^{1/2}\mathbf{U}_A^H\mathbf{Q}_x\mathbf{U}_A\mathbf{D}_A^{1/2}$ and $\mathbf{A} = \mathbf{U}_A\mathbf{D}_A\mathbf{U}_A^H$ is the eigenvalue decomposition of the positive-definite matrix $\mathbf{A}$ [71]. The solution to (P1-2) is given by the waterfilling algorithm and therefore omitted for brevity [76]. The optimal solution to (P1-1) is $\mathbf{Q}_{x,opt}^{(\mathrm{WIT})} = \mathbf{U}_A\mathbf{D}_A^{-1/2}\tilde{\mathbf{Q}}_x^*\mathbf{D}_A^{-1/2}\mathbf{U}_A^H$, where $\tilde{\mathbf{Q}}_x^*$ is the solution to (P1-2).

Secondly, we consider finding the transmit covariance matrix $\mathbf{Q}_{x,opt}^{(\mathrm{WPT})}$ that maximizes the total harvested power. The optimization problem is

Max Harvested Power Waveform

$$\begin{aligned} \arg\max_{\mathbf{Q}_x} \quad & \mathrm{tr}(\mathbf{G}\mathbf{Q}_x\mathbf{G}^H) && \text{(P2-1)} \\ \text{subject to} \quad & \mathrm{tr}(\mathbf{Q}_x\mathbf{A}) \leq P_T, \\ & \mathbf{Q}_x \succeq 0. \end{aligned}$$

The problem (P2-1) can be equivalently written as

$$\begin{aligned} \arg\max_{\tilde{\mathbf{Q}}_x} \quad & \mathrm{tr}\left(\tilde{\mathbf{G}}\tilde{\mathbf{Q}}_x\tilde{\mathbf{G}}^H\right) \\ \text{subject to} \quad & \mathrm{tr}(\tilde{\mathbf{Q}}_x) \le P_T, \\ & \tilde{\mathbf{Q}}_x \succeq 0, \end{aligned} \tag{P2-2}$$

where $\tilde{\mathbf{G}} \triangleq \mathbf{G}\mathbf{U}_A\mathbf{D}_A^{-1/2}$. The solution to (P2-2) is given by $\tilde{\mathbf{Q}}_x = P_T\mathbf{v}\mathbf{v}^H$ where $\tilde{\mathbf{G}} = \mathbf{U}_{\tilde{G}}\mathbf{D}_{\tilde{G}}\mathbf{V}_{\tilde{G}}^H$ is the singular value decomposition (SVD) of $\tilde{\mathbf{G}}$, and $\mathbf{v}$ is the column of $\mathbf{V}_{\tilde{G}}$ which corresponds to the largest singular value [6]. The optimal solution to (P2-1) is given by $\mathbf{Q}_{x,opt}^{(\mathrm{WPT})} = P_T\mathbf{f}\mathbf{f}^H$, where $\mathbf{f} = \mathbf{U}_A\mathbf{D}_A^{-1/2}\mathbf{v}$.

This result shows that the harvested power is maximized by generating a common signal (e.g., a tone) and setting the gain and phase of the i-th transmitter's incident wave by $\sqrt{P_T}f_i$, where f_i is the i-th entry of $\mathbf{f}$. From a signal processing point of view, this solution can also be seen as beamforming.

Lastly, we consider finding the transmit covariance matrix $\mathbf{Q}_{x,opt}^{(\mathrm{SWIPT})}$ that maximizes the capacity subject to the minimum harvested power constraint. The optimization problem is

Max Capacity s.t. Min Harvested Power Waveform

$$\begin{aligned} \arg\max_{\mathbf{Q}_x} \quad & \log_2\det\left(\mathbf{I} + \mathbf{K}_w^{-1}\mathbf{H}\mathbf{Q}_x\mathbf{H}^H\right) && \text{(P3-1)} \\ \text{subject to} \quad & \mathrm{tr}(\mathbf{G}\mathbf{Q}_x\mathbf{G}^H) \ge P_{min}, && (3.16) \\ & \mathrm{tr}(\mathbf{Q}_x\mathbf{A}) \le P_T, && (3.17) \\ & \mathbf{Q}_x \succeq 0, && (3.18) \end{aligned}$$

where (3.16) is the minimum harvested power constraint. The problem (P3-1) is then equivalently written as

$$\begin{aligned} \underset{\tilde{\mathbf{Q}}_x}{\arg\max} \quad & \log_2 \det\left(\mathbf{I} + \tilde{\mathbf{H}}\tilde{\mathbf{Q}}_x\tilde{\mathbf{H}}^H\right), && \text{(P3-2)} \\ \text{subject to} \quad & \operatorname{tr}\left(\tilde{\mathbf{G}}\tilde{\mathbf{Q}}_x\tilde{\mathbf{G}}^H\right) \geq P_{min}, && (3.19) \\ & \operatorname{tr}(\tilde{\mathbf{Q}}_x) \leq P_T, && (3.20) \\ & \tilde{\mathbf{Q}}_x \succeq 0. && (3.21) \end{aligned}$$

The solution to (P3-2) is given in [6] and omitted for brevity. The solution to (P3-1) is given by $\mathbf{Q}_{x,opt}^{(\text{SWIPT})} = \mathbf{U}_A\mathbf{D}_A^{-1/2}\tilde{\mathbf{Q}}_x^*\mathbf{D}_A^{-1/2}\mathbf{U}_A^H$, where $\tilde{\mathbf{Q}}_x^*$ is the solution to (P3-2).

The performance of SWIPT is characterized by the rate-energy (R-E) region. The region for the total available generated power P_T is defined as

$$\begin{aligned} C_{\text{R-E}}(P_T) = &\{(R,P) : R \leq \log_2 \det\left(\mathbf{I} + \mathbf{K}_w^{-1}\mathbf{H}\mathbf{Q}_x\mathbf{H}^H\right), \\ & P \leq \operatorname{tr}(\mathbf{G}\mathbf{Q}_x\mathbf{G}^H), \operatorname{tr}(\mathbf{Q}_x\mathbf{A}) \leq P_T, \mathbf{Q}_x \succeq 0\}. \end{aligned}$$

The difference from the R-E region defined in [6] is that the parameters $\mathbf{K}_w$ and $\mathbf{A}$ are explicitly given in order to capture the correlated noise and signal reflections, respectively. In general, the maximum harvested power is linearly proportional to ρ_{EH}, while the capacity is proportional to $\log(\rho_{\text{ID}})$ in the high SNR regime.

3.4 Estimating S-Parameters and Noise Distribution

The knowledge of scattering parameters and the distribution of received noise is required to compute the optimal transmit covariance as discussed in Section 3.3. Since the scattering parameters may vary when the location of coils or the surrounding environment changes, the system needs to adapt to the channel in real-time. While it is a common practice in nearly all modern communication systems to obtain receive-side channel knowledge by having the transmitter send a known pilot sequence, the scattering parameter of an unknown network is often measured directly using a device such as a vector network analyzer (VNA) [69].

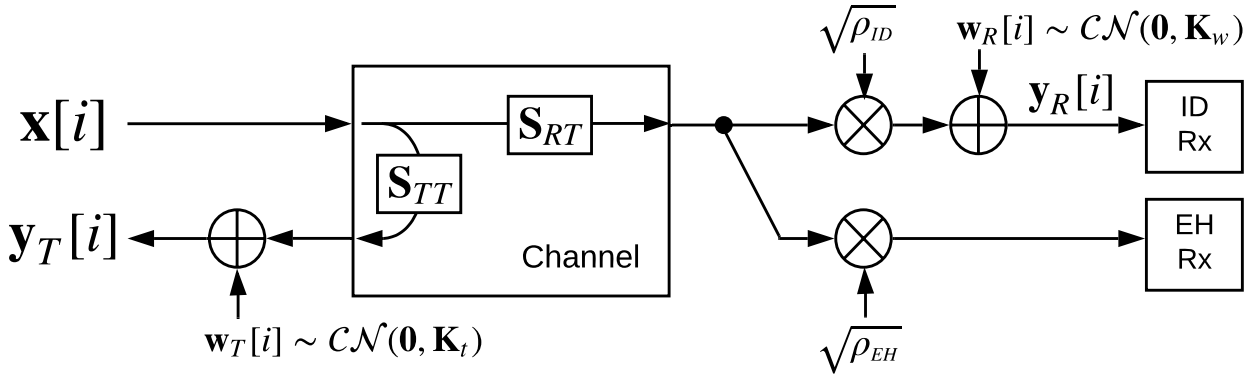

Figure 3.5. Block diagram of IC-SWIPT model. $\mathbf{S}_{TT}$, $\mathbf{S}_{RT}$, and $\mathbf{K}_w$ are estimated by received $\mathbf{y}_T[i]$ and $\mathbf{y}_R[i]$.

We propose a simple procedure to estimate the unknown scattering parameters and noise covariance matrix based on channel sounding. This approach is inspired by the RF channel estimation [41] and the real-time circuit sounding technique proposed for WPT systems in [10]. The parameters required to compute the optimal transmit waveforms are $\mathbf{S}_{TT}$, $\mathbf{S}_{RT}$, and $\mathbf{K}_w$. The scattering matrix $\mathbf{S}_{TT}$ is estimated at the transmitter by observing the reflected signal, and $\mathbf{S}_{RT}$ and $\mathbf{K}_w$ are estimated at the ID receiver by observing the transmitted signal as shown in Fig. 3.5.

We incorporate the knowledge that the law of conservation of energy requires that the sum of power delivered to the receiver and reflected to the transmitter must be less than the generated power, i.e., $\|\mathbf{S}_{TT}\|^2 + \|\mathbf{S}_{RT}\|^2 \leq 1$. This constraint is physically valid since the channels are defined based on scattering parameters. However, the constraint requires a joint estimation of $\mathbf{S}_{TT}$ and $\mathbf{S}_{RT}$, which is not practical for a system in which the channels are estimated in a distributed manner. Therefore, we relax the constraint to $\|\mathbf{S}_{TT}\|^2 \leq 1$ and $\|\mathbf{S}_{RT}\|^2 \leq 1$. This constraint is usually ignored in the standard channel estimation problems since the gain of an RF channel is very small and the constraint is almost always satisfied.

At the ID receiver, both the channel $\mathbf{S}_{RT}$ and the noise covariance matrix $\mathbf{K}_w$ need to be estimated. We assume a sequence of pilot symbols $\mathbf{x}[1], \mathbf{x}[2], \ldots, \mathbf{x}[M] \in \mathbb{C}^{N_t \times 1}$, known by both transmitter and receiver, is transmitted. Using the communication channel defined

in (3.5), when the i-th pilot symbol $\mathbf{x}[i]$ is transmitted, the received symbol at the ID receiver is

$$\mathbf{y}_R[i] = \mathbf{H}\mathbf{x}[i] + \mathbf{w}_R[i], \tag{3.22}$$

where $\mathbf{w}_R[i]$ is the noise with $\mathbf{w}_R[i] \sim \mathcal{CN}(\mathbf{0}, \mathbf{K}_w)$. The received pilot sequence can be written in a vector form as

$$\mathbf{y}_{\text{vec}} = \mathbf{V}\mathbf{h}_{\text{vec}} + \mathbf{w}_{\text{vec}},$$

where $\mathbf{y}_{\text{vec}} = \text{vec}\left(\mathbf{y}_R[i], \ldots, \mathbf{y}_R[M]\right)$, $\mathbf{h}_{\text{vec}} = \text{vec}(\mathbf{H})$, $\mathbf{w}_{\text{vec}} = \text{vec}(\mathbf{w}_R[1], \ldots, \mathbf{w}_R[M])$, and $\mathbf{V} = \mathbf{X}^T \otimes \mathbf{I}$ with $\mathbf{X} = [\mathbf{x}[i], \ldots, \mathbf{x}[M]] \in \mathbb{C}^{N_t \times M}$. The operator $\otimes$ indicates the Kronecker product and $\text{vec}(\cdot)$ is the vectorization operator.

We consider maximum likelihood (ML) estimation of $\mathbf{S}_{RT}$ and $\mathbf{K}_w$ with the constraint of the law of conservation of energy. A scaled version of the log-likelihood function is

$$\begin{aligned} L\left(\mathbf{y}_{\text{vec}} \middle| \mathbf{h}_{\text{vec}}, \mathbf{K}_w\right) = \\ &- (\mathbf{y}_{\text{vec}} - \mathbf{V}\mathbf{h}_{\text{vec}})^H (\mathbf{I} \otimes \mathbf{K}_w)^{-1} (\mathbf{y}_{\text{vec}} - \mathbf{V}\mathbf{h}_{\text{vec}}) \\ &- \ln(\det(\mathbf{I} \otimes \mathbf{K}_w)). \end{aligned} \tag{3.23}$$

The optimization problem is

$$\begin{aligned} &\arg\max_{\hat{\mathbf{h}}_{\text{vec}}, \hat{\mathbf{K}}_w} && L\left(\mathbf{y}_{\text{vec}} \middle| \hat{\mathbf{h}}_{\text{vec}}, \hat{\mathbf{K}}_w\right) && \text{(P5)} \\ &\text{subject to} && ||\hat{\mathbf{h}}_{\text{vec}}||^2 \leq \rho_{\text{ID}}. && (3.24) \end{aligned}$$

Since the optimization problem (P5) does not have a closed-form solution, we consider solving the problem iteratively similar to the expectation conditional maximization (ECM) algorithm [77]. An iteration consists of i) maximization of the likelihood function $L(\mathbf{y}_{\text{vec}} \,|\, \hat{\mathbf{h}}_{\text{vec}}^{(t+1)}, \hat{\mathbf{K}}_w^{(t)})$ for a known $\hat{\mathbf{K}}_w^{(t)}$subject to the constraint (3.24) and ii) maximization of $L(\mathbf{y}_{\text{vec}} \,|\, \hat{\mathbf{h}}_{\text{vec}}^{(t+1)}, \hat{\mathbf{K}}_w^{(t+1)})$ for a known $\hat{\mathbf{h}}_{\text{vec}}^{(t+1)}$.

First, we obtain $\hat{\mathbf{h}}_{\text{vec}}^{(t+1)}$ that maximizes the likelihood function for a given $\hat{\mathbf{K}}_w^{(t)}$. The optimization problem is

$$\begin{aligned} &\arg\max_{\hat{\mathbf{h}}_{\text{vec}}^{(t+1)}} && L\left(\mathbf{y}_{\text{vec}} \middle| \hat{\mathbf{h}}_{\text{vec}}^{(t+1)}, \hat{\mathbf{K}}_w^{(t)}\right) \\ &\text{subject to} && ||\hat{\mathbf{h}}_{\text{vec}}^{(t+1)}||^2 \leq \rho_{\text{ID}}. \end{aligned} \tag{P5-1}$$

For convenience, let $\mathbf{\Omega}^{(t)} = \mathbf{I} \otimes \mathbf{K}_w^{(t)}$. Then, the optimal solution to (P5-1) is

$$\hat{\mathbf{h}}_{\text{vec}}^{(t+1)} = \left[\mathbf{V}^H \left(\mathbf{\Omega}^{(t)}\right)^{-1} \mathbf{V} + \lambda \mathbf{I}\right]^{-1} \mathbf{V}^H \left(\mathbf{\Omega}^{(t)}\right)^{-1} \mathbf{y}_{\text{vec}}, \tag{3.25}$$

where if $||[\mathbf{V}^H \left(\mathbf{\Omega}^{(t)}\right)^{-1} \mathbf{V}]^{-1} \mathbf{V}^H \left(\mathbf{\Omega}^{(t)}\right)^{-1} \mathbf{y}_{\text{vec}}||^2 > \rho_{\text{ID}}$ then $\lambda > 0$ is selected such that $||\hat{\mathbf{h}}_{\text{vec}}^{(t+1)}||^2 = \rho_{\text{ID}}$, otherwise $\lambda = 0$. The proof of the solution is given in Appendix 3.A.

Secondly, we obtain the optimal $\hat{\mathbf{K}}_w^{(t+1)}$ that maximizes (3.23) for a given $\hat{\mathbf{h}}_{\text{vec}}^{(t+1)}$. The optimization problem is

$$\arg\max_{\hat{\mathbf{K}}_w^{(t+1)}} \quad L\left(\mathbf{y}_{\text{vec}} \middle| \hat{\mathbf{h}}_{\text{vec}}^{(t+1)}, \hat{\mathbf{K}}_w^{(t+1)}\right). \tag{P5-2}$$

The optimal solution to (P5-2) is given as

$$\mathbf{K}_w^{(t+1)} = \frac{1}{M} \sum_{i=1}^{M} \mathbf{e}_i^{(t+1)} \mathbf{e}_i^{(t+1)^H}, \tag{3.26}$$

where $\mathbf{e}_i^{(t)} = \mathbf{y}_R[i] - \mathbf{H}^{(t)}\mathbf{x}[i]$ and $\mathbf{H}^{(t)} = \text{vec}^{-1}\left(\mathbf{h}^{(t)}\right) \in \mathbb{C}^{N_r \times N_t}$. The estimates (3.25) and (3.26) are computed iteratively until they converge.

To optimize the transmit covariance matrix, a feedback channel is required to send the channel and noise covariance estimates to the transmitter. The implementation and performance of the feedback channel of communication systems have been extensively studied [78], [79]. Possible feedback channel implementations include load modulation, an uplink communication technique for RFID and near-field communication (NFC) systems [11]. A detailed discussion of the implementation is deferred to future work.

The channel $\mathbf{S}_{TT}$ is estimated using ML estimation in the same manner as the previous estimation procedure. The reflected pilot symbol is $\mathbf{y}_T[i] = \mathbf{S}_{TT}\mathbf{x}[i] + \mathbf{w}_T[i]$ where $\mathbf{w}_T[i]$ is

the additive noise with $\mathbf{w}_T[i] \sim \mathcal{CN}(\mathbf{0}, \mathbf{K}_t)$ as shown in Fig. 3.5. Note that the estimator for $\mathbf{K}_t$ can be treated as a nuisance parameter since the estimation of this noise covariance matrix is not required for optimizing $\mathbf{Q}_x$.

3.5 Simulation

3.5.1 Overview

The performance of IC-SWIPT is investigated by numerical analysis and FEM simulation. Throughout the simulations, we use the center frequency of $f_c = 13.56\,\text{MHz}$. The source impedance R_s and the reference impedance Z_R are $50\,\Omega$ and the total available transmit power is $1\,\text{W}$. The power splitting coefficients are $\rho_{\text{EH}} = 0.9$ and $\rho_{\text{ID}} = 0.1$. The noise covariance matrix is generated based on Bosma's theorem [74], [75] as $\mathbf{K}_w = \sigma^2\rho_{\text{ID}}(\mathbf{I} - \mathbf{S}_{RR}\mathbf{S}_{RR}^H)$ where $\sigma^2 = 1\,\text{mW}$. For simplicity, we do not consider impedance matching in this simulation.[4]

We consider the direct-fed and indirect-fed inductively coupled models [80]. In the direct-fed model, each coil is directly connected to a source or a load in series. The indirect-fed model is often referred to as strongly coupled magnetic resonance, in which secondary coils are employed for resonance [4].

For each of the models, the simulation is performed as follows. First, the scattering matrices $\mathbf{S}_{TT}$, $\mathbf{S}_{RT}$, and $\mathbf{S}_{RR}$ are computed using ANSYS HFSS [81]. Then, the maximum capacity waveform, the maximum harvested power waveform, and the R-E region are numerically computed. Lastly, The average magnitude of magnetic field is computed for each of the optimal waveforms by averaging field realizations. Each transmitted signal is generated from a realization of a random vector with distribution $\mathbf{Q}_{x,opt}$.

3.5.2 Direct-Fed Resonant 2×2 MIMO Model

We first consider a direct-fed resonantly-coupled 2×2 MIMO IC-SWIPT model ($N_t = N_r = 2$). This simple setup is intended to show how the magnetic fields change depending

[4]↑The framework proposed in this paper is readily applicable to a model with linear impedance matching circuits by having the scattering parameters capture the matching network as well.

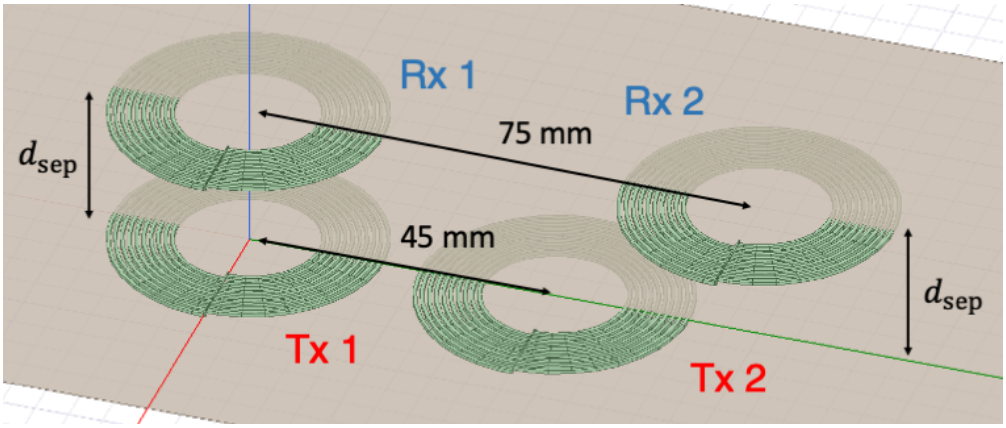

(a)

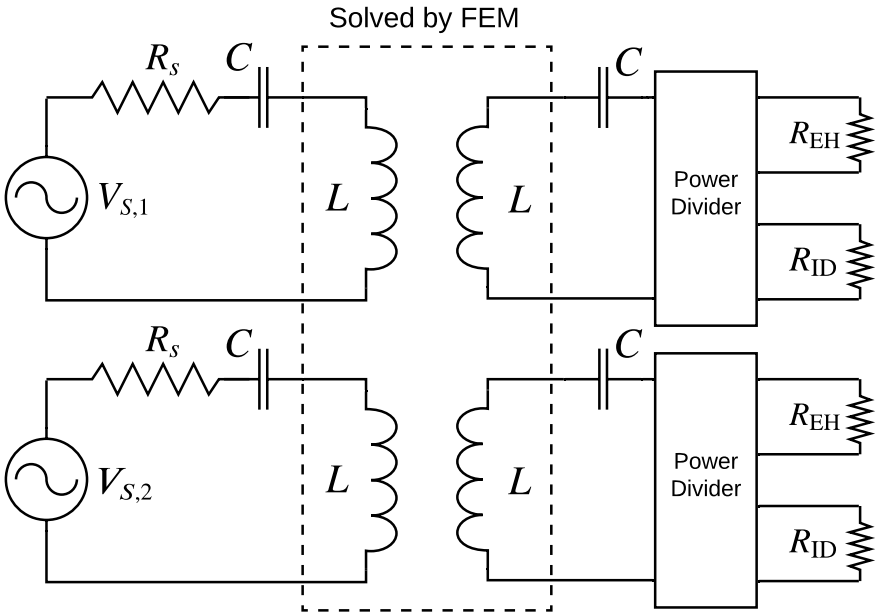

(b)

Figure 3.6. Direct-fed 2×2 MIMO IC-SWIPT model. (a) Coil geometry. The shaded plane that goes through the centers of each coil indicates the surface in which the field strength is to be plotted. (b) Equivalent circuit configuration.

on the optimization objective. The model consists of two pairs of co-planer coils as shown in Fig. 3.6. The separation distance between the transmitter and receiver is denoted by d_{sep}. The four flat spiral coils have the same shape, with each having 10 turns. Each coil having inductance L is connected to a capacitor C in series for resonance. The inductance and capacitance satisfy $f_c = 1/(2\pi\sqrt{LC})$.

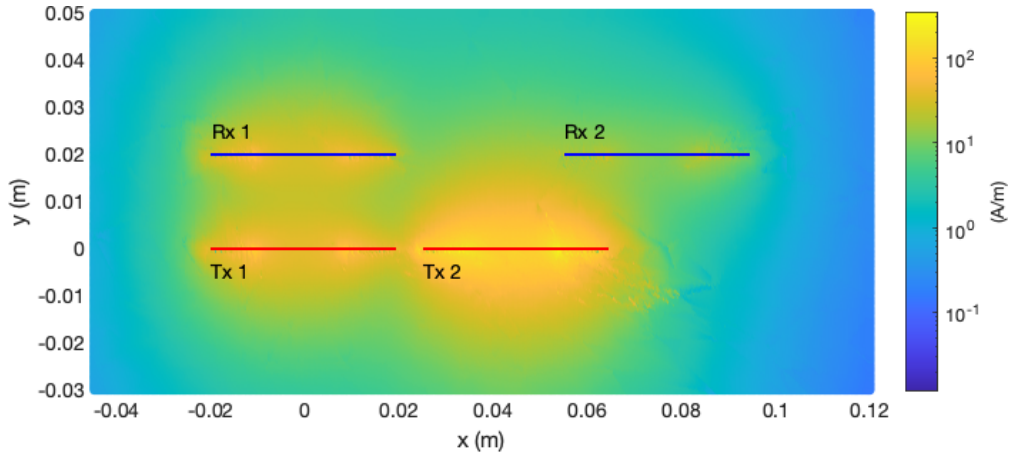

(a)

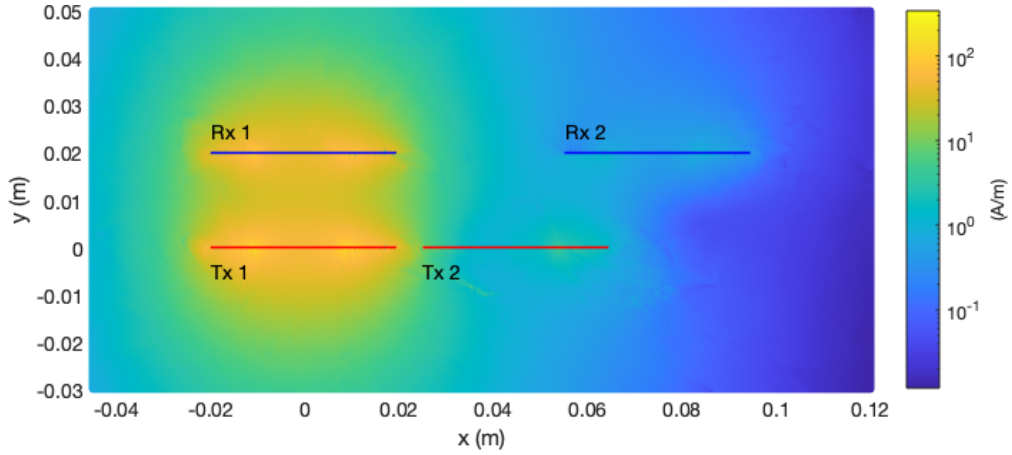

(b)

Figure 3.7. Average magnetic field strength of direct-fed 2×2 MIMO model. (a) Maximum capacity waveform. (b) Maximum harvested power waveform.

The R-E region and the average strength of the magnetic field for $d_{\text{sep}} = 20\,\text{mm}$ are shown in Fig. 3.7 and 3.8, respectively. With the maximum capacity waveform, a large portion of the available power is allocated to transmit coil 2, which results in a strong magnetic field around transmit coil 2. This is because receive coil 2 is distant from both transmitters and, therefore, has smaller magnitude of the channel compared to receive coil 1. With the maximum harvested power waveform, almost none of the available power is allocated to transmit coil 2. Figure 3.7b suggests that most of the power was transferred over the channel from transmit coil 1 to receive coil 1. This can be justified by the fact that the channel from

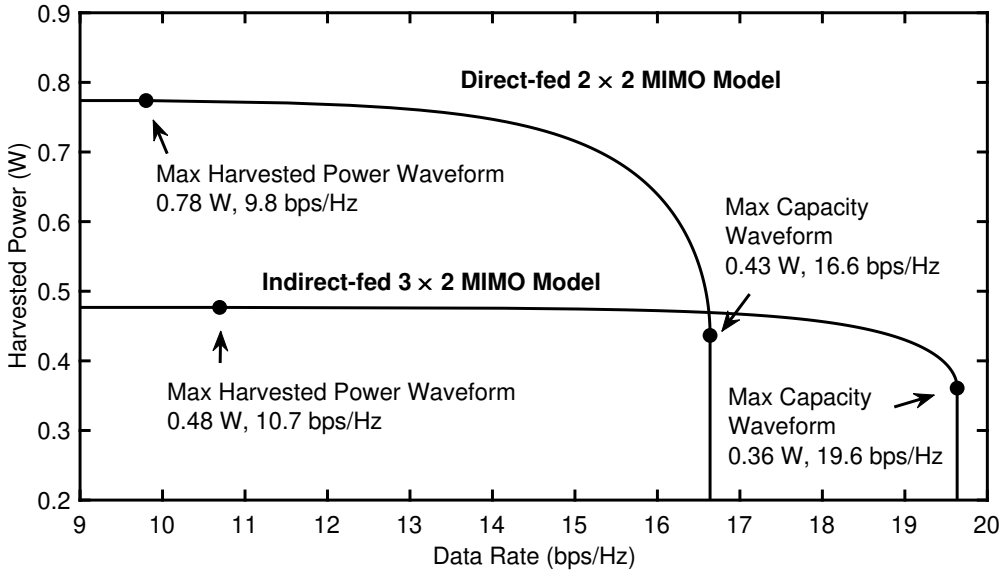

Figure 3.8. R-E regions of direct-fed 2×2 and indirect-fed 3×2 MIMO models. The solid lines represent boundaries of the regions.

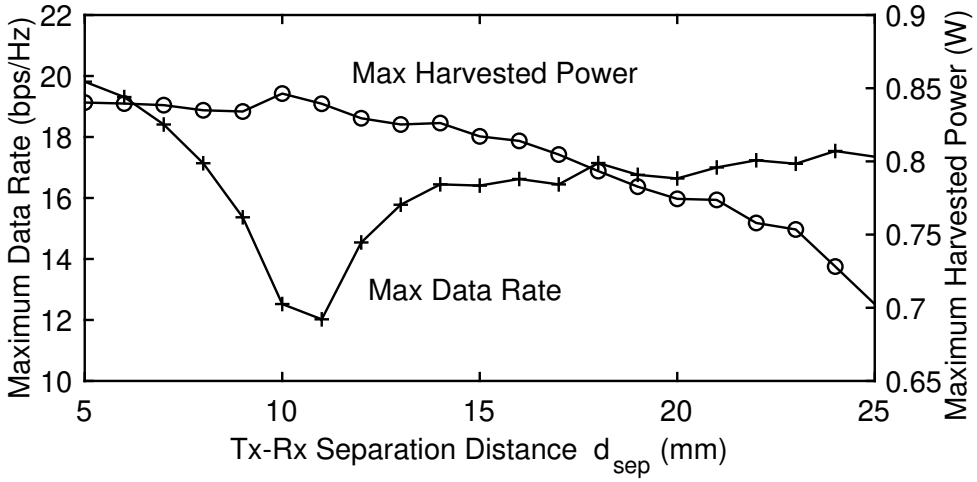

Figure 3.9. Maximum data rate and delivered power for separation distance d_{sep}.

transmit coil 1 to receive coil 1 has a higher gain than the channel from transmit coil 2 to receive coil 2.

Figure 3.9 shows how d_{sep} affects the maximum harvested power and maximum data rate. Since power transfer mostly occurs between transmit coil 1 and receive coil 1, the maximum harvested power decreases as the separation between the coils increases. In contrast, the

maximum data rate significantly drops near $d_{\text{sep}} = 11\,\text{mm}$ because the location of coils resulted in a low channel gain between transmitter 2 and receiver 2.

3.5.3 Indirect-Fed Resonant 3×2 MIMO Model

We now consider an indirect-fed 3×2 MIMO IC-SWIPT model ($N_t = 3, N_r = 2$) as shown in Fig. 3.10. This model is designed to show the performance of a practical IC-SWIPT model with a larger transmitter-receiver distance. Each primary coil is constructed by a single-turn circular loop and a connection port for coil excitation. Each secondary coil has five turns and is connected to a capacitor in series. The secondary coil circuits are tuned to the frequency of f_c.

The R-E region and the average field strengths are shown in Fig. 3.8 and 3.11, respectively. Since the resonant secondary coils are used in this setup, the receive coils are strongly excited even when they are distant from the transmit coils. Transmit coils 1 and 2 are both highly excited with the maximum capacity waveform, while the maximum harvested power waveform allocated a large portion of the available power to transmit coil 3. When the transmit covariance matrix is optimized for the maximum harvested power, this model achieves the harvested power of 0.48 W and the capacity of $10.7\,\text{bit}\,\text{s}^{-1}\,\text{Hz}^{-1}$. When the transmit covariance matrix is optimized for the maximum capacity, this model gives the harvested power of 0.36 W and the capacity of $19.6\,\text{bit}\,\text{s}^{-1}\,\text{Hz}^{-1}$.

3.6 Conclusion

We proposed a new framework to define the input-output relationship and analyzed the performance of a MIMO IC-SWIPT system by utilizing the traveling waves and scattering parameters. The framework represents the unknown channel as a two-port vector-input vector-output network, which captures properties of coils, inductively coupled channels, and other linear circuit elements as well as parasitic components. The information capacity and the harvested power were derived as functions of the scattering parameters and a covariance matrix of the incident wave to the channel. We showed how to find the transmit waveform that i) maximizes information capacity, ii) maximizes harvested power, and iii) maximizes

information capacity subject to a minimum harvested power constraint. In addition, a simple technique to estimate the unknown scattering parameters that accounts for the law of conservation of energy was proposed. We computed the rate-energy regions and the average magnetic field strengths for direct-fed 2×2 MIMO and indirect-fed 3×2 MIMO models.

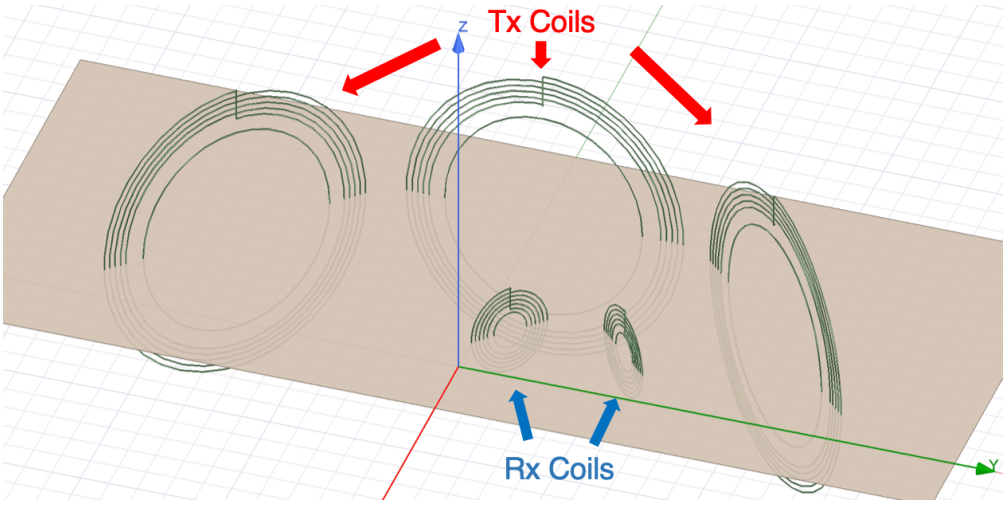

(a)

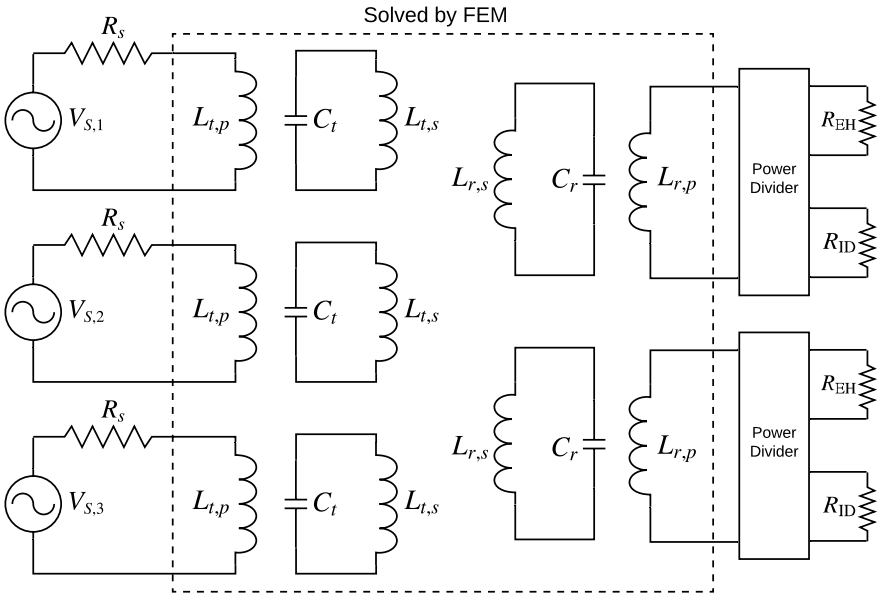

(b)

Figure 3.10. Indirect-fed 3×2 MIMO IC-SWIPT model. (a) Coil geometry. The shaded plane indicates the surface in which the field strength is to be plotted. (b) Equivalent circuit configuration.

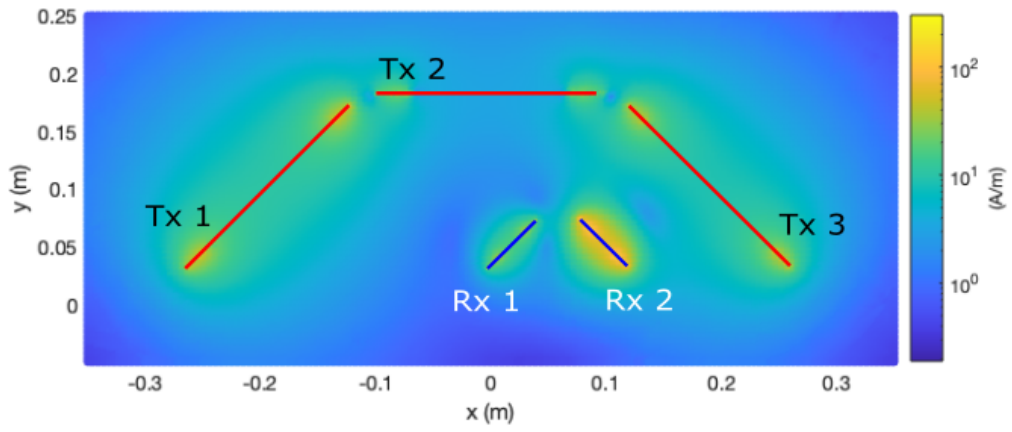

(a)

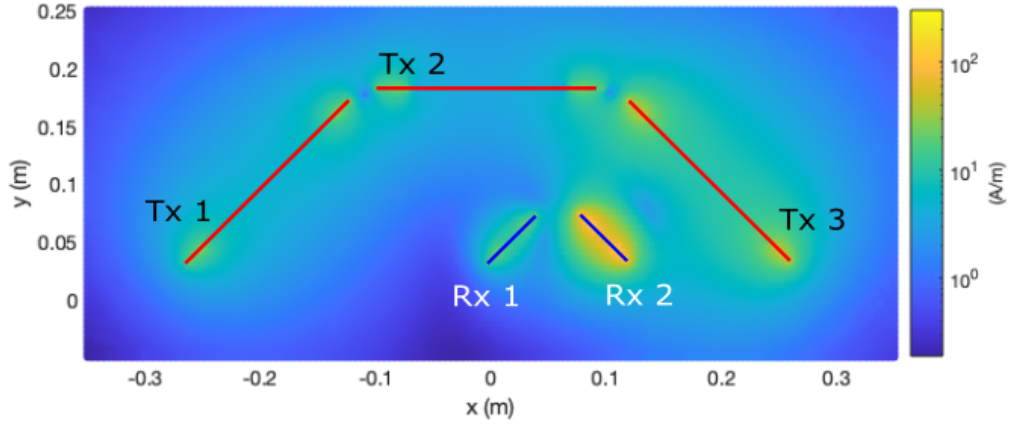

(b)

Figure 3.11. Average magnetic field strength of indirect-fed 3×2 MIMO model. (a) Maximum capacity waveform. (b) Maximum harvested power waveform.

3.A Proof of Maximum Likelihood Channel Estimation with Constraint

The optimization problem (P5-1) can be rewritten as

$$\begin{aligned} &\arg\min_{\mathbf{h}_{\text{vec}}} && (\mathbf{y}_{\text{vec}} - \mathbf{V}\mathbf{h}_{\text{vec}})^H \mathbf{\Omega}^{-1} (\mathbf{y}_{\text{vec}} - \mathbf{V}\mathbf{h}_{\text{vec}}) \\ &\text{subject to} && ||\mathbf{h}_{\text{vec}}||^2 \leq \rho_{\text{ID}}, \end{aligned} \tag{3.27}$$

where $\mathbf{\Omega} = \mathbf{I} \otimes \mathbf{K}_w$. The superscripts "$(t)$" and "$(t+1)$" are omitted. The Lagrangian is

$$L(\mathbf{h}_{\text{vec}}, \lambda) = (\mathbf{V}\mathbf{h}_{\text{vec}} - \mathbf{y}_{\text{vec}})^H \mathbf{\Omega}^{-1} (\mathbf{V}\mathbf{h}_{\text{vec}} - \mathbf{y}_{\text{vec}}) + \lambda \left(||\mathbf{h}_{\text{vec}}||^2 - \rho_{\text{ID}} \right),$$

where $\lambda \geq 0$ is the Lagrange multiplier. Setting $\nabla L(\mathbf{h}_{\text{vec}}, \lambda) = 0$ gives

$$\mathbf{h}_{\text{vec}} = \left(\mathbf{V}^H \mathbf{\Omega}^{-1} \mathbf{V} + \lambda \mathbf{I} \right)^{-1} \mathbf{V}^H \mathbf{\Omega}^{-1} \mathbf{y}_{\text{vec}}.$$

Therefore, it follows from the Karush-Kuhn-Tucker (KKT) conditions that if $||\mathbf{h}_{\text{vec}}||^2 \leq \rho_{\text{ID}}$ with $\lambda = 0$, then the solution is equivalent to that of generalized least squares (GLS), i.e.,

$$\mathbf{h}_{\text{vec}} = \left(\mathbf{V}^H \mathbf{\Omega}^{-1} \mathbf{V} \right)^{-1} \mathbf{V}^H \mathbf{\Omega}^{-1} \mathbf{y}_{\text{vec}}.$$

Otherwise, λ is chosen such that

$$||(\mathbf{V}^H \mathbf{\Omega}^{-1} \mathbf{V} + \lambda \mathbf{I})^{-1} \mathbf{V}^H \mathbf{\Omega}^{-1} \mathbf{y}_{\text{vec}}||^2 = \rho_{\text{ID}}.$$

The parameter λ can be found using an iterative algorithm (e.g., the bisection method).

4. NEAR-FIELD WIRELESS POWERED COMMUNICATION NETWORK USING A COIL ARRAY

4.1 Introduction

The rapid growth of the IoT has drawn significant attention to WPCN in which remote devices are powered wirelessly over a downlink channel, while transferring information using the uplink channel [1], [82]. One of the most well-known WPCN applications is RFID, in which a reader transmits energy to tags that use the received energy to send information back to the reader [11], [16], but there are many emerging use cases that accompany the growing and widespread IoT use cases in agriculture, manufacturing, and daily life. Recently, WPCN has been extensively studied in signal the signal processing community. The system is considered from various aspects including the data rate, PTE, network structure, scheduling, and hardware design of transmitter and receiver mainly based on microwave signals [1], [8], [83].

In short and middle-range transmission scenarios, near-field inductive coupling, which primarily uses a non-radiative magnetic field, has various advantages over a far-field model, which is based on a propagating electromagnetic field. Firstly, inductive coupling achieves higher PTE compared to RF WPT since inductive coupling primarily uses a non-radiative magnetic field [2]. The recent progress in near-field wireless power transfer techniques including magnetic resonant coupling and multi-coil transmission can provide robust power transfer at a longer distance [4], [10]. Secondly, uplink information transfer can be easily implemented over inductively coupled circuits using load modulation (LM) [11]. This is due to the mutual coupling effect in which the state (e.g., voltages and currents) of one circuit is affected by the states of the other coupled circuits. Lastly, an inductively coupled link is less susceptible to surrounding obstacles such as water, concrete walls, and soils than far-field transmission systems. This property allows near-field WPCNs to be used in traditionally harsh environments including underground and underwater [64], [84].

Despite the various advantages of inductive coupling, most of the previous studies on WPCNs are based on a far-field transmission model. Therefore, this paper models a near-field WPCN over inductively coupled circuits and investigates the optimal strategies for

wireless information and power transfer. We consider the use of multiple coils at the reader, and we find that the analysis is similar to that of multiple antenna communication techniques used in today's high-rate RF communication systems.

Specifically, the main contributions of this paper are:

- Modeling an inductive WPCN based on the "black-box" approach in which the properties of the network are captured by a small number of measurable parameters;
- Deriving optimal source signal vectors that maximize the harvested and reflected powers;
- Presenting methods to design load impedance values for communication;
- Analyzing effects of different load impedance values to the energy and information transfer performances;
- Proposing a scattering parameter (S-parameter) estimation technique based on the combination of channel sounding and a sequence of reflection coefficients.

WPCNs over an inductively coupled circuits using a coil array was initially studied in [9]. The relationship between voltages and currents of the circuits was modeled based on the black-box approach using a small number of transconductance values, in a similar way to the technique originally proposed in [10]. While modeling a WPCN using transconductance values allows us to straightforwardly relate the parameters that appear in the analysis to the corresponding voltages and currents, it is nontrivial to optimize the circuit parameters such as load impedance.

In this paper, we utilize the S-parameters to represent the black-box, instead of transconductance values. By representing the current and voltage by a pair of an incident and reflected waves, the tools from signal processing such as beamforming can be directly applied while preserving the meaningful physical effects.

The model and optimizations presented in this paper are readily applicable to far-field backscattering, which is a mathematically similar technique that can be used to implement WPCN, while it is regarded as a distinct physical phenomenon from near-field coupling in

general [16]. Far-field backscattering is a technique to send back information from remote devices to an AP using the backscattering effect of microwaves. Backscattering can be seen as a special case of the model presented in this paper, in which signal reflections *from* the "black-box" are zero. The related works of backscattering include MIMO communication [85], beamforming for power transfer [86], and channel estimation [87].

The following notations are used throughout this paper. $\mathbf{A}^*$, $\mathbf{A}^\mathsf{T}$, $\mathbf{A}^\mathsf{H}$, and $\mathrm{tr}(\mathbf{A})$ indicate the conjugate, transpose, Hermitian transpose, and trace of a matrix $\mathbf{A}$, respectively. $\mathrm{Re}\{a\}$ represents the real component of complex scalar a. The $n \times n$ identity matrix is represented by $\mathbf{I}_n$. Lastly, $\mathbb{C}$ denotes the set of complex numbers.

4.2 System Model

In this section, we describe the power transfer and communication set-up we consider in this paper.

4.2.1 Overview

Consider an inductive WPCN model with a *reader* denoted by $\mathcal{R}$ with N coils and a *transponder* denoted by $\mathcal{T}$ with a single coil as shown in Fig. 4.1. The reader coils are used for transferring energy to and receiving information from $\mathcal{T}$ with an average total transmit power constraint P. The transponder coil is connected to a load, which is used for passive load modulation and energy harvesting.

The WPCN model is represented by an *abstract circuit model* in which all the interconnections between $\mathcal{R}$ and $\mathcal{T}$ are treated as a "black-box" as shown in Fig. 4.2. The abstract circuit model allows us to capture the properties of circuit system by a small number of measurable parameters [10], [88]. The connection between $\mathcal{R}$ and $\mathcal{T}$ is fully characterized by an $N+1$ port network. In addition, the modulator and the energy harvester are represented by a passive variable load with impedance Z_L, which is connected to port 0 of the network. The harvested power is defined to be the power dissipated at the load Z_L. The sources of $\mathcal{R}$, with each having the structure shown in Fig. 4.3, are connected to ports 1 to N. Throughout the paper, the transponder coil and its related parameters are exclusively denoted by the

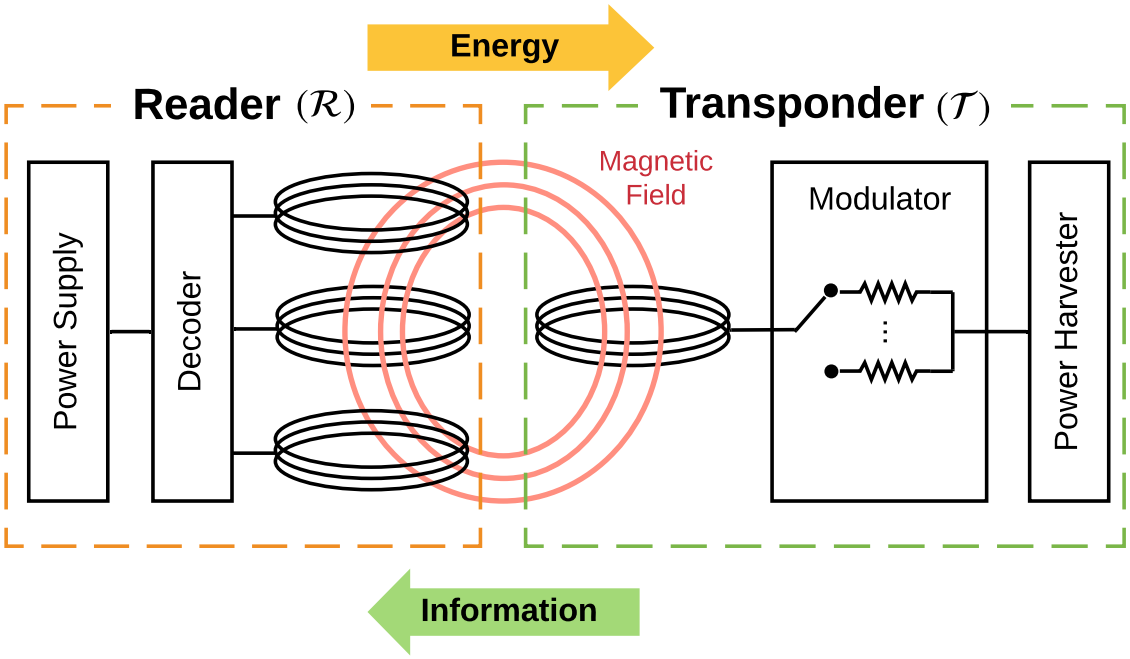

Figure 4.1. Illustration of a near-field WPCN model.

index 0. The reader coils and the corresponding parameters are indexed by 1 to N. Also, the scattering parameter from port i to j in Fig. 4.2 is denoted by[1] $s_{j,i}$.

In this paper, the WPCN is modeled using traveling waves and S-parameters, instead of voltages, currents, and impedance or admittance values. This representation allows us to apply tools from signal processing while preserving the properties of the circuits (e.g., impedance mismatches). The incident signal x_i and reflected signal y_i for port i are defined as

$$x_i = \frac{V_i + R_{\text{ref}} I_i}{2\sqrt{R_{\text{ref}}}}, \quad y_i = \frac{V_i - R_{\text{ref}} I_i}{2\sqrt{R_{\text{ref}}}}, \tag{4.1}$$

where $R_{\text{ref}} > 0$ is a reference impedance, and V_i and I_i are RMS values of the voltage and current of port i, respectively. The definitions (4.1) can be seen as a special case of power waves with a real reference impedance [69].

[1]↑Note the order of i and j in the subscript. We adopted the standard notation of scattering parameters from microwave network theory.

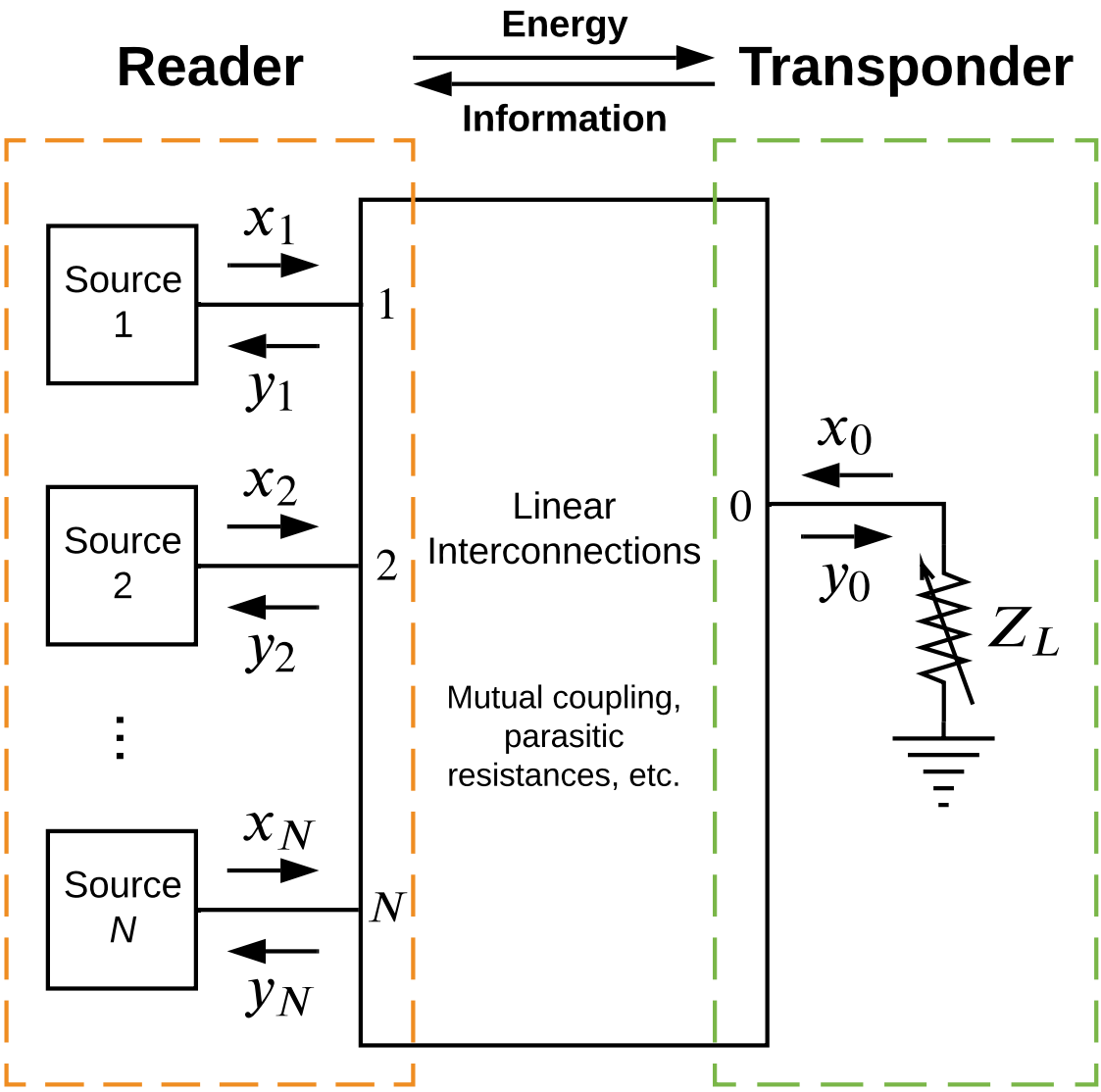

Figure 4.2. Abstract circuit model of near-field WPCN model.

The load impedance Z_L is converted to a reflection coefficient Γ, rather than directly using it in the formulation. The reflection coefficient of the load with impedance Z_L is given by [69]

$$\Gamma = \frac{Z_L - R_{\text{ref}}}{Z_L + R_{\text{ref}}}. \tag{4.2}$$

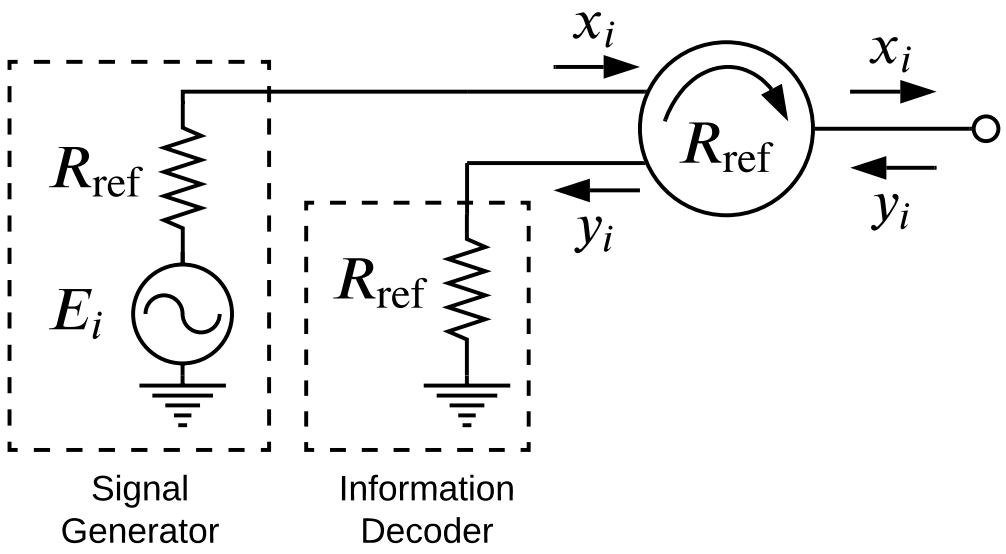

Figure 4.3. Circuit model for i-th source. The model was originally proposed in [89].

Note that $|\Gamma| \leq 1$ since the load is passive and the reference impedance is real. The reflection coefficient Γ is dynamically modulated by $\mathcal{T}$ in order to transfer information. As such, Γ is treated as a random variable that takes one of the values in $\mathcal{G}$, which is defined as

$$\mathcal{G} = \left\{\Gamma^{(1)}, \Gamma^{(2)}, \cdots, \Gamma^{(M)}\right\}, \tag{4.3}$$

where M is the total number of available reflection coefficients. The design methods of $\mathcal{G}$ will be discussed in Section 4.3.2.

We assume that the interconnections between $\mathcal{R}$ and $\mathcal{T}$ are represented by a reciprocal network, i.e., $s_{i,j} = s_{j,i}$ for $i = 0, \ldots, N$ and $j = 0, \ldots, N$. It is known that the reciprocity property is valid for any passive network that contains only isotropic materials [69].

A block diagram representing the flow of the signals in the abstract circuit model is shown in Fig. 4.4. For notational convenience, we use three parameters, $\mathbf{S}_{\mathcal{R}}$, $\mathbf{s}$, and $s_{0,0}$, to denote partial sections of the scattering matrix that represents the interconnections as illustrated in Fig. 4.5. Specifically, $\mathbf{S}_{\mathcal{R}}$ is an $N \times N$ matrix whose (i,j)-element is $s_{i+1,j+1}$, $\mathbf{s}$ is a row vector given by $\mathbf{s} = \begin{bmatrix} s_{0,1} & s_{0,2} & \cdots & s_{0,N} \end{bmatrix}$, and $s_{0,0}$ is a scalar value. Intuitively, $\mathbf{S}_{\mathcal{R}}$, $\mathbf{s}$, and $s_{0,0}$ represent $\mathcal{R}$-to-$\mathcal{R}$, $\mathcal{T}$-to-$\mathcal{T}$, and $\mathcal{T}$-to-$\mathcal{T}$ interconnections, respectively.

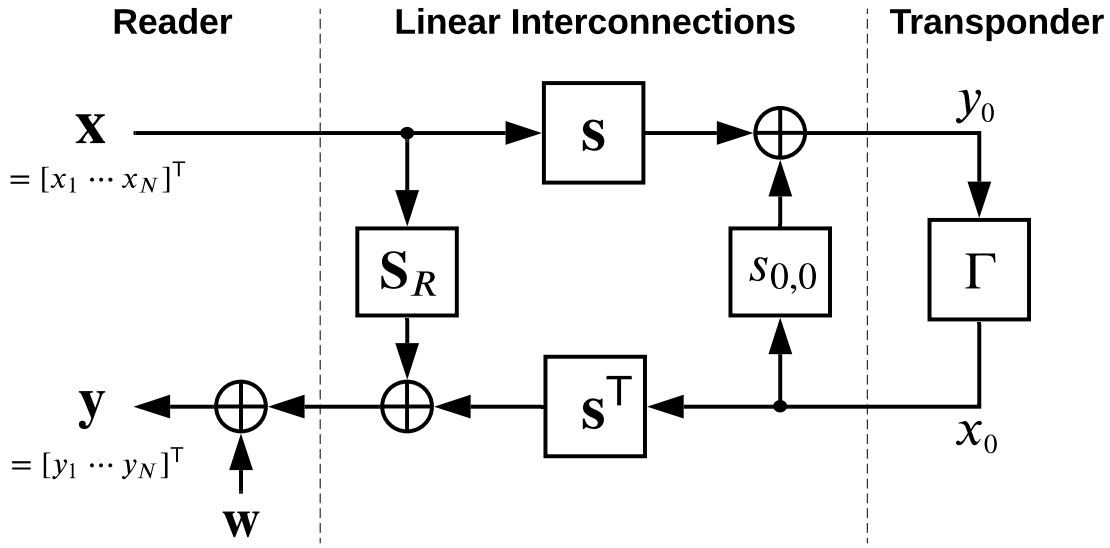

Figure 4.4. Block diagram of an inductive WPCN.

4.2.2 Power Transfer

We first consider the downlink channel from $\mathcal{R}$ to $\mathcal{T}$, which is used for power transfer. Since the interconnection is linear, the signal admitted to the load Z_L can be written as a linear combination of continuous wave (CW) signals supplied by the sources,

$$y_0 = \mathbf{h}_D(\Gamma)\,\mathbf{x} + \mathbf{w}_\tau, \tag{4.4}$$

where $\mathbf{x} = \left[x_1\, x_2 \ldots x_N\right]^\mathsf{T}$ is the source signal vector which represents a CW applied to the system by $\mathcal{R}$,

$$\mathbf{h}_D(\Gamma) = \frac{1}{1 - s_{0,0}\Gamma}\,\mathbf{s} \tag{4.5}$$

is the downlink channel from $\mathcal{R}$ to $\mathcal{T}$. Derivation of (4.5) from the abstract model shown in Fig. 4.2 is given in Appendix 4.A.

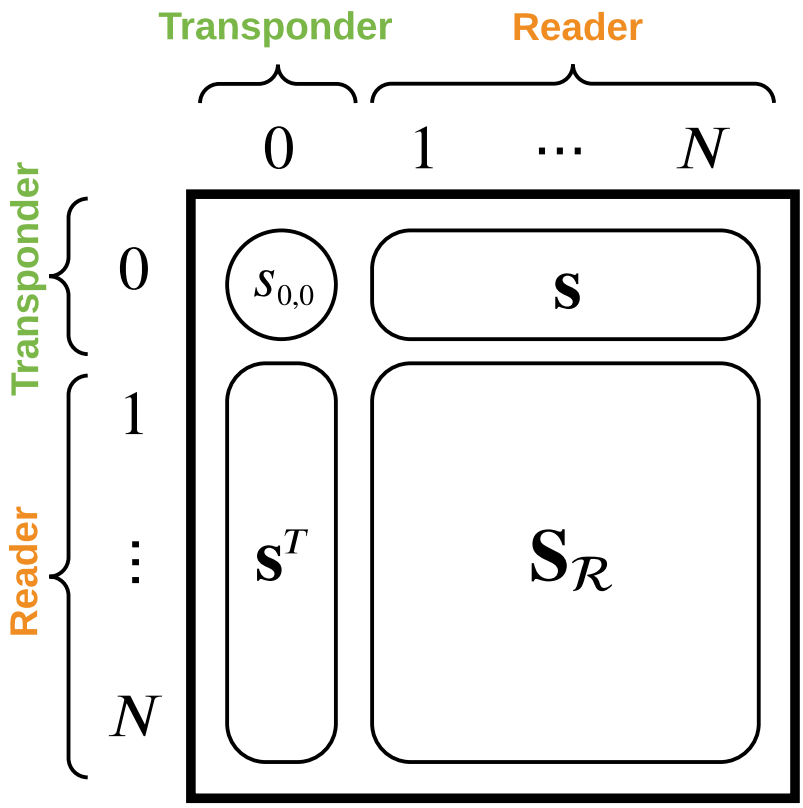

Figure 4.5. Structure of scattering matrix representing the black-box.

Since the harvested power is defined to be the power dissipated at the load, the harvested power is given by the difference of the incident and reflected power of the load, which is written as

$$\begin{aligned} P_H(\Gamma, \mathbf{x}) &= |y_0|^2 - |\Gamma\, y_0|^2 \\ &= \left(1 - |\Gamma|^2\right) y_0^* y_0 \\ &= \left(1 - |\Gamma|^2\right) \mathbf{x}^{\mathsf{H}} \mathbf{h}_D^{\mathsf{H}}(\Gamma) \mathbf{h}_D(\Gamma) \mathbf{x}, \\ &= \frac{1 - |\Gamma|^2}{|1 - s_{0,0}\Gamma|^2} \mathbf{x}^{\mathsf{H}} \mathbf{s}^{\mathsf{H}} \mathbf{s}\, \mathbf{x}. \end{aligned} \tag{4.6}$$

The average harvested power for the source vector $\mathbf{x}$ is

$$\bar{P}_H(\mathbf{x}) = \mathrm{E}\left\{P_H(\Gamma, \mathbf{x})\right\} = \alpha\, \mathbf{x}^{\mathsf{H}} \mathbf{s}^{\mathsf{H}} \mathbf{s}\, \mathbf{x}, \tag{4.7}$$

where $\alpha \triangleq \mathrm{E}\left\{(1-|\Gamma|^2)/\left|1-s_{0,0}\Gamma\right|^2\right\}$ and the expectation is taken over Γ.

The total power supplied to the black-box by transmitting a CW signal $\mathbf{x}$ from $\mathcal{R}$ is

$$P_T(\mathbf{x}) = \|\mathbf{x}\|^2 = \mathbf{x}^{\mathsf{H}}\mathbf{x}, \tag{4.8}$$

which has units of Watts[2]. Since $\mathbf{x}$ is independent of Γ, the average transmit power with respect to Γ is equal to (4.8), i.e., $\bar{P_T}(\mathbf{x}) = P_T(\mathbf{x})$.

The average PTE for $P_T(\mathbf{x}) > 0$ is defined as

$$\bar{\eta}(\mathbf{x}) \triangleq \frac{\bar{P_H}(\mathbf{x})}{\bar{P_T}(\mathbf{x})} = \frac{\alpha\,\mathbf{x}^{\mathsf{H}}\mathbf{s}^{\mathsf{H}}\mathbf{s}\,\mathbf{x}}{\mathbf{x}^{\mathsf{H}}\mathbf{x}}, \tag{4.9}$$

which is independent of the transmit power. Therefore, average PTE is described by a kind of Rayleigh quotient.

4.2.3 Information Transfer

The information is transferred using the uplink channel from $\mathcal{T}$ to $\mathcal{R}$ by passive LM. Changing the load impedance Z alters the reflection coefficient Γ of $\mathcal{T}$ as given in (4.2), which is detected from the reflected signal $\mathbf{y}$ by $\mathcal{R}$ to extract information. Therefore, information transfer involves the wireless channel from $\mathcal{R}$ to $\mathcal{R}$ via $\mathcal{T}$.

The reflected signal received by $\mathcal{R}$ is given by

$$\mathbf{y} = \mathbf{H}(\Gamma)\,\mathbf{x} + \mathbf{w}_{\mathcal{R}}, \tag{4.10}$$

where $\mathbf{y} = \begin{bmatrix} y_1\, y_2 \ldots y_N \end{bmatrix}^{\mathsf{T}}$, $\mathbf{H}(\Gamma) \in \mathbb{C}^{N\times N}$ represents a channel from $\mathcal{R}$ to $\mathcal{R}$ via $\mathcal{T}$, which is a channel matrix as a function of the load reflection coefficient Γ, and $\mathbf{w}_{\mathcal{R}} \sim \mathcal{CN}(\mathbf{0}, \sigma^2\mathbf{I}_N)$ is zero-mean complex Gaussian noise with covariance matrix $\sigma^2\mathbf{I}_M$.

[2]↑Signal processing oriented papers usually do not consider the units. An advantage of scattering parameter-based approach is being able to relate each quantity to measurable physical units.

The channel matrix $\mathbf{H}(\Gamma)$ can be explicitly written in terms of scattering parameters and the load reflection coefficient. The channel is given by

$$\mathbf{H}(\Gamma) = \underbrace{\frac{\Gamma}{1 - s_{0,0}\Gamma}}_{\zeta(\Gamma)} \mathbf{s}^{\mathsf{T}}\mathbf{s} + \mathbf{S}_{\mathcal{R}}. \tag{4.11}$$

Derivation of (4.11) is given in Appendix 4.A. For ease of notation, we define $\zeta(\Gamma)$ as shown in (4.11).

The transmitted data symbols are detected by $\mathcal{R}$ using the received (reflected) signal $\mathbf{y}$. By plugging (4.11) into (4.10), the noisy received signal is

$$\mathbf{y} = \left[\zeta(\Gamma)\,\mathbf{s}^{\mathsf{T}}\mathbf{s} + \mathbf{S}_{\mathcal{R}}\right]\mathbf{x} + \mathbf{w}_{\mathcal{R}}. \tag{4.12}$$

Recall that the transmitted information is embedded in the value of Γ. To detect the transmitted symbol, the receiver cancels out the self interference (i.e., tones) and generate y as

$$\begin{aligned} y &= \mathbf{f}\,(\mathbf{y} - \mathbf{S}_{\mathcal{R}}\mathbf{x}) \\ &= \zeta(\Gamma)\,\mathbf{f}\,\mathbf{s}^{\mathsf{T}}\mathbf{s}\,\mathbf{x} + \mathbf{f}\,\mathbf{w}_{\mathcal{R}}, \end{aligned} \tag{4.13}$$

where $\mathbf{f}$ is a receive combiner.

The instantaneous receive SNR of the combiner output y is defined as

$$\gamma(\Gamma, \mathbf{x}) = \frac{\left|\zeta(\Gamma)\,\mathbf{f}\,\mathbf{s}^{\mathsf{T}}\mathbf{s}\,\mathbf{x}\right|^2}{\|\mathbf{f}\|^2\,\sigma^2}. \tag{4.14}$$

The SNR (4.14) represents the ratio of $\mathcal{T}$'s reflected power associated with $\zeta(\Gamma)$ to the noise power. Since symbol detection is performed based on the combiner output y, the detection

performance is directly related to the SNR defined in (4.14). The instantaneous SNR given Γ and $\mathbf{x}$ is bounded by

$$\gamma(\Gamma, \mathbf{x}) = \frac{|\zeta(\Gamma)\,\mathbf{s}\,\mathbf{x}|^2 \left|\mathbf{f}\,\mathbf{s}^{\mathsf{T}}\right|^2}{\|\mathbf{f}\|^2 \sigma^2} \leq \frac{|\zeta(\Gamma)\,\mathbf{s}\,\mathbf{x}|^2 \|\mathbf{s}\|^2}{\sigma^2},$$

where equality holds if and only if

$$\mathbf{f} = \frac{\mathbf{s}^*}{\|\mathbf{s}\|}, \tag{4.15}$$

which is the maximum ratio combining (MRC) [90]. The combiner (4.15) is independent of $\mathbf{x}$ because $\mathbf{s}\,\mathbf{x}$ is a scalar.

The average receive SNR is

$$\bar{\gamma}(\mathbf{x}) = \frac{\beta \left|\mathbf{f}\mathbf{s}^{\mathsf{T}}\mathbf{s}\,\mathbf{x}\right|^2}{\|\mathbf{f}\|^2 \sigma^2} \tag{4.16}$$

where $\beta \triangleq \mathrm{E}\left\{|\zeta(\Gamma)|^2\right\} = \mathrm{E}\left\{|\Gamma|^2 / |1 - s_{0,0}\Gamma|^2\right\}$.

Remark. *In general, the received signal y is nonlinear in Γ due to the nonlinear structure of function $\zeta(\Gamma)$. A common assumption in far-field (RF) models is that the ports are matched (i.e., $s_{0,0} = s_{1,1} = \cdots = s_{N,N} = 0$). Under this assumption, y is linear in Γ, since $\zeta(\Gamma) = \Gamma$. This result aligns with the widely-used far-field backscattering models (e.g., [87]).*

4.3 Wireless Powered Communication Network

In this section, we discuss optimizing the source signal vector, methods to design the reflection coefficients of the transponder, and a SNR-power region to characterize the performance of an inductive WPCN system.

4.3.1 Optimizing Source Signal Vector

The harvested power and the received signal at $\mathcal{R}$ are both functions of the transmit CW vector $\mathbf{x}$, according to (4.6) and (4.10). Therefore, the optimization problems to find the optimal $\mathbf{x}$ are considered in this section.

We start with showing that the receive the SNR γ is a scalar multiple of the harvested power, and therefore the optimal $\mathbf{x}$ that maximizes SNR also maximizes the harvested power, and vice versa. The instantaneous receive SNR (4.14) can be rewritten as

$$\gamma(\Gamma, \mathbf{x}) = \frac{\left|\zeta(\Gamma)\, \mathbf{f}\, \mathbf{s}^{\mathsf{T}}\right|^2}{\|\mathbf{f}\|^2 \sigma^2} \mathbf{x}^{\mathsf{H}} \mathbf{s}^{\mathsf{H}} \mathbf{s}\, \mathbf{x}. \tag{4.17}$$

By comparing (4.6) and (4.17), we conclude that

$$\gamma(\Gamma, \mathbf{x}) = \ell\, P_H(\Gamma, \mathbf{x}),$$

where $\ell > 0$ is a scalar.

We now consider optimizing the source signal vector $\mathbf{x}$ that maximizes both the harvested power and the receive SNR. The optimization problem is formally written as

$$\mathbf{x}_{\text{opt}} = \underset{\mathbf{x}}{\text{argmax}} \;\; \mathbf{x}^{\mathsf{H}} \mathbf{s}^{\mathsf{H}} \mathbf{s}\, \mathbf{x} \tag{P1}$$

$$\text{subject to} \;\; \mathbf{x}^{\mathsf{H}} \mathbf{x} \leq P, \tag{4.18}$$

where (4.18) is the maximum average source power constraint. The positive scalar of the cost function is omitted since it does not change the result of a maximization problem. The optimal solution to (P1) is a an eigenvector with magnitude $\sqrt{P}$ that corresponds to the largest eigenvalue of $\mathbf{s}^{\mathsf{H}}\mathbf{s}$, which is $\mathbf{x}_{\text{opt}} = \sqrt{P}\, \mathbf{s}^{\mathsf{H}} / \|\mathbf{s}\|$. Therefore, this solution can be seen as beamforming from $\mathcal{R}$ to $\mathcal{T}$. It is worth noting that the optimum solution also maximizes the PTE (4.9). This is not to be confused with the maximum power transfer theorem in circuit analysis, which is the result of impedance matching.

4.3.2 Load Design Methods

A choice of reflection coefficients $\mathcal{G}$ defined in (4.3) affects the harvested power and the receive SNR of information transfer, since both (4.7) and (4.16) depend on $\mathcal{G}$. The fact that y is nonlinear in Γ as can be seen in (4.10) provides us with two approaches to design $\mathcal{G}$, namely, a *direct design* and *predistortion-based design*, which we present in this section.

Since the load is passive (i.e., the reflected power does not exceed the incident power), every $\mathcal{G}$ must satisfy $\mathcal{G} \subset \bar{\mathcal{G}}$, where $\bar{\mathcal{G}}$ is a set of all of the "valid" reflection coefficients, defined as

$$\bar{\mathcal{G}} = \{\Gamma : \Gamma \in \mathbb{C}, |\Gamma| \leq 1\}. \tag{4.19}$$

For a given $\mathcal{G}$, the reader observes the constellation $\mathcal{C} = \left\{c^{(1)}, \ldots, c^{(M)}\right\}$ where $c^{(m)} = \zeta\left(\Gamma^{(m)}\right)$. Since every $\mathcal{C}$ must generate a valid $\mathcal{G}$, we have $\mathcal{C} \subset \bar{\mathcal{C}}$ where $\bar{\mathcal{C}}$ is the set of all constellation points that generate the valid reflection coefficients, defined as

$$\bar{\mathcal{C}} = \left\{\zeta(\Gamma) : \Gamma \in \bar{\mathcal{G}}\right\}. \tag{4.20}$$

While it can be easily seen that $\bar{\mathcal{G}}$ is a disk centered at zero with radius 1 from the definition (4.19), the region that is defined by $\bar{\mathcal{C}}$ is relatively difficult to observe. As such, we provide the following theorem that provides the constraint on $\mathcal{C}$ in order for it to be a "valid" constellation.

Theorem 4.3.1. *Assume $|s_{0,0}| < 1$. If a constellation point $c \in \mathbb{C}$ satisfies $|c - a| \leq r$ where $r = |p_1 - p_2|/2$, $a = (p_1 + p_2)/2$, $p_1 = \zeta(|s_{0,0}|/s_{0,0})$, and $p_2 = \zeta(-|s_{0,0}|/s_{0,0})$, then $|\zeta^{-1}(c)| \leq 1$.*

Proof. See Appendix 4.B.

Theorem 1 provides a useful property that any constellation $\mathcal{C}$ that is confined to a circle with center a and radius r generates a valid set of reflection coefficients $\mathcal{G} = \{\zeta^{-1}(c) : c \in \mathcal{C}\}$ where $\zeta^{-1}(c) = c/(1 + s_{0,0}\, c)$.

We now present two approaches to designing the reflection coefficients.

Direct load design

Since $\bar{\mathcal{G}}$ is a disk, a straightforward but naïve approach is to design $\mathcal{G}$ directly. For example, a binary phase shift keying (BPSK) constellation can be directly defined as a set of reflection coefficients $\mathcal{G} = \{-1, 1\}$, which clearly satisfies $\mathcal{G} \subset \bar{\mathcal{G}}$. Note that while the distance between the two symbols (-1 and 1) is maximized under $\bar{\mathcal{G}}$ in this example, it does

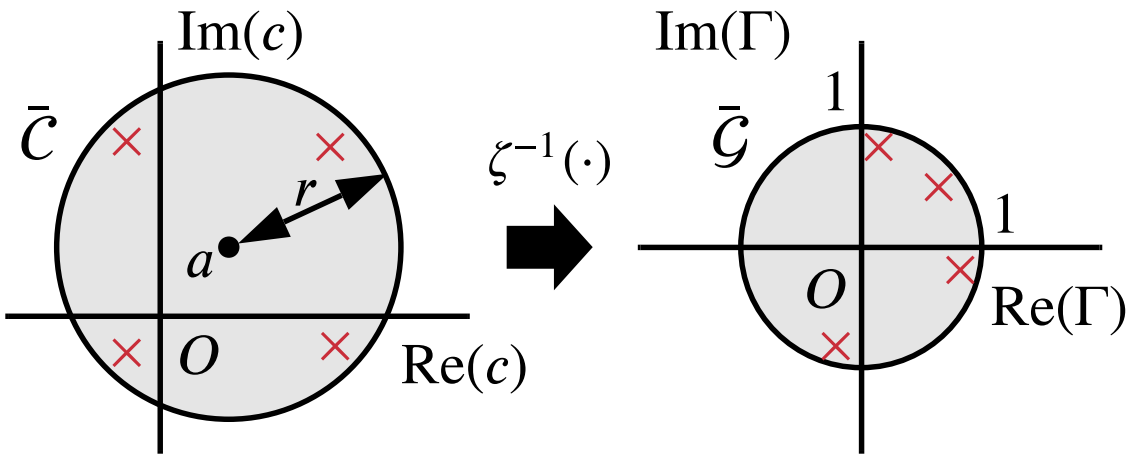

Figure 4.6. Illustration of transformation of QPSK constellation to reflection coefficients.

not imply the maximum distance under $\bar{\mathcal{C}}$ due to the nonlinearity of $\zeta(\cdot)$. This approach does not require channel state information (CSI) and is best suited for low-cost transponders that need to be manufactured with a fixed set of reflection coefficients. This approach can be seen as constellation design based on $\mathcal{T}$'s perspective.

Predistortion-based load design

If the transponder's reflection coefficients are reconfigurable, $\mathcal{G}$ can be designed in a way that a desired constellation appears at $\mathcal{R}$ by predistorting the reflection coefficient. Specifically, a constellation $\mathcal{C} = \left\{c^{(1)}, \ldots, c^{(M)}\right\}$ where $\mathcal{C} \subset \bar{\mathcal{C}}$ is designed using the property from Theorem 1 and the corresponding $\mathcal{G} = \{\zeta^{-1}(c) : c \in \mathcal{C}\}$ is generated. An illustration of transformation of quadrature phase shift keying (QPSK) to a set of reflection coefficients is shown in Fig. 4.6 as an example.

4.3.3 SNR-Power Tradeoff

There is a fundamental tradeoff between the downlink energy transfer and uplink information transfer performances. The tradeoff arises from the fact that a portion of the power received by $\mathcal{T}$ is used for uplink data transfer. To observe the tradeoff, consider reflection coefficients $\mathcal{G} = \{-a, a\}$, which can be used for binary transmission. When $a = 1$, no power

is harvested by $\mathcal{T}$ according to (4.6) since $1 - |\Gamma|^2$ is always zero. When $a = 0$, $\mathcal{T}$ does not reflect any energy to $\mathcal{R}$ since $\zeta(\Gamma)$ is always zero and therefore no information can be transferred.

To characterize the performance tradeoff, we define an SNR-power region [91]. The SNR-power region for an inductive WPCN is defined as

$$C_{\text{SNR}-\text{P}}(P_T) = \{(\rho, P) : \rho \leq \gamma(\Gamma, \mathbf{x}),\ P \leq P_H(\Gamma, \mathbf{x}), \\ \mathbf{x}^{\mathsf{H}}\mathbf{x} \leq P_T,\ |\Gamma| \leq 1\}. \tag{4.21}$$

An SNR-power pair $(\rho, P) \in C_{\text{R-E}}(P_T)$ is interpreted as, the transponder is able to harvest P Watts of power while transferring information to $\mathcal{R}$ at the SNR of less than or equal to ρ.

4.4 Circuit Estimation

The knowledge of scattering parameters is required for the source signal optimization, receive signal combining, and predistortion-based reflection coefficient designing, as discussed in the previous sections. This section proposes a novel method to estimate the unknown scattering parameters $s_{0,0}$, $\mathbf{s}$, and $\mathbf{S}_{\mathcal{R}}$.

Determining unknown scattering parameters of a multi-port network usually involves the transmission of CW and measurement of reflected signal at each port (e.g., measurement using a vector network analyzer). However, this technique is not suitable for the proposed WPCN model since active signal transmission or reflected signal measurement at the transponder is not feasible. Therefore, we propose an S-parameter estimation method that does not require active transmission or signal measurement at the transponder.

The channel estimation uses a *active pilot sequence* $\mathbf{X} = \begin{bmatrix}\mathbf{x}_1 \cdots \mathbf{x}_L\end{bmatrix} \in \mathbb{C}^{N\times L}$ and a *passive load sequence* $\mathbf{g} = \begin{bmatrix}\Gamma_1 \cdots \Gamma_L\end{bmatrix}$, both having L symbols as illustrated in Fig. 4.7. The first L_0 symbols of the passive load sequence, $\Gamma_1, \ldots, \Gamma_{L_0}$ are all zeros, where $N \leq L_0 < L$. The active pilot symbols $\mathbf{x}_\ell$ and the passive load symbols Γ_ℓ are transmitted and selected in a synchronized manner. The reader's ℓ-th received signal $\mathbf{y}_\ell \in \mathbb{C}^{N\times 1}$ is written using (4.10) as

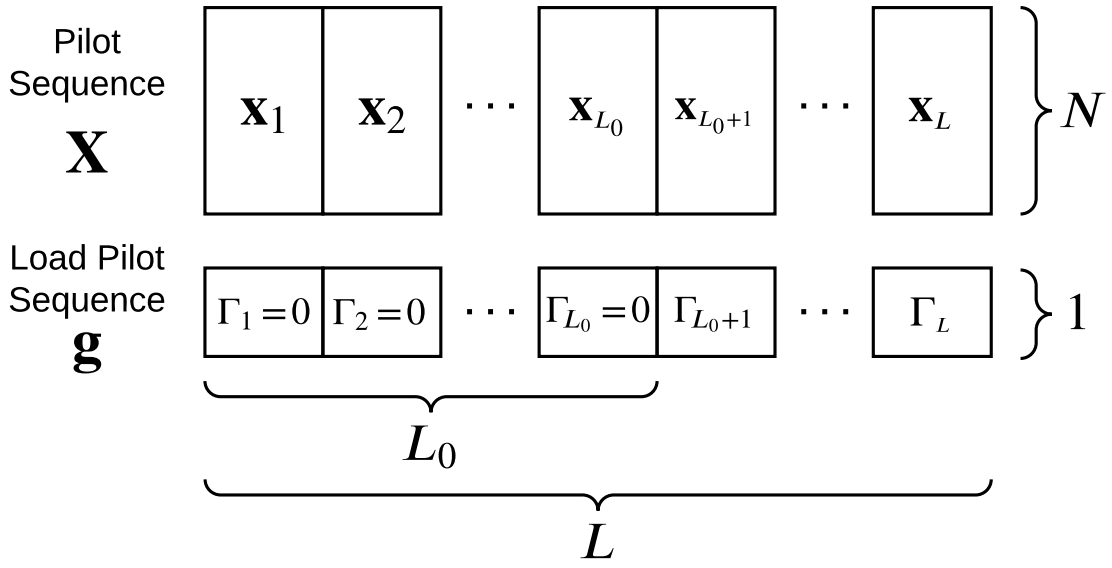

Figure 4.7. Illustration of pilot sequence for channel estimation.

$$\mathbf{y}_\ell = \left[\frac{\Gamma_\ell}{1 - s_{0,0}\Gamma_\ell}\,\mathbf{s}^\mathsf{T}\mathbf{s} + \mathbf{S}_\mathcal{R}\right]\mathbf{x}_\ell + \mathbf{w}_\ell. \tag{4.22}$$

The received signals (4.22) can be written in a matrix form $\mathbf{Y} = [\mathbf{y}_1 \ \cdots \ \mathbf{y}_L] \in \mathbb{C}^{N\times L}$ as

$$\mathbf{Y} = \mathbf{s}^\mathsf{T}\mathbf{s}\mathbf{X}\mathbf{\Gamma}\left(\mathbf{I}_L - s_{0,0}\mathbf{\Gamma}\right)^{-1} + \mathbf{S}_\mathcal{R}\mathbf{X} + \mathbf{W}, \tag{4.23}$$

where $\mathbf{\Gamma} = \mathrm{diag}(\mathbf{g}) \in \mathbb{C}^{L\times L}$ is a diagnonal reflection coefficient matrix and $\mathbf{W} = \left[\mathbf{w}_1 \ \cdots \ \mathbf{w}_L\right] \mathbb{C}^{N\times L}$ is noise.

The least squares (LS) channel estimation problem can now be formally written as

$$\underset{\hat{\mathbf{S}}_\mathcal{R},\,\hat{\mathbf{s}},\,\hat{s}_{0,0}}{\mathrm{argmin}} \left\|\mathbf{Y} - \hat{\mathbf{s}}^\mathsf{T}\hat{\mathbf{s}}\mathbf{X}\mathbf{\Gamma}\left(\mathbf{I}_L - \hat{s}_{0,0}\mathbf{\Gamma}\right)^{-1} - \hat{\mathbf{S}}_\mathcal{R}\mathbf{X}\right\|_F^2. \tag{4.24}$$

To solve this problem, we use an iterative method in which each iteration consists of the following initialization and three estimation steps.

Initialization: Find an initial estimate of $\hat{\mathbf{S}}_\mathcal{R}$. For a faster convergence, the initial estimate of $\hat{\mathbf{S}}_\mathcal{R}$ is obtained using the first L_0 estimation symbols. The received signal (4.22) for the first L_0 estimation symbols is simplified to $\mathbf{y}_\ell = \mathbf{S}_\mathcal{R}\mathbf{x}_\ell + \mathbf{w}_\ell$ since $\Gamma_\ell = 0$ where

$\ell = 1, \cdots, L_0$. Therefore, the received signals for the first L_0 symbols can be written in a matrix form as

$$\mathbf{Y}_0 = \mathbf{S}_{\mathcal{R}}\mathbf{X}_0 + \mathbf{W}_0, \tag{4.25}$$

where $\mathbf{Y}_0 = [\mathbf{y}_1 \ \cdots \ \mathbf{y}_{L_0}] \in \mathbb{C}^{N\times L_0}$, $\mathbf{X}_0 = \begin{bmatrix}\mathbf{x}_1 \ \cdots \ \mathbf{x}_{L_0}\end{bmatrix} \in \mathbb{C}^{N\times L_0}$ and $\mathbf{W}_0 = \begin{bmatrix}\mathbf{w}_1 \ \cdots \ \mathbf{w}_{L_0}\end{bmatrix} \in \mathbb{C}^{N\times L_0}$. The problem to compute the initial estimate of $\hat{\mathbf{S}}_{\mathcal{R}}$ is

$$\underset{\hat{\mathbf{S}}_{\mathcal{R}}}{\operatorname{argmin}} \left\|\mathbf{Y}_0 - \hat{\mathbf{S}}_{\mathcal{R}}\mathbf{X}_0\right\|_F^2. \tag{4.26}$$

The optimal solution to (4.26) is [92]

$$\hat{\mathbf{S}}_{\mathcal{R}} = \mathbf{Y}_0\mathbf{X}_0^{\mathsf{H}}\left(\mathbf{X}_0\mathbf{X}_0^{\mathsf{H}}\right)^{-1}.$$

Step 1: Optimize $\hat{\mathbf{s}}$ given $\hat{\mathbf{S}}_{\mathcal{R}}$ and $\hat{s}_{0,0}$. In this case, we consider the following optimization problem.

$$\underset{\hat{\mathbf{s}}}{\operatorname{argmin}} \left\|\mathbf{Y}_1 - \hat{\mathbf{s}}^{\mathsf{T}}\hat{\mathbf{s}}\mathbf{X}\boldsymbol{\Gamma}\left(\mathbf{I}_L - \hat{s}_{0,0}\boldsymbol{\Gamma}\right)^{-1}\right\|_F^2, \tag{4.27}$$

where

$$\mathbf{Y}_1 = \mathbf{Y} - \hat{\mathbf{S}}_{\mathcal{R}}\mathbf{X}$$

is the received signal after self-interference cancellation. Note that this optimization problem leaves a π-phase ambiguity in $\hat{\mathbf{s}}$ since $(-\hat{\mathbf{s}})^{\mathsf{T}}(-\hat{\mathbf{s}}) = \hat{\mathbf{s}}^{\mathsf{T}}\hat{\mathbf{s}}$. However, the phase ambiguity can be practically ignored in the system discussed in this paper.

To solve (4.27), we first replace $\hat{\mathbf{s}}^{\mathsf{T}}\hat{\mathbf{s}}$ with a new matrix $\hat{\mathbf{S}} \in \mathbb{C}^{N\times N}$ and the optimal $\hat{\mathbf{s}}$ is obtained from $\hat{\mathbf{S}}$ by enforcing the rank-one constraint. Specifically, we consider the following relaxed problem of (4.27).

$$\underset{\hat{\mathbf{S}}}{\operatorname{argmin}} \left\|\mathbf{Y}_1 - \hat{\mathbf{S}}\mathbf{Q}\right\|_F^2, \tag{4.28}$$

where

$$\mathbf{Q} = \mathbf{X}\boldsymbol{\Gamma}\left(\mathbf{I}_L - \hat{s}_{0,0}\boldsymbol{\Gamma}\right)^{-1}.$$

The optimal solution to (4.28) is

$$\hat{\mathbf{S}} = \mathbf{Y}_1\mathbf{Q}^{\mathsf{H}}\left(\mathbf{Q}\mathbf{Q}^{\mathsf{H}}\right)^{-1}.$$

The optimal solution to (4.27) is obtained by minimizing $\left\|\hat{\mathbf{S}} - \hat{\mathbf{s}}^{\mathsf{T}}\hat{\mathbf{s}}\right\|^2$, where $\hat{\mathbf{S}}$ is a sufficient statistic to estimate $\hat{\mathbf{S}}$ [87]. A rank-one approximation algorithm to find $\hat{\mathbf{s}}$ from $\hat{\mathbf{S}}$ is provided in [87]. Therefore, the procedure to find $\hat{\mathbf{s}}$ is omitted for brevity.

Step 2: Optimize $\hat{s}_{0,0}$ given $\hat{\mathbf{S}}_{\mathcal{R}}$ and $\hat{\mathbf{s}}$. To optimize $\hat{s}_{0,0}$, we consider the following optimization problem.

$$\underset{\hat{s}_{0,0}}{\operatorname{argmin}} \left\|\mathbf{Y}_1 - \hat{\mathbf{s}}^{\mathsf{T}}\hat{\mathbf{s}}\mathbf{X}\mathbf{\Gamma}\left(\mathbf{I}_L - \hat{s}_{0,0}\mathbf{\Gamma}\right)^{-1}\right\|_F^2 \tag{4.29}$$

It can be seen from (4.29) that $\hat{s}_{0,0}$ is nonlinear in $\mathbf{X}$ and $\mathbf{\Gamma}$. The optimal value of $\hat{s}_{0,0}$ can be found by a simple grid search by noting that $|s_{0,0}| \leq 1$ since the network is passive.

Step 3: Optimize $\hat{\mathbf{S}}_{\mathcal{R}}$ given $\hat{\mathbf{s}}$ and $\hat{s}_{0,0}$. Given the previous estimates $\hat{\mathbf{s}}$ and $\hat{s}_{0,0}$, compute a new estimate $\hat{\mathbf{S}}_{\mathcal{R}}$. The optimization problem is

$$\underset{\hat{\mathbf{S}}_{\mathcal{R}}}{\operatorname{argmin}} \left\|\mathbf{Y}_2 - \hat{\mathbf{S}}_{\mathcal{R}}\mathbf{X}\right\|_F^2, \tag{4.30}$$

where

$$\mathbf{Y}_2 = \mathbf{Y} - \hat{\mathbf{s}}^{\mathsf{T}}\hat{\mathbf{s}}\mathbf{X}\mathbf{\Gamma}\left(\mathbf{I}_L - \hat{s}_{0,0}\mathbf{\Gamma}\right)^{-1}.$$

The optimal solution to (4.30) is

$$\hat{\mathbf{S}}_{\mathcal{R}} = \mathbf{Y}_2\mathbf{X}^{\mathsf{H}}\left(\mathbf{X}\mathbf{X}^{\mathsf{H}}\right)^{-1}.$$

Note that the main difference between (4.26) and (4.30) is that all of the L estimation symbols are used to optimize $\hat{\mathbf{S}}_{\mathcal{R}}$ in (4.30) while only the first L_0 estimation symbols are used in (4.26).

The three estimation steps described above are iteratively performed until it satisfies a predetermined stopping condition (e.g., the difference in the squared error). Also, the least-

squares error (i.e., the cost function of (4.24)) is monotonically decreasing in the iterations since each of the optimal solutions to (4.27), (4.29), and (4.30) always reduces or keeps the previous error.

4.5 Simulation

In this section, the performances of the proposed wireless communication and power transfer methods are numerically analyzed using a practical inductive WPCN model.

4.5.1 System Setup

We consider a MISO inductive WPCN model in which a multi-coil reader communicates with a transponder equipped with a single coil. The model consists of four reader coils (coils 1 to 4) and a transponder coil, which is placed 25 mm below the reader coils, as shown in Fig. 4.8. This configuration is intended to simulate communication and power transfer with an agricultural sensor buried in the soil.

All of the reader coils have the same shape, with each having four turns and 42 mm in radius. The transponder coil has four turns and a 22 mm radius. Each of the five coils is connected to a compensating capacitor in series to make the coil resonant at the center frequency $f_c = 13.56\,\text{MHz}$. The scattering parameters are computed using ANSYS High Frequency Structure Simulator (HFSS). Throughout the simulation, the total transmit power and the receiver noise power are assumed to be $P_T = 1\,\text{W}$ and $\sigma^2 = 1\,\mu\text{W}$, respectively.

4.5.2 SNR-Power Regions for Coil Misalignment Scenarios

An advantage of a multi-coil reader is that misalignment of reader and transponder coils can be tolerated by adapting the transmit signal. In a conventional single-input single-output (SISO) inductively coupled model, a small coil misalignment may cause significant performance degradation. This section compares SNR-power regions of the proposed the multi-coil reader model against a conventional SISO model.

In this simulation, we consider two coil misalignment scenarios shown in Fig. 4.9, using MISO and SISO models. A conventional SISO WPCN is modeled by removing reader coils

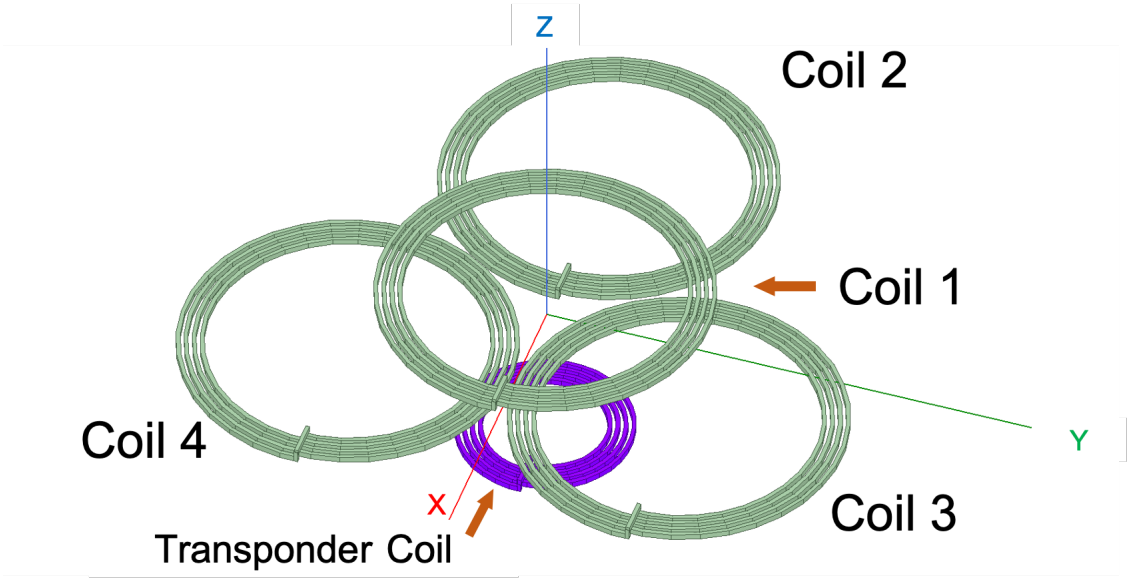

Figure 4.8. Reader and transponder coils for simulation. All coils are activated for the four-coil reader model. For a single-coil reader model, coils 2 to 4 are removed.

2, 3, and 4 from the configuration shown in Fig. 4.8. The first misalignment model is a non-coaxial coil scenario where the transponder coil is shifted by 40 mm to the y-direction with respect to the reader coil 1, as shown in Fig. 4.9a. The second scenario considers a case where the transponder coil is rotated 60° counterclockwise, as shown in Fig. 4.9b. For both scenarios, full CSI (S-parameters) at the reader is assumed.

The computed SNR-power regions are shown in Fig. 4.10. In both misalignment scenarios, the proposed multi-coil reader model achieved higher receive SNR and harvested power than the conventional single-coil reader model. Specifically, the multi-coil reader model harvests 3.5 times larger power and provides 11.6 dB higher receive SNR compared to the single-coil model in the 40 mm offset scenario. The performance improvement in the 60° rotation scenario is slightly smaller and the multi-coil reader model harvests 21 % more energy and gives 1.73 dB higher SNR than the single-coil reader model.

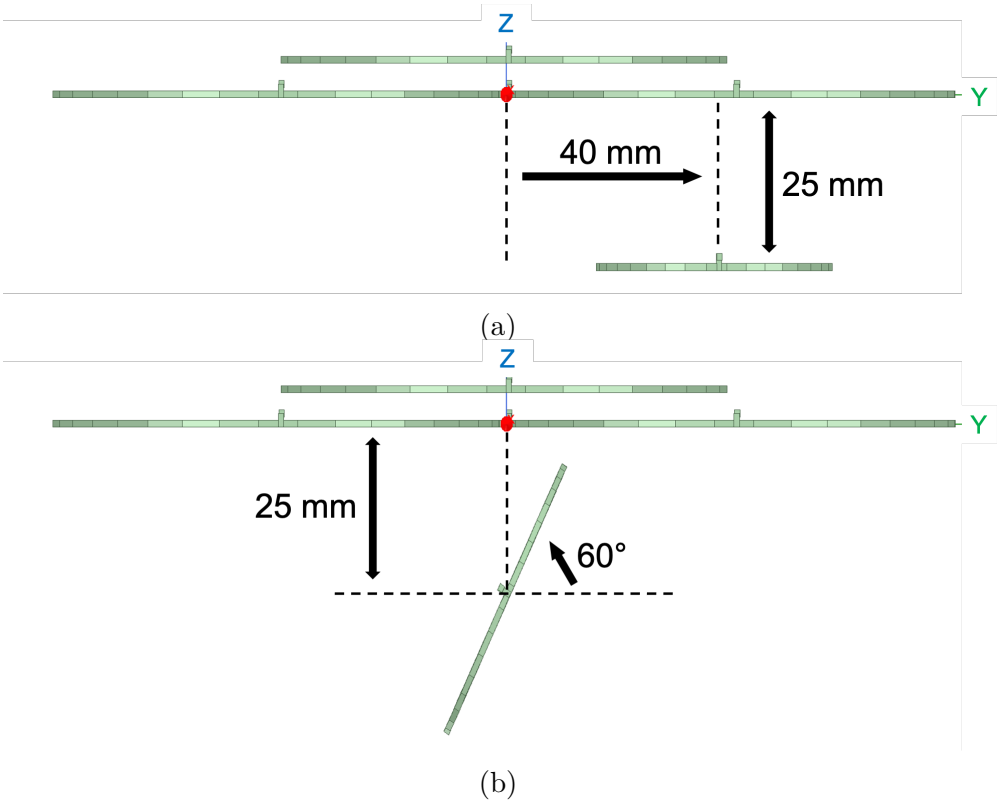

Figure 4.9. Front views of two misalignment scenarios. (a) The transponder coil is shifted by 40 mm in the y-direction. (b) The transponder coil is rotated 60° counterclockwise.

4.5.3 Channel Estimation

The performance of the proposed S-parameter estimation method was evaluated using the four-coil reader model shown in Fig. 4.8. Specifically, we computed the least-squares error (i.e., the cost function of (4.24)) and the squared errors $||\mathbf{S}_{\mathcal{R}} - \hat{\mathbf{S}}_{\mathcal{R}}||_F^2$, $\left\|\mathbf{s}^{\mathsf{T}}\mathbf{s} - \hat{\mathbf{s}}^{\mathsf{T}}\hat{\mathbf{s}}\right\|_F^2$, and $|s_{0,0} - \hat{s}_{0,0}|^2$. Note that we use $\mathbf{s}^{\mathsf{T}}\mathbf{s}$ instead of $\mathbf{s}$ to evaluate the error of $\hat{\mathbf{s}}$ since there exists a π-phase ambiguity in $\hat{\mathbf{s}}$ as discussed in Section 4.4.

In this simulation, we used an estimation sequence with length $L = 40$, which is generated from the first N rows of the $L \times L$ discrete Fourier transform (DFT) matrix. The first $L_0 = N$ symbols of the passive pilot sequence are all zeros, and the remaining $L - L_0$ symbols are generated by $\Gamma_\ell = \exp(j\theta_\ell)$, where $\theta_\ell = 2\pi(\ell - L_0)/(L - L_0)$ and $\ell = L_0 + 1, \ldots, L$. The grid search in the channel estimation used a set of complex numbers, which was generated

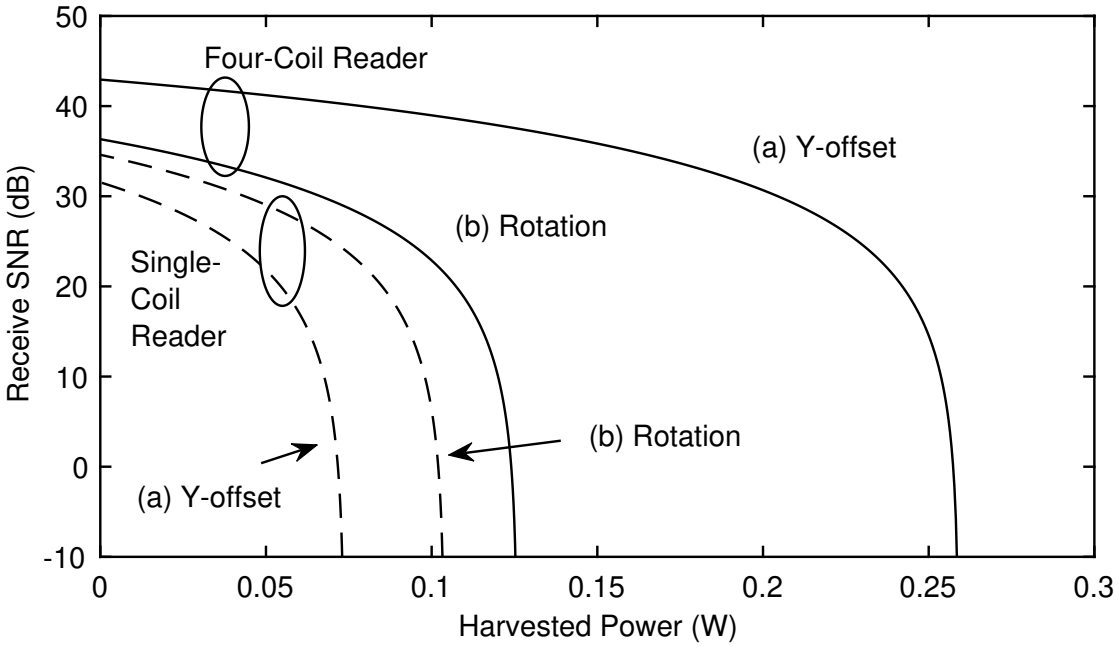

Figure 4.10. SNR-Power regions for two misalignment scenarios.

by incrementing each of the real and imaginary parts of a reflection coefficient from -1 to 1 by 0.01 step.

The simulation result is shown in Fig. 4.11. It can be seen that the squared errors reached less than 10^{-3} within the first ten iterations. The squared error in $\hat{s}_{0,0}$ significantly dropped in the first three iterations and remained at approximately 6×10^{-5} for the rest of the iterations. This behavior is due to the grid search in which only a discrete set of $s_{0,0}$ values are evaluated. The loss in the maximum harvested power and receive SNR due to the estimation error at iteration 20 are 1.4 % and 0.13 dB, respectively, compared to the full-CSI case.

4.5.4 Comparison of Load Design Methods

The symbol error rates (SERs) of the direct and predistortion-based load design methods are analyzed by Monte Carlo simulation. In this simulation, BPSK, QPSK, and 16-quadrature amplitude modulation (QAM) constellations are used, and the ratio of total signal source power P_T to the noise power σ^2 is varied from 0 dB to 25 dB. The result is

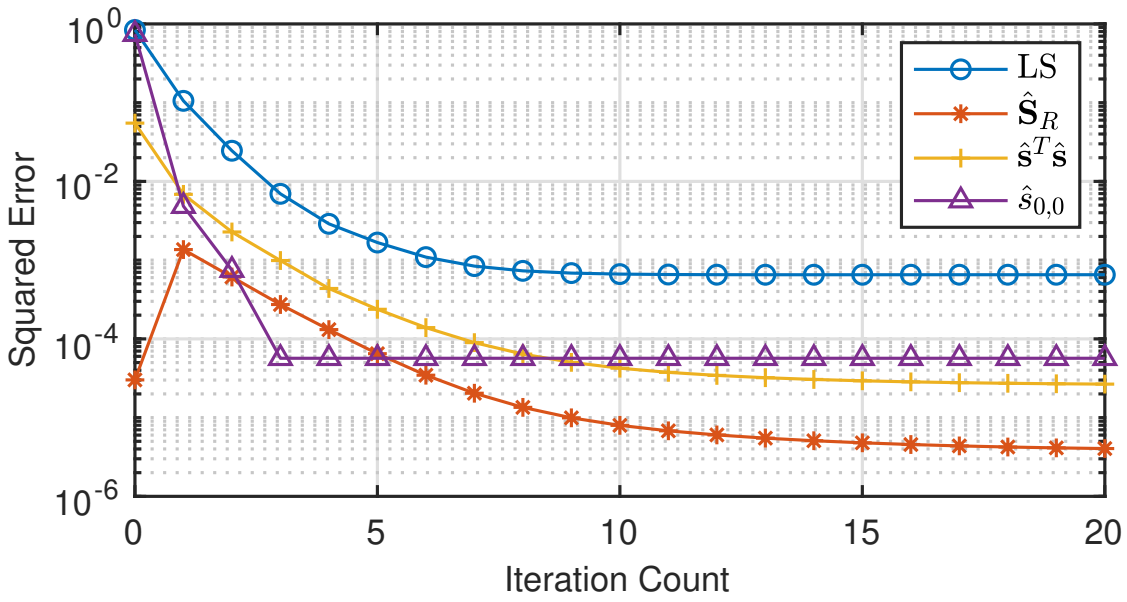

Figure 4.11. Least-squares error and the estimation errors in $\hat{\mathbf{S}}_{\mathcal{R}}$, $\hat{\mathbf{s}}^{\mathsf{T}}\hat{\mathbf{s}}$, and $\hat{s}_{0,0}$.

shown in Fig. 4.12. For all three constellations, the predistortion-based design method outperformed the direct design method. In particular, the error rate performances of the direct design method for QPSK and 16-QAM constellations are significantly worse than those of the predistortion design method.

To observe the cause of the significant SER degradation of the direct load design method with higher-order modulation schemes, the reflection coefficients and receive constellation of 16-QAM are shown in Fig. 4.13. The predistortion-based load design method generates equispaced 16-QAM constellation points, as can be seen from Fig. 4.13b. The direct load design method results in smaller distances between constellation points than the predistortion-based design method, making the constellation more vulnerable to additive noise.

4.6 Conclusion and Future Research Directions

An inductive WPCN was modeled based on the black-box approach, in which the channel and properties of coils are represented by a small number of scattering parameters. The optimal source signal vector that maximizes both the harvested and reflected powers is derived as a function of the scattering parameters. Since the inductive channel introduces a non-

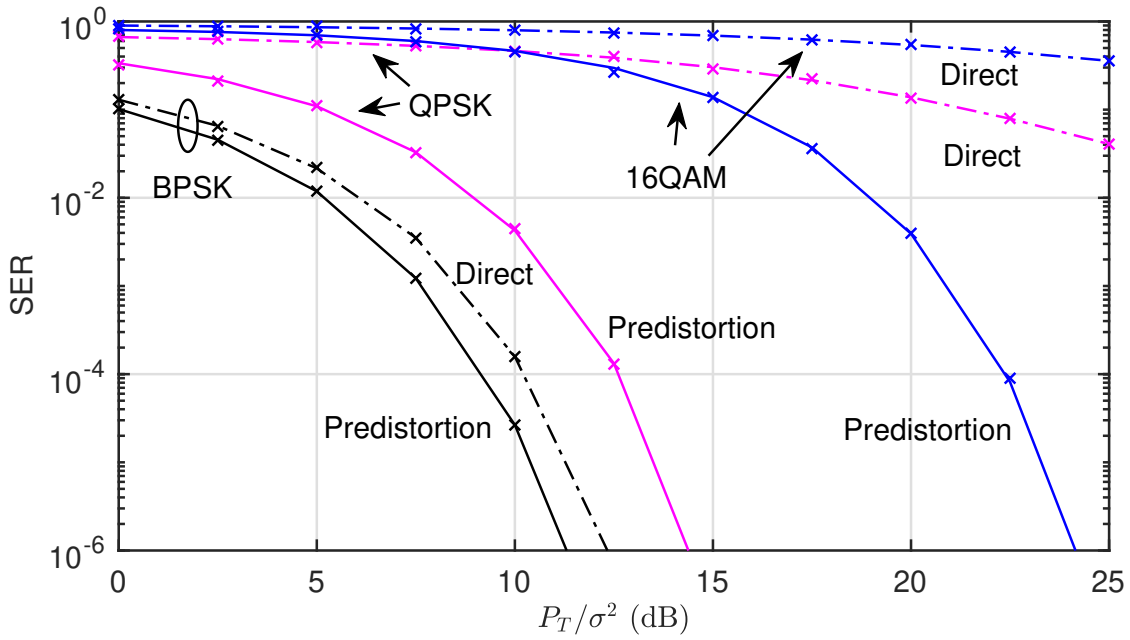

Figure 4.12. Symbol error rates for BPSK, QPSK, and 16-QAM.

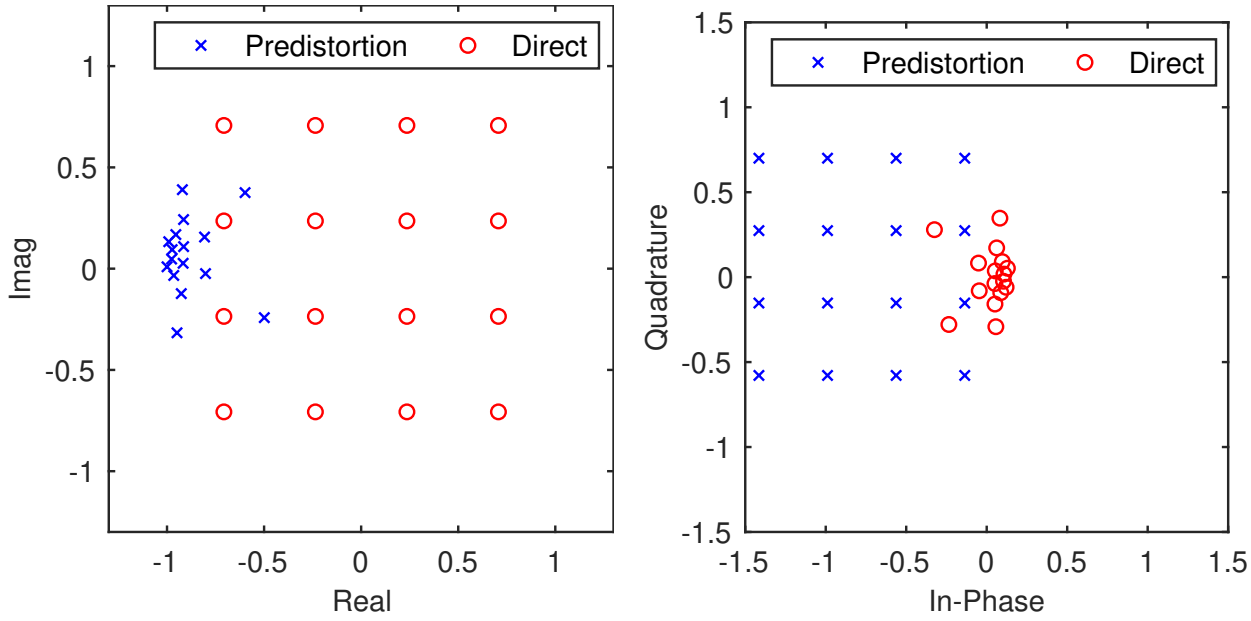

(a) Reflection coefficients $\mathcal{G}$

(b) Receive constellation $\mathcal{C}$

Figure 4.13. 16-QAM reflection coefficients $\mathcal{G}$ and receive constellation $\mathcal{C}$ of direct and predistortion-based load design methods.

linear transformation of the reflected signal, we proposed a method to design the reflection coefficients by predistorting the reflected signal by the load. A circuit estimation method

that simultaneously uses the active and passive pilot sequences was presented. The simulation showed that the proposed multi-coil reader model achieves higher SNR and delivered power than a single-coil reader model in coil misalignment scenarios. The performances of the proposed circuit estimation method and two load design methods were evaluated by numerical analysis using the multi-coil reader model.

The system model and analysis techniques for inductive WPCN discussed in this chapter provide various future research directions. Some of the potential research problems are listed below.

- **DC offset in receiver constellation**. The predistortion based load design often results in a receiver constellation with a constant DC offset from the origin. However, a DC offset is undesirable in standard wireless communication systems since it "wastes" the transmit signal power without improving communication performances. Therefore, the effect of DC offset in the receive constellation on the communication and power transfer performances should be further investigated.

- **Definition of signal power**. We defined the SNR as the ratio of the "signal power" associated with $\zeta(\Gamma)$ to the noise power. However, unlike conventional digital communication models in which the signal power is fully controlled by a transmitter, the signal power in the inductive WPCN model is determined by both the transponder, which is the source of the information, and the reader, which is the power source. Therefore, the definition of the "signal power" is somewhat vague in inductive WPCN. For a rigorous analysis of communication and power transfer performances, the definition of the signal power should be further discussed.

- **Error in load impedance**. As shown in the simulation on the predistortion-based load design, accurate control of the load reflection coefficient is essential. Since production tolerance or other environmental factors (e.g., ambient temperature) may cause a change in the load impedance value, performance degradation due to the error of impedance as well as methods to compensate for the error should be studied.

4.A Derivation of Channel Matrices

The channels $\mathbf{h}_D(\Gamma)$ and $\mathbf{H}(\Gamma_L)$ are derived from the scattering matrix of the $N+1$ port network shown in Fig. 4.2. The channels are obtained by solving the input-output relationship from the definition of the scattering parameters.

To find $\mathbf{h}_D(\Gamma)$ from the definition of scattering parameters, first recall that the signal y_i can be written as

$$y_i = \sum_{j=0}^{N} s_{i,j} x_j. \tag{4.31}$$

Since the reflection coefficient of the load is Γ, the relationship between the incident and reflected signals of port 0 is

$$x_0 = \Gamma y_0. \tag{4.32}$$

Using (4.31) and (4.32), the incident signal to the load (y_0) can be written as

$$\begin{aligned} y_0 &= \sum_{j=1}^{N} s_{0,j} x_j + s_{0,0}\Gamma y_0 \\ &= \mathbf{s}\mathbf{x} + s_{0,0}\Gamma y_0, \end{aligned} \tag{4.33}$$

where $\mathbf{s} = \begin{bmatrix} s_{0,1}\, s_{0,2}\, \cdots\, s_{0,N} \end{bmatrix}$ and $\mathbf{x} = \begin{bmatrix} x_1\, x_2 \ldots x_N \end{bmatrix}^{\mathsf{T}}$. Solving (4.33) for y_0, we get

$$y_0 = \underbrace{\frac{1}{1 - s_{0,0}\Gamma}}_{\mathbf{h}_D(\Gamma)} \mathbf{s}\,\mathbf{x}. \tag{4.34}$$

Therefore, the channel $\mathbf{h}_D(\Gamma)$ is obtained as shown in (4.34).

To find $\mathbf{H}(\Gamma)$, write for the incident signal to the i-th port, where $i = 1, 2, \ldots, N$, using (4.31), (4.32), and (4.34) as

$$\begin{aligned} y_i &= s_{i,0}\Gamma y_0 + \sum_{j=1}^{N} s_{i,j} x_j \\ &= \frac{s_{i,0}\Gamma}{1 - s_{0,0}\Gamma}\mathbf{s}\mathbf{x} + \sum_{j=1}^{N} s_{i,j} x_j. \end{aligned}$$

Noting the reciprocity assumption $s_{i,j} = s_{j,i}$, we can write y_i's in a vector form as

$$\mathbf{y} = \underbrace{\left(\frac{\Gamma}{1 - s_{0,0}\Gamma} \mathbf{s}^{\mathsf{T}}\mathbf{s} + \mathbf{S}_{\mathcal{R}} \right)}_{\mathbf{H}(\Gamma)} \mathbf{x}, \tag{4.35}$$

where $\mathbf{y} = \begin{bmatrix} y_1 \cdots y_N \end{bmatrix}^{\mathsf{T}}$ and $\mathbf{S}_{\mathcal{R}}$ is an $N \times N$ matrix whose (i, j)-element is $s_{i+1,j+1}$. Therefore, the channel $\mathbf{H}(\Gamma)$ is obtained as shown in (4.35).

4.B Proof of Theorem 1

Proof. $\zeta(\cdot)$ is a Möbius transformation [93]. Since $|s_{0,0}| < 1$ and $|\Gamma| \leq 1$, we have $1 - s_{0,0}\Gamma \neq 0$. Thus, $\zeta(\cdot)$ transforms a disk $D_1 = \{\Gamma \in \mathbb{C} : |\Gamma| \leq 1\}$ to another disk $D_2 = \{z \in \mathbb{C} : |z - a| \leq r\}$, where a and r are the center and radius of the disk D_2. To find a and r, first consider antipodal points $\pm |s_{0,0}| / s_{0,0}$ on the boundary of D_1. Since these two points are also on a line that passes through both the center of D_1 and the center of inversion $1/s_{0,0}$, the transformed points $p_1 = \zeta(|s_{0,0}| / s_{0,0})$ and $p_2 = \zeta(- |s_{0,0}| / s_{0,0})$ are also antipodal points on the boundary of D_2. Thus, a and r are given by $r = |p_1 - p_2| / 2$ and $a = (p_1 + p_2)/2$. □

5. SUMMARY

In this dissertation, three types of inductive WPC operating modes, namely, WPT, SWIPT, and WPCN, were considered. The black-box model, a well-known technique in the wireless communications and signal processing community to represent unknown channel properties by a small number of measurable parameters, is applied to the inductively coupled circuit systems. This approach eliminates the necessity of solving a complex circuit system that involves self and mutual inductances of coils and parasitic components that exist in various parts of an inductive WPC system. Furthermore, this approach allows us to apply well-studied signal processing techniques, including beamforming, receive combining, and channel estimations, to inductively coupled systems.

First, we studied PTE optimizations for WPT from multiple transmit coils to a single receiver coil that is connected to a passive load. We applied the black-box approach to a MISO inductive WPT model. Based on the proposed model, the optimal source current vector that maximizes the power transfer efficiency was derived. Also, a simple estimation method to determine the unknown channel parameters was proposed. An experimental model consisting of four transmit and two receive coils showed an improvement in efficiency compared to the conventional equal power and conjugate beamforming solutions.

Secondly, an inductive MIMO SWIPT system, in which both data and energy are transferred from a multi-coil transmitter to a multi-coil receiver, was considered. The system was modeled based on the black-box approach in which the unknown channel was represented by scattering parameters. We derived the optimal transmit covariance matrices for the maximum harvested power, maximum data rate, and the maximum data rate with the minimum harvested power constraint. We modeled direct-fed and indirect-fed inductive MIMO SWIPT configurations and presented a rate-energy region for each of the models using FEM simulations.

Lastly, we investigated an inductive WPCN where energy is transferred from a multi-coil reader to a single-coil transponder while data is transferred from the transponder to the reader. The information is transferred by a complex passive load modulation which dynamically changes the transponder's load impedance to embed information to the reflected

signal. The black-box circuit system is represented by scattering parameters, similar to the SWIPT model. We derived the optimal transmit signal vector and receive combiners that maximize the harvested energy and the receive SNR. Furthermore, we proposed a least-squares channel estimation method that does not require signal measurement or active signal transmission at the transponder. The improvements in the harvested power and receive SNR were shown by comparing the proposed multi-coil reader model to the conventional single-coil reader model in coil misalignment scenarios. Furthermore, the performance of the proposed channel estimation technique was evaluated by numerical analysis.

The inductive WPC systems proposed in this dissertation open up various research opportunities. Some of the open research problems on inductive WPC are listed below.

- **Stochastic channel modeling**. Throughout the dissertation, inductive wireless channels (i.e., the parameters that define the properties of black-boxes) are assumed to be deterministic. However, the wireless channels in practical deployment scenarios involve impairment due to mobility or random coil misalignments, which may be stochastically modeled in analogous to far-field channel modeling techniques.

- **Multi-user WPC**. Wireless charging and communication for multiple devices would be of interest in order to make the proposed WPC systems more scalable. This may require changes to the black-box network models. Note that all three proposed models can be used without any modifications in a scenario where a transmitter (or a reader) communicates with or transfers energy to one of the multiple devices at a time. This can be done by treating all the other devices as loss elements of a wireless channel.

- **Wideband channel analysis**. Wireless communication requires nonzero bandwidth to transfer information. In the SWIPT and WPCN analyses of this dissertation, it was assumed that the bandwidth was sufficiently narrow and the gain was constant over the bandwidth of interest. However, it is known that the inductively coupled circuits form a frequency selective channel since the inductors (and capacitors for resonant coupling systems) act as an analog filter [88], [94]. Therefore, a performance analysis that takes into account the frequency selectivity of the inductive channels would be necessary, especially when a high data-rate communication channel is considered.

- **Coil design**. The mutual inductances of coils are affected by the shape and geometry of inductors. While this dissertation did not consider optimizations of coil shapes or placements, careful consideration of coil properties is necessary to deploy the system.

- **Experimental verification**. The information and power transfer performances of the proposed SWIPT and WPCN systems are analyzed using the coil models designed on FEM software. In order to confirm the validity of the proposed schemes, it is desirable to implement the WPC hardware and obtain the experimental results.

Inductive WPC is a new research area with great potential to achieve robust and energy-efficient wireless power transfer and communication using the near-field inductive coupling technique. In order to utilize the proposed systems in practical deployment scenarios, further analysis of models and performances of inductive WPC is desired.

REFERENCES

[1] S. Bi, C. K. Ho, and R. Zhang, "Wireless powered communication: Opportunities and challenges," *IEEE Communications Magazine*, vol. 53, no. 4, pp. 117–125, Apr. 2015, ISSN: 0163-6804. DOI: 10.1109/MCOM.2015.7081084. [Online]. Available: http://ieeexplore.ieee.org/document/7081084/.

[2] S. Y. R. Hui, W. Zhong, and C. K. Lee, "A critical review of recent progress in mid-range wireless power transfer," *IEEE Transactions on Power Electronics*, vol. 29, no. 9, pp. 4500–4511, Sep. 2014, ISSN: 0885-8993. DOI: 10.1109/TPEL.2013.2249670. [Online]. Available: http://ieeexplore.ieee.org/document/6472081/.

[3] N. Tesla, "Apparatus for transmitting electrical energy," US Patent 1,119,732, Dec. 1914.

[4] A. Kurs, A. Karalis, R. Moffatt, J. D. Joannopoulos, P. Fisher, and M. Soljacic, "Wireless power transfer via strongly coupled magnetic resonances," *Science*, vol. 317, no. 5834, pp. 83–86, Jul. 2007. DOI: 10.1126/science.1143254. [Online]. Available: http://science.sciencemag.org/content/317/5834/83.short.

[5] I. Cortes and W.-J. Kim, "Lateral position error reduction using misalignment-sensing coils in inductive power transfer systems," *IEEE/ASME Transactions on Mechatronics*, vol. 23, no. 2, pp. 875–882, Apr. 2018. DOI: 10.1109/tmech.2018.2801250.

[6] R. Zhang and C. Ho, "MIMO broadcasting for simultaneous wireless information and power transfer," *IEEE Transactions on Wireless Communications*, vol. 12, no. 5, pp. 1989–2001, May 2013, ISSN: 1536-1276. DOI: 10.1109/TWC.2013.031813.120224.

[7] T. Arakawa, J. V. Krogmeier, and D. J. Love, "Simultaneous wireless information and power transfer: An S-parameter approach," in *Proc. 2019 Asilomar Conf. Sig., Sys, and Comp*, Nov. 2019, pp. 1896–1900.

[8] S. Bi, Y. Zeng, and R. Zhang, "Wireless powered communication networks: An overview," *IEEE Wireless Communications*, vol. 23, no. 2, pp. 10–18, Apr. 2016. DOI: 10.1109/mwc.2016.7462480.

[9] T. Arakawa, J. V. Krogmeier, and D. J. Love, "Waveform optimization for near-field wireless powered communication using a coil array," in *Proc. 2020 Asilomar Conf. Sig., Sys, and Comp*, to be published, Nov. 2020.

[10] T. Arakawa, S. Goguri, J. V. Krogmeier, A. Kruger, D. J. Love, R. Mudumbai, and M. A. Swabey, "Optimizing wireless power transfer from multiple transmit coils," *IEEE Access*, vol. 6, pp. 23 828–23 838, 2018. DOI: 10.1109/ACCESS.2018.2825290.

[11] K. Finkenzeller, *RFID Handbook: Fundamentals and Applications in Contactless Smart Cards, Radio Frequency Identification and near-Field Communication*. Wiley, 2010, ISBN: 9780470695067. DOI: 10.1002/9780470665121.

[12] J. Garnica, R. A. Chinga, and J. Lin, "Wireless Power Transmission: From Far Field to Near Field," *Proceedings of the IEEE*, vol. 101, no. 6, pp. 1321–1331, Jun. 2013, ISSN: 0018-9219. DOI: 10.1109/JPROC.2013.2251411. [Online]. Available: http://ieeexplore.ieee.org/document/6494253/.

[13] A. Costanzo, M. Dionigi, D. Masotti, M. Mongiardo, G. Monti, L. Tarricone, and R. Sorrentino, "Electromagnetic energy harvesting and wireless power transmission: A unified approach," *Proceedings of the IEEE*, vol. 102, no. 11, pp. 1692–1711, Nov. 2014, ISSN: 0018-9219. DOI: 10.1109/JPROC.2014.2355261. [Online]. Available: http://ieeexplore.ieee.org/document/6916985/.

[14] X. Lu, D. Niyato, P. Wang, and D. I. Kim, "Wireless charger networking for mobile devices: Fundamentals, standards, and applications," *IEEE Wireless Communications*, vol. 22, no. 2, pp. 126–135, Apr. 2015, ISSN: 1536-1284. DOI: 10.1109/MWC.2015.7096295. [Online]. Available: http://ieeexplore.ieee.org/document/7096295/.

[15] S. Hui and W. Ho, "A new generation of universal contactless battery charging platform for portable consumer electronic equipment," in *2004 IEEE 35th Annual Power Electronics Specialists Conference*, IEEE, Jun. 2004, pp. 638–644, ISBN: 0-7803-8399-0. DOI: 10.1109/PESC.2004.1355823.

[16] V. Chawla and D. S. Ha, "An overview of passive RFID," *IEEE Communications Magazine*, vol. 45, no. 9, pp. 11–17, Apr. 2007. DOI: 10.1109/MCOM.2007.4342873.

[17] B. H. Waters, A. P. Sample, P. Bonde, and J. R. Smith, "Powering a Ventricular Assist Device (VAD) With the Free-Range Resonant Electrical Energy Delivery (FREE-D) System," *Proceedings of the IEEE*, vol. 100, no. 1, pp. 138–149, Jan. 2012, ISSN: 0018-9219. DOI: 10.1109/JPROC.2011.2165309. [Online]. Available: http://ieeexplore.ieee.org/document/6032700/.

[18] S. Mutashar, M. A. Hannan, S. A. Samad, and A. Hussain, "Analysis of transcutaneous inductive powering links," in *ICIAS 2012 - 2012 4th International Conference on Intelligent and Advanced Systems: A Conference of World Engineering, Science and Technology Congress (ESTCON) - Conference Proceedings*, 2012, ISBN: 9781457719677. DOI: 10.1109/ICIAS.2012.6306160.

[19] G. A. Covic and J. T. Boys, "Modern trends in inductive power transfer for transportation applications," *IEEE Journal of Emerging and Selected Topics in Power Electronics*, vol. 1, no. 1, pp. 28–41, Mar. 2013. DOI: 10.1109/jestpe.2013.2264473.

[20] *System description wireless power transfer*, Wireless Power Consortium Standards, Apr. 2011.

[21] *A4wp wireless power transfer system baseline system specification (bss)*, AirFuel Alliance, Nov. 2014.

[22] Z. N. Low, R. A. Chinga, R. Tseng, and J. Lin, "Design and test of a high-power high-efficiency loosely coupled planar wireless power transfer system," *IEEE Transactions on Industrial Electronics*, vol. 56, no. 5, pp. 1801–1812, May 2009.

[23] G. Wang, W. Liu, M. Sivaprakasam, and G. A. Kendir, "Design and analysis of an adaptive transcutaneous power telemetry for biomedical implants," *IEEE Transactions on Circuits and Systems—Part I: Fundamental Theory and Applications*, vol. 52, no. 10, pp. 2109–2117, Oct. 2005.

[24] M. Kiani and M. Ghovanloo, "The circuit theory behind coupled-mode magnetic resonance-based wireless power transmission," *IEEE Transactions on Circuits and Systems—Part I: Regular Papers*, vol. 59, no. 9, pp. 2065–2074, Sep. 2012. DOI: 10.1109/tcsi.2011.2180446.

[25] S. Cheon, Y.-H. Kim, S.-Y. Kang, M. L. Lee, J.-M. Lee, and T. Zyung, "Circuit-model-based analysis of a wireless energy-transfer system via coupled magnetic resonances," *IEEE Transactions on Industrial Electronics*, vol. 58, no. 7, pp. 2906–2914, Jul. 2011, ISSN: 0278-0046. DOI: 10.1109/TIE.2010.2072893. [Online]. Available: http://ieeexplore.ieee.org/document/5560805/.

[26] W. Hu, L. Yi, Z. Liu, and H. Yan, "Loss analysis and improvement of all parts of magnetic resonant wireless power transfer system," in *2015 Chinese Automation Congress (CAC)*, IEEE, Nov. 2015, pp. 2251–2256, ISBN: 978-1-4673-7189-6. DOI: 10.1109/CAC.2015.7382878. [Online]. Available: http://ieeexplore.ieee.org/document/7382878/.

[27] D. Chen, L. Wang, C. Liao, and Y. Guo, "The power loss analysis for resonant wireless power transfer," in *2014 IEEE Conference and Expo Transportation Electrification Asia-Pacific (ITEC Asia-Pacific)*, IEEE, Aug. 2014, pp. 1–4, ISBN: 978-1-4799-4239-8. DOI: 10.1109/ITEC-AP.2014.6940952. [Online]. Available: http://ieeexplore.ieee.org/lpdocs/epic03/wrapper.htm?arnumber=6940952.

[28] T. C. Beh, M. Kato, T. Imura, S. Oh, and Y. Hori, "Automated Impedance Matching System for Robust Wireless Power Transfer via Magnetic Resonance Coupling," *IEEE Transactions on Industrial Electronics*, vol. 60, no. 9, pp. 3689–3698, Sep. 2013, ISSN: 0278-0046. DOI: 10.1109/TIE.2012.2206337. [Online]. Available: http://ieeexplore.ieee.org/document/6226848/.

[29] D. Nie, B. M. Hochwald, and E. Stauffer, "Systematic Design of Large-Scale Multiport Decoupling Networks," *IEEE Transactions on Circuits and Systems—Part I: Regular Papers*, vol. 61, no. 7, pp. 2172–2181, Jul. 2014, ISSN: 1549-8328. DOI: 10.1109/TCSI.2014.2304666. [Online]. Available: http://ieeexplore.ieee.org/document/6776537/.

[30] R. Fano, "Theoretical limitations on the broadband matching of arbitrary impedances," *J. Franklin Inst.*, vol. 249, no. 1, pp. 57–83, 1950, ISSN: 0016-0032. DOI: https://doi.org/10.1016/0016-0032(50)90006-8.

[31] A. P. Sample, D. A. Meyer, and J. R. Smith, "Analysis, experimental results, and range adaptation of magnetically coupled resonators for wireless power transfer," *IEEE Transactions on Industrial Electronics*, vol. 58, no. 2, pp. 544–554, Feb. 2011. DOI: 10.1109/TIE.2010.2046002.

[32] R. Johari, J. V. Krogmeier, and D. J. Love, "Analysis and practical considerations in implementing multiple transmitters for wireless power transfer via coupled magnetic resonance," *IEEE Trans. Ind. Electron.*, vol. 61, no. 4, pp. 1774–1783, Apr. 2014, ISSN: 0278-0046. DOI: 10.1109/TIE.2013.2263780. [Online]. Available: http://ieeexplore.ieee.org/lpdocs/epic03/wrapper.htm?arnumber=6517242.

[33] D. Ahn and S. Hong, "Effect of coupling between multiple transmitters or multiple receivers on wireless power transfer," *IEEE Transactions on Industrial Electronics*, vol. 60, no. 7, pp. 2602–2613, Jul. 2013, ISSN: 0278-0046. DOI: 10.1109/TIE.2012.2196902. [Online]. Available: http://ieeexplore.ieee.org/document/6192319/.

[34] *Electronic Code of Federal Regulations, Part 15: Radio Frequency Devices, F. C. Commission*, vol. Title 47: Telecommunication (47 CFR 15), 2014.

[35] N. Oodachi, K. Ogawa, H. Kudo, H. Shoki, S. Obayashi, and T. Morooka, "Efficiency improvement of wireless power transfer via magnetic resonance using transmission coil array," in *2011 IEEE Int. Symp. Antennas and Propagation (APSURSI)*, Jul. 2011, pp. 1707–1710.

[36] I.-J. Yoon and H. Ling, "Investigation of near-field wireless power transfer under multiple transmitters," *IEEE Antennas and Wireless Propagation Letters*, vol. 10, pp. 662–665, Jun. 2011.

[37] J. Jadidian and D. Katabi, "Magnetic MIMO: how to charge your phone in your pocket," in *Proc. 20th annual international conference on Mobile computing and networking (MobiCom '14)*, New York, New York, USA: ACM Press, 2014, pp. 495–506, ISBN: 9781450327831. DOI: 10.1145/2639108.2639130. [Online]. Available: http://dl.acm.org/citation.cfm?doid=2639108.2639130.

[38] B. H. Waters, B. J. Mahoney, V. Ranganathan, and J. R. Smith, "Power delivery and leakage field control using an adaptive phased array wireless power system," *IEEE Transactions on Power Electronics*, vol. 30, no. 11, pp. 6298–6309, Nov. 2015.

[39] H.-D. Lang, A. Ludwig, and C. D. Sarris, "Convex optimization of wireless power transfer systems with multiple transmitters," *IEEE Transactions on Antennas and Propagation*, vol. 62, no. 9, pp. 4623–4636, Sep. 2014. DOI: 10.1109/tap.2014.2330584.

[40] G. Yang, M. R. V. Moghadam, and R. Zhang, "Magnetic MIMO signal processing and optimization for wireless power transfer," *IEEE Transactions on Signal Processing*, vol. 65, no. 11, pp. 2860–2874, Jun. 2017. DOI: 10.1109/tsp.2017.2673816.

[41] M. Biguesh and A. Gershman, "Training-based MIMO channel estimation: A study of estimator tradeoffs and optimal training signals," *IEEE Transactions on Signal Processing*, vol. 54, no. 3, pp. 884–893, Mar. 2006, ISSN: 1053-587X. DOI: 10.1109/TSP.2005.863008. [Online]. Available: http://ieeexplore.ieee.org/document/1597555/.

[42] R. A. DeCarlo and P.-M. Lin, *Linear Circuit Analysis: Time Domain, Phasor, and Laplace Transform Approaches*, 2nd. Oxford University Press, 2001, p. 1024.

[43] B. Zhao, N.-C. Kuo, and A. M. Niknejad, "A gain boosting array technique for weakly-coupled wireless power transfer," *IEEE Transactions on Power Electronics*, vol. 32, no. 9, pp. 7130–7139, Sep. 2017, ISSN: 0885-8993. DOI: 10.1109/TPEL.2016.2626473. [Online]. Available: http://ieeexplore.ieee.org/document/7738583/.

[44] T. Arakawa, J. V. Krogmeier, and D. J. Love, "MIMO simultaneous wireless information and power transfer over inductively coupled circuits," submitted for publication.

[45] L. R. Varshney, "Transporting information and energy simultaneously," in *Proc. IEEE Int. Symp. Inf. Theory*, IEEE, Jul. 2008, pp. 1612–1616. DOI: 10.1109/isit.2008.4595260.

[46] B. Clerckx, R. Zhang, R. Schober, D. W. K. Ng, D. I. Kim, and H. V. Poor, "Fundamentals of wireless information and power transfer: From RF energy harvester models to signal and system designs," *IEEE Journal on Selected Areas in Communications*, vol. 37, no. 1, pp. 4–33, Jan. 2019. DOI: 10.1109/jsac.2018.2872615.

[47] I. Krikidis, S. Timotheou, S. Nikolaou, G. Zheng, D. W. K. Ng, and R. Schober, "Simultaneous wireless information and power transfer in modern communication systems," *IEEE Communications Magazine*, vol. 52, no. 11, pp. 104–110, Nov. 2014, ISSN: 0163-6804. DOI: 10.1109/MCOM.2014.6957150. [Online]. Available: http://ieeexplore.ieee.org/lpdocs/epic03/wrapper.htm?arnumber=6957150.

[48] A. Costanzo and D. Masotti, "Energizing 5G: Near- and far-field wireless energy and data trantransfer as an enabling technology for the 5G IoT," *IEEE Microwave Magazine*, vol. 18, no. 3, pp. 125–136, May 2017. DOI: 10.1109/mmm.2017.2664001.

[49] T. D. P. Perera, D. N. K. Jayakody, S. K. Sharma, S. Chatzinotas, and J. Li, "Simultaneous wireless information and power transfer (SWIPT): Recent advances and future challenges," *IEEE Communications Surveys and Tutorials*, vol. 20, no. 1, pp. 264–302, 2018. DOI: 10.1109/comst.2017.2783901.

[50] K. Huang and E. Larsson, "Simultaneous information and power transfer for broadband wireless systems," *IEEE Transactions on Signal Processing*, vol. 61, no. 23, pp. 5972–5986, Dec. 2013. DOI: 10.1109/tsp.2013.2281026.

[51] J. Xu, L. Liu, and R. Zhang, "Multiuser MISO beamforming for simultaneous wireless information and power transfer," *IEEE Transactions on Signal Processing*, vol. 62, no. 18, pp. 4798–4810, Sep. 2014. DOI: 10.1109/tsp.2014.2340817.

[52] Z. Zhang, H. Pang, A. Georgiadis, and C. Cecati, "Wireless power transfer - an overview," *IEEE Transactions on Industrial Electronics*, pp. 1044–1058, 2018. DOI: 10.1109/tie.2018.2835378.

[53] Cost Action IC1301 Team, "Europe and the future for WPT : European contributions to wireless power transfer technology," *IEEE Microw. Mag.*, vol. 18, no. 4, pp. 56–87, Jun. 2017. DOI: 10.1109/mmm.2017.2680078.

[54] I. Mayordomo, T. Drager, P. Spies, J. Bernhard, and A. Pflaum, "An overview of technical challenges and advances of inductive wireless power transmission," *Proceedings of the IEEE*, vol. 101, no. 6, pp. 1302–1311, Jun. 2013. DOI: 10.1109/jproc.2013.2243691.

[55] Z. Liu, Z. Chen, C. Peng, J. Liang, P. Xiao, L. Bian, Y. Qiu, and G. Li, "A misalignment resilient system for magnetically coupled resonant wireless power transfer," *IEEE Transactions on Antennas and Propagation*, vol. 68, no. 12, pp. 8260–8265, Dec. 2020. DOI: 10.1109/tap.2020.2996749.

[56] F. Jolani, Y. Yu, and Z. Chen, "A planar magnetically coupled resonant wireless power transfer system using printed spiral coils," *IEEE Antennas and Wireless Propagation Letters*, vol. 13, pp. 1648–1651, 2014. DOI: 10.1109/lawp.2014.2349481.

[57] Q. Yuan, Q. Chen, L. Li, and K. Sawaya, "Numerical analysis on transmission efficiency of evanescent resonant coupling wireless power transfer system," *IEEE Transactions on Antennas and Propagation*, vol. 58, no. 5, pp. 1751–1758, May 2010. DOI: 10.1109/tap.2010.2044321.

[58] J. Park, Y. Tak, Y. Kim, Y. Kim, and S. Nam, "Investigation of adaptive matching methods for near-field wireless power transfer," *IEEE Transactions on Antennas and Propagation*, vol. 59, no. 5, pp. 1769–1773, May 2011. DOI: 10.1109/tap.2011.2123061.

[59] R. Bansal, "Near-field magnetic communication," *IEEE Antennas and Propagation Magazine*, vol. 46, no. 2, pp. 114–115, Apr. 2004, ISSN: 1045-9243. DOI: 10.1109/MAP.2004.1305555.

[60] U. Azad, H. C. Jing, and Y. E. Wang, "Link budget and capacity performance of inductively coupled resonant loops," *IEEE Transactions on Antennas and Propagation*, vol. 60, no. 5, pp. 2453–2461, May 2012. DOI: 10.1109/tap.2012.2189696.

[61] H.-J. Kim, J. Park, K.-S. Oh, J. P. Choi, J. E. Jang, and J.-W. Choi, "Near-field magnetic induction MIMO communication using heterogeneous multipole loop antenna array for higher data rate transmission," *IEEE Transactions on Antennas and Propagation*, vol. 64, no. 5, pp. 1952–1962, May 2016. DOI: 10.1109/tap.2016.2539371.

[62] Y. Morag, N. Tal, Y. Leviatan, and Y. Levron, "Channel capacity of magnetic communication in a general medium incorporating full-wave analysis and high-frequency effects," *IEEE Transactions on Antennas and Propagation*, vol. 67, no. 6, pp. 4104–4118, Jun. 2019. DOI: 10.1109/tap.2019.2902707.

[63] Z. Sun and I. F. Akyildiz, "Magnetic induction communications for wireless underground sensor networks," *IEEE Transactions on Antennas and Propagation*, vol. 58, no. 7, pp. 2426–2435, Jul. 2010, ISSN: 0018-926X. DOI: 10.1109/TAP.2010.2048858. [Online]. Available: http://ieeexplore.ieee.org/lpdocs/epic03/wrapper.htm?arnumber=5452976.

[64] M. C. Domingo, "Magnetic induction for underwater wireless communication networks," *IEEE Transactions on Antennas and Propagation*, vol. 60, no. 6, pp. 2929–2939, Jun. 2012. DOI: 10.1109/tap.2012.2194670.

[65] P. Grover and A. Sahai, "Shannon meets Tesla: Wireless information and power transfer," in *Proc. IEEE Int. Symp. Inf. Theory*, Jun. 2010, pp. 2363–2367, ISBN: 978-1-4244-7892-7. DOI: 10.1109/ISIT.2010.5513714.

[66] S. Kisseleff, I. F. Akyildiz, and W. H. Gerstacker, "Magnetic induction based simultaneous wireless information and power transfer for single information and multiple power receivers," *IEEE Transactions on Communications*, vol. 65, no. 3, pp. 1396–1410, Mar. 2017, ISSN: 0090-6778. DOI: 10.1109/TCOMM.2016.2646684. [Online]. Available: http://ieeexplore.ieee.org/document/7802585/.

[67] D. Tse and P. Viswanath, *Fundamentals of Wireless Communication*. New York: Cambridge University Press, 2005, ISBN: 0521845270.

[68] Z. Sun, I. F. Akyildiz, S. Kisseleff, and W. Gerstacker, "Increasing the capacity of magnetic induction communications in RF-challenged environments," *IEEE Transactions on Communications*, vol. 61, no. 9, pp. 3943–3952, Sep. 2013. DOI: 10.1109/tcomm.2013.071813.120600.

[69] D. M. Pozar, *Microwave Engineering*, 2nd ed. Wiley, 2005, p. 700, ISBN: 0471448788.

[70] J.-M. Jin, *The finite element method in electromagnetics*. John Wiley & Sons, 2015.

[71] J. Wallace and M. Jensen, "Mutual coupling in MIMO wireless systems: A rigorous network theory analysis," *IEEE Transactions on Wireless Communications*, vol. 3, no. 4, pp. 1317–1325, Jul. 2004. DOI: 10.1109/twc.2004.830854.

[72] M. Morris and M. Jensen, "Network model for MIMO systems with coupled antennas and noisy amplifiers," *IEEE Transactions on Antennas and Propagation*, vol. 53, no. 1, pp. 545–552, Jan. 2005. DOI: 10.1109/tap.2004.838774.

[73] C. Domizioli, B. Hughes, K. Gard, and G. Lazzi, "Noise correlation in compact diversity receivers," *IEEE Transactions on Communications*, vol. 58, no. 5, pp. 1426–1436, May 2010. DOI: 10.1109/tcomm.2010.05.080601.

[74] H. Bosma, "On the theory of linear noisy systems," *Philips research reports*, no. 10, 1967.

[75] S. Wedge and D. Rutledge, "Noise waves and passive linear multiports," *IEEE Microwave and Guided Wave Letters*, vol. 1, no. 5, pp. 117–119, May 1991. DOI: 10.1109/75.89082.

[76] E. Telatar, "Capacity of multi-antenna gaussian channels," *Eur. Trans. Telecommun.*, vol. 10, no. 6, pp. 585–595, Nov. 1999. DOI: 10.1002/ett.4460100604.

[77] X.-L. Meng and D. B. Rubin, "Maximum likelihood estimation via the ECM algorithm: A general framework," *Biometrika*, vol. 80, no. 2, pp. 267–278, Jun. 1993. DOI: 10.1093/biomet/80.2.267.

[78] D. J. Love, R. W. Heath, W. Santipach, and M. L. Honig, "What is the value of limited feedback for MIMO channels?" *IEEE Communications Magazine*, vol. 42, no. 10, pp. 54–59, Oct. 2004. DOI: 10.1109/mcom.2004.1341261.

[79] D. J. Love, R. Heath, V. N. Lau, D. Gesbert, B. Rao, and M. Andrews, "An overview of limited feedback in wireless communication systems," *IEEE Journal on Selected Areas in Communications*, vol. 26, no. 8, pp. 1341–1365, Oct. 2008. DOI: 10.1109/jsac.2008.081002.

[80] J. Kim, J. Kim, S. Kong, H. Kim, I.-S. Suh, N. P. Suh, D.-H. Cho, J. Kim, and S. Ahn, "Coil design and shielding methods for a magnetic resonant wireless power transfer system," *Proceedings of the IEEE*, vol. 101, no. 6, pp. 1332–1342, Jun. 2013. DOI: 10.1109/jproc.2013.2247551.

[81] *ANSYS High Frequency Structure Simulator (HFSS), Release 2019 R2*, Ansys, Inc.

[82] K. Han and K. Huang, "Wirelessly powered backscatter communication networks: Modeling, coverage, and capacity," *IEEE Transactions on Wireless Communications*, vol. 16, no. 4, pp. 2548–2561, Apr. 2017, ISSN: 1536-1276. DOI: 10.1109/TWC.2017.2665629. [Online]. Available: http://ieeexplore.ieee.org/document/7876867/.

[83] D. Niyato, D. I. Kim, M. Maso, and Z. Han, "Wireless powered communication networks: Research directions and technological approaches," *IEEE Wireless Communications*, vol. 24, no. 6, pp. 88–97, Dec. 2017. DOI: 10.1109/mwc.2017.1600116.

[84] X. Tan, Z. Sun, and I. F. Akyildiz, "Wireless underground sensor networks: MI-based communication systems for underground applications.," *IEEE Antennas and Propagation Magazine*, vol. 57, no. 4, pp. 74–87, Aug. 2015. DOI: 10.1109/map.2015.2453917.

[85] C. Boyer and S. Roy, "Backscatter communication and RFID: Coding, energy, and MIMO analysis," *IEEE Transactions on Communications*, vol. 62, no. 3, pp. 770–785, Mar. 2014. DOI: 10.1109/TCOMM.2013.120713.130417.

[86] G. Yang, C. K. Ho, and Y. L. Guan, "Multi-antenna wireless energy transfer for backscatter communication systems," *IEEE Journal on Selected Areas in Communications*, vol. 33, no. 12, pp. 2974–2987, Dec. 2015. DOI: 10.1109/jsac.2015.2481258.

[87] D. Mishra and E. G. Larsson, "Optimal channel estimation for reciprocity-based backscattering with a full-duplex MIMO reader," *IEEE Transactions on Signal Processing*, vol. 67, no. 6, pp. 1662–1677, Mar. 2019. DOI: 10.1109/tsp.2019.2893859.

[88] T. Arakawa, J. V. Krogmeier, and D. J. Love, "Channel modeling for wireless information and power transfer using inductive coupling," in *Proc. 52nd Asilomar Conf. Sig., Sys, and Comp*, Oct. 2018. DOI: 10.1109/acssc.2018.8645307.

[89] K. Kurokawa, "Power waves and the scattering matrix," *IEEE Transactions on Microwave Theory and Techniques*, vol. 13, no. 2, pp. 194–202, Mar. 1965. DOI: 10.1109/tmtt.1965.1125964.

[90] J. G. Proakis and M. Salehi, *Digital Communications*, 5th editio. McGraw-Hill, New York, 2007, p. 1150, ISBN: 2007036509.

[91] B. Clerckx, Z. B. Zawawi, and K. Huang, "Wirelessly powered backscatter communications: Waveform design and SNR-energy tradeoff," *IEEE Communications Letters*, vol. 21, no. 10, pp. 2234–2237, Oct. 2017. DOI: 10.1109/lcomm.2017.2716341.

[92] S. M. Kay, *Fundamentals of Statistical Processing, Volume I: Estimation Theory*. Prentice Hall, Mar. 26, 1993, 608 pp., ISBN: 0133457117.

[93] J. Brown, R. Churchill, and B. James, *Complex Variables and Applications*. McGraw-Hill Higher Education, 2004, ISBN: 9780072878349.

[94] T. Arakawa, A. C. Marcum, J. V. Krogmeier, and D. J. Love, "Simultaneous wireless information and power transfer over inductively coupled circuits," in *Proc. IEEE Int. Conf. on Acoustics, Speech, and Sig. Process. (ICASSP)*, Mar. 2017, pp. 3769–3773. DOI: 10.1109/ICASSP.2017.7952861.

VITA

Tomohiro Arakawa received the B.Eng. degree from the National Institution for Academic Degrees and Quality Enhancement of Higher Education, Japan, upon completion of the Advanced Course of Mechanical and Computer Systems Engineering at the National Institute of Technology, Tokyo College, Japan, in 2015. He is currently pursuing a Ph.D. degree in electrical and computer engineering at Purdue University, West Lafayette, IN, USA. His research interests include signal processing for wireless communications and wireless power transfer systems.